UNIVERSITAT DE BARCELONA

Novel carbon-based nanoscale therapeutics for the modulation of macrophages in liver inflammation, fibrosis, and regeneration

Alazne Moreno Lanceta

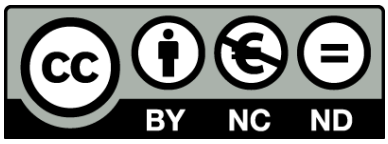

Novel carbon-based nanoscale therapeutics for the modulation of macrophages in liver inflammation, fibrosis, and regeneration

Doctoral thesis dissertation presented by

Alazne Moreno Lanceta

to apply for the degree of doctor at the University of Barcelona

Thesis director: **Dr. Pedro Melgar Lesmes**[1,2]

Tutor: **Dr. Wladimiro Jiménez Povedano**[1]

[1]Department of Biomedicine, School of Medicine, University of Barcelona, Institut d'Investigacions Biomèdiques August Pi-Sunyer (IDIBAPS), Biochemistry and Molecular Genetics Service, Hospital Clínic de Barcelona

[2]Institute for Medical Engineering and Science, Massachusetts Institute of Technology

Doctoral program in Medicine and Translational Research

School of Medicine and Health Sciences. University of Barcelona

Barcelona, June 2024

INDEX

FUNDING 7

INDEX OF FIGURES AND TABLES 8

ABBREVIATIONS 9

LIST OF ARTICLES IN THE THESIS 12

RESUMEN 13

INTRODUCTION 17

1. Chronic liver disease 18
    1.1. Overview 18
    1.2. Liver fibrosis 19
        1.2.1. Cellular and molecular mechanisms 21
        1.2.2. Fibrosis regression 24
    1.3. Liver regeneration 26
2. Macrophages 28
    2.1. Macrophages as key players in the liver 29
    2.2. Macrophage polarization 35
        2.2.1. Inflammation-related signaling pathways 35
            2.2.1.1. PPARγ 38
        2.2.2. Ubiquitin ligases 41
            2.2.2.1. RNF41 42
3. Nanoparticles 43
    3.1. Nanoparticles in liver diseases 45
    3.2. Carbon-based nanoparticles 46

HYPOTHESIS 50

OBJECTIVES 52

MATERIAL, METHODS, AND RESULTS 55

- Article 1 56

"PPAR-γ agonist GW1929 targeted to macrophages with dendrimer–graphene nanostars reduces liver fibrosis and inflammation"

Article 1: supplementary materials 73

- Article 2 74

"RNF41 orchestrates macrophage-driven fibrosis resolution and hepatic regeneration"

Article 2: supplementary materials 89

DISCUSSION 115

CONCLUSIONS 131

REFERENCES 134

FUNDING

This thesis is framed within the projects RTI2018-094734-B-C21 and PID2021-123426OB-I00, funded by the Spanish Ministry of Science, Innovation and Universities (MCIN/AEI/10.13039/501100011033 and "ERDF A way of making Europe"). Alazne Moreno Lanceta had a Formación de Personal Investigador (FPI) grant from the Spanish Ministry of Science, Innovation and Universities and FSE invierte en tu futuro (reference: PRE2019-088097).

INDEX OF FIGURES AND TABLES

Figure 1: Stages of chronic liver disease 18
Figure 2: Macroscopic and microscopic structure of the liver 22
Figure 3: Major molecular and cellular mechanisms modulating fibrogenesis 23
Figure 4: Functions, features, and phenotypes of HSCs in fibrosis perpetuation and resolution 25
Figure 5: Role of monocyte-derived macrophages in the initiation, progression, and resolution of liver inflammation and fibrosis 32
Figure 6: Monocyte-endothelial cell interaction 34
Figure 7: Molecular mechanisms of PPARγ 39
Figure 8: The ubiquitin system 41
Figure 9: Schematic representation of graphene, graphene nanostar, and graphite nanoparticle structure 47
Figure 10: Functionalization of oxidized graphene nanostars and graphene nanoparticles with PAMAM dendrimers 48
Figure 11: Schematic representation of the therapeutic effects of a pDNA expressing MMP9 selectively delivered with dendrimer-graphene nanostars to liver macrophages in fibrotic mice 49
Figure 12: Schematic representation of the state of macrophages in CLD and the therapeutic potential of their polarization 120
Figure 13: Schematic illustration of the effects of macrophage-selective PPARγ activation and RNF41 restoration in liver inflammation, fibrosis, and regeneration 129

Table 1: Classification and characteristics of the main liver immune cells in homeostasis and hepatic inflammation and fibrosis 30

ABBREVIATIONS

APC	antigen-presenting cells
ARG1	arginase-1
C/EBPβ	CCAAT enhancer-binding protein beta
CCl_4	carbon tetrachloride
CLD	chronic liver disease
COX-2	cyclooxygenase 2
CREB-C	cAMP response element-binding C
DAMP	damage-associated molecular patters
DGNP	dendrimer-graphite nanoparticles
DGNS	dendrimer-graphene nanostars
ECM	extracellular matrix
EGF	epidermal growth factor
ERK	extracellular signal-regulated kinases
FLRF	fetal liver ring finger
G5 PAMAM	generation 5 polyamidoamine
GNP	graphite nanoparticles
GNS	graphene nanostars
GW1929	PPARγ agonist
HCC	hepatocellular carcinoma
HECT	homologous to the E6AP carboxyl terminus
HSC	hepatic stellate cells
ICAM-1	intracellular adhesion molecule 1
IFN-γ	interferon gamma
IGF-1	insulin-like growth factor 1
IκB	inhibitor of NF-κB
IKK	IκB kinase
IL-1β	interleukin 1 beta

KC	Kupffer cells
LPS	lipopolysaccharide
LSEC	liver sinusoidal endothelial cells
MASH	metabolic dysfunction-associated steatohepatitis
MDM	monocyte-derived macrophages
MMP	metalloproteinase
MRC	mannose receptors
NASH	non-alcoholic steatohepatitis
NF-κB	nuclear factor kappa-B
NIK	NF-kB inducing kinase
NOS-2	including nitric oxide synthase 2
NP	nanoparticles
NRDP1	neuregulin receptor degradation protein 1
OSM	oncostatin M
PAMAM	polyamidoamine
PBC	primary biliary cirrhosis
PDGF-BB	platelet-derived growth factor
pDNA	plasmid DNA
PPARγ	peroxisome proliferator-activated receptor γ
PPRE	proliferator responsive element
pRNF41-DGNP	pRNF41 with dendrimer-graphite nanoparticles
pshRNF41-DGNP	pshRNF41 with dendrimer-graphite nanoparticles
RETNLA	resistin-like alpha
RING	really interesting new gene
RNF	RING finger
RNF41	RING finger 41
ROS	reactive oxygen species
RXR	retinoid X receptor
STAT	signal transducer and activator of transcription

SWCNH	single-walled carbon nanohorns
TAA	thioacetamide
TBK1	TANK-binding kinase 1
TGF-β	transforming growth factor-beta
TIMP	tissue inhibitor metalloproteinases
TLR	toll-like receptor
TNF-α	tumor necrosis factor alpha
TNFR	tumor necrosis factor receptor
TREM2	triggering receptor expressed on myeloid cells 2
TZD	thiazolidinediones
Ub	ubiquitin
UbR	ubiquitin receptors
USP8	ubiquitin specific peptidase 8
VEGF	vascular endothelial growth factor
Wnt	wingless-related integration site
α-SMA	alpha-smooth muscle actin

LIST OF ARTICLES IN THE THESIS

This thesis is presented in compendium of publications format. The thesis consists of two principal objectives and two published articles:

Article 1: **Moreno-Lanceta A**, Medrano-Bosch M, Simón-Codina B, Barber-González M, Jiménez W and Melgar-Lesmes P. PPAR-γ agonist GW1929 targeted to macrophages with dendrimer–graphene nanostars reduces liver fibrosis and inflammation. Pharmaceutics. 2023; *15*(5), 1452.

- Journal impact factor (JCR) (2022): 5.4
- Quartile: Q1
- Area of knowledge: Pharmacology & Pharmacy (rank 50/278).

Article 2: **Moreno-Lanceta A,** Medrano-Bosch M, Fundora Y, Perramón M, Aspas J, Parra-Robert M, Baena S, Fondevila C, Edelman ER, Jiménez W, Melgar-Lesmes P. RNF41 orchestrates macrophage-driven fibrosis resolution and hepatic regeneration. Science Translational Medicine. 2023; *15*(704): eabq6225.

- Journal impact factor (JCR) (2022): 17.1
- Quartile: Q1
- Area of knowledge: Cell biology (rank 13/191); Medicine, research & experimental (rank 2/136).

RESUMEN

Título: Nuevas terapias en la nanoescala basadas en nanopartículas de carbono para la modulación de los macrófagos en inflamación, fibrosis y regeneración hepática.

Introducción: La enfermedad hepática crónica (EHC) es la consecuencia de un daño hepático prolongado y se caracteriza por un proceso de inflamación y fibrosis en el hígado, que causa alrededor de 2 millones de muertes al año. La EHC puede tardar varios años en progresar desde fibrosis temprana hasta cirrosis, y en última instancia, producir insuficiencia hepática y muerte. Actualmente no existen terapias curativas para la cirrosis más allá del trasplante hepático y, por tanto, es necesario el desarrollo de nuevas estrategias terapéuticas. Los macrófagos hepáticos desempeñan funciones esenciales en todas las etapas de la EHC, tanto en el inicio y progresión de la respuesta inflamatoria como en el desarrollo de fibrosis. El microentorno de inflamación hepática crónica perpetúa la actividad proinflamatoria y profibrogénica de los macrófagos hepáticos. Sin embargo, los macrófagos también son esenciales en los procesos que regulan la resolución de la fibrosis, tanto promoviendo una respuesta antiinflamatoria y regenerativa, como mediante la secreción de enzimas que remodelen la matriz extracelular. El receptor gamma activado por el proliferador de peroxisomas (PPARγ) y la E3 ubiquitina ligasa RNF41 se han asociado a la polarización antiinflamatoria de los macrófagos.

Hipótesis: La activación selectiva de las vías antiinflamatorias PPARγ y RNF41 en macrófagos hepáticos mediante nanopartículas de carbono macrófago-selectivas puede inducir un fenotipo pro-resolutivo en estas células inmunitarias que promueva una reducción de la inflamación y la fibrosis, y estimule la regeneración del hígado en la EHC.

Objetivos: El primer objetivo fue analizar los efectos que produce una activación macrófago-selectiva de PPARγ en el hígado de ratones con fibrosis hepática mediante nanoestrellas de dendrímero-grafeno unidas al agonista de PPARγ GW1929. El segundo objetivo fue investigar el papel que desempeña RNF41 en la regulación de los macrófagos hepáticos en la EHC, y estudiar los efectos de la modulación macrófago-selectiva de RNF41 sobre la inflamación, fibrosis y regeneración hepática en modelos animales de EHC mediante nanopartículas de dendrímero-grafito.

Métodos: En el primer estudio, se sintetizaron y caracterizaron nanoestrellas macrófago-selectivas de dendrímero-grafeno unidas al agonista de PPARγ GW1929 (NSDG-GW) o a manitol (NSDG-Man) como control. Se evaluó la capacidad de incorporación de NSDG-GW y su actividad antiinflamatoria en macrófagos murinos estimulados con el factor de necrosis tumoral alfa (TNF-α). Se administraron NSDG-GW de manera intravenosa a ratones con fibrosis hepática inducida por tetracloruro de carbono (CCl_4). El efecto terapéutico de NSDG-GW sobre la inflamación, fibrosis y regeneración hepática se evaluó mediante técnicas de histología y PCR en tiempo real. En el segundo estudio, se aislaron macrófagos $CD11b^+$ del hígado de pacientes cirróticos y de ratones con fibrosis hepática inducida por CCl_4, para cuantificar la expresión de RNF41 mediante PCR en tiempo real. Se sintetizaron y caracterizaron nanopartículas de dendrímero-grafito (NPDG) unidas a plásmidos que inducían (pRNF41) o inhibían (pshRNF41) la expresión de RNF41. Estas nanopartículas se administraron de manera intravenosa a ratones con fibrosis hepática y/o hepatectomía parcial. Se analizó la biodistribución de dichas nanopartículas y los efectos de la inducción o inhibición de RNF41 sobre la inflamación, fibrosis, función hepática y regeneración mediante técnicas de histología y PCR en tiempo real. Se

llevaron a cabo estudios *in vitro* en macrófagos para analizar el mecanismo de acción de RNF41 sobre la fibrosis y la regeneración.

Resultados: En el primer estudio, las NSDG-GW y NSDG-Man mostraron una distribución de tamaños uniforme y carga de superficie negativa adecuada para su administración *in vivo*. Macrófagos estimulados *in vitro* con TNF-α captaron mayor cantidad de NSDG-GW y mostraron menor expresión de genes pro-inflamatorios en comparación con los tratados con NSDG-Man. La activación selectiva de PPARγ en macrófagos hepáticos de ratones fibróticos con NSDG-GW redujo la expresión de genes proinflamatorios e incrementó la expresión de genes antiinflamatorios en comparación con los ratones tratados con NSDG-Man. Asimismo, el tratamiento con NSDG-GW produjo una regresión histológica parcial en la fibrosis y una disminución de la expresión de α-actina, sin observarse diferencias significativas en el daño hepático, ni en la expresión de los inhibidores de metaloproteinasas ni de colágeno 1A. La disminución en la fibrosis se asoció a un aumento en la expresión de metaloproteinasas. Las NSDG-GW también produjeron un aumento en la regeneración hepática en ratones fibróticos que se asoció a un aumento en la expresión del factor de crecimiento endotelial vascular. En el segundo estudio, los macrófagos aislados de hígado de pacientes cirróticos y ratones fibróticos mostraron una menor expresión de RNF41. *In vitro,* esta disminución en la expresión de RNF41 en macrófagos se asoció al proceso de inflamación crónica. Las NPDG demostraron una acumulación selectiva en macrófagos de hígados fibróticos y una alta eficiencia como vehículo de terapia génica mediante plásmidos. La inducción de la expresión de RNF41 en macrófagos de ratones fibróticos mediante pRNF41-NPDG produjo la regresión histológica de la fibrosis, una reducción notable en el daño hepático, un aumento en la expresión de

genes antiinflamatorios y una menor expresión de genes proinflamatorios y profibrogénicos. Asimismo, las pRNF41-NPDG produjeron un aumento en la regeneración hepática en ratones hepatectomizados con y sin fibrosis. Mecanísticamente, el efecto terapéutico de la inducción de RNF41 en macrófagos fue, en parte, mediado por el factor de crecimiento insulínico tipo 1 y la estimulación de PPARγ. El bloqueo de la expresión de RNF41 en los macrófagos hepáticos de ratones fibróticos mediante pshRNF41-NPDG produjo una sobreexpresión de citocinas inflamatorias acompañada de una mayor fibrosis, daño hepático y una menor supervivencia.

Conclusiones: La activación selectiva de PPARγ así como la inducción de la expresión de RNF41 en los macrófagos hepáticos en la EHC estimula un fenotipo antiinflamatorio y pro-resolutivo en los macrófagos que da lugar a una reducción en la fibrosis y promueve la regeneración hepática. Además, el uso de nanopartículas macrófago-selectivas basadas en carbono para la administración de terapia farmacológica o la modulación de la expresión génica supone una estrategia terapéutica prometedora para modular el comportamiento de los macrófagos proinflamatorios en la EHC.

INTRODUCTION

1. CHRONIC LIVER DISEASE

1.1. Overview

Chronic liver disease (CLD) is the consequence of a long-standing process of sustained injury and inflammation in the liver, which leads to a progressive deterioration of the hepatic tissue and its functions (1). CLD accounts for around 2 million deaths per year and is responsible for 1 out of 25 deaths worldwide (2). CLD is characterized by an active process of injury/destruction and regeneration of the liver parenchyma that leads to the development of liver fibrosis to restrict the areas with liver injury (3). Liver fibrosis is commonly asymptomatic. The development of liver dysfunction and measurable symptoms may take several years to progress from early fibrosis towards cirrhosis and ultimately liver failure and death (4) **(Figure 1)**. Liver cirrhosis is among the top 15 causes of disability-adjusted life years and years of life lost (2). Moreover, cirrhosis is a major risk factor for the development of hepatocellular carcinoma (HCC) (5). Indeed, CLD mortality is principally attributable to complications of cirrhosis and HCC (2,5).

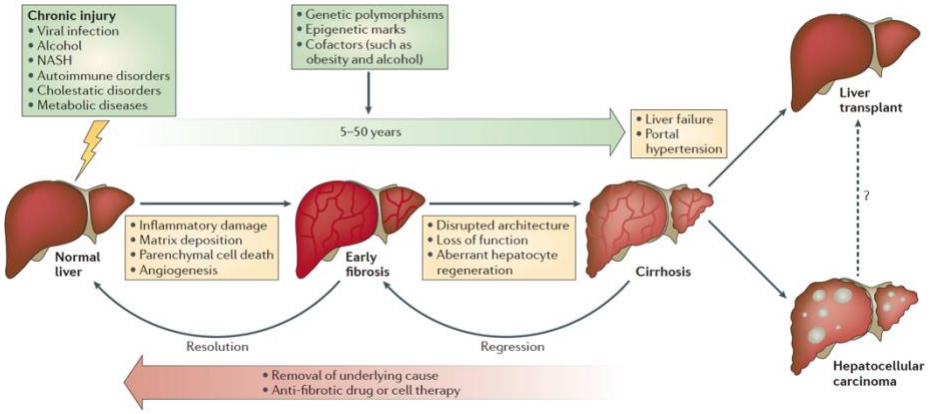

Figure 1: Stages of chronic liver disease. After initial liver injury, sustained inflammation and matrix deposition leads to early fibrosis. Fibrosis progression may disrupt liver architecture and function leading to a cirrhotic stage, which may eventually trigger hepatocellular carcinoma. The only available treatment for advanced stage chronic liver disease nowadays is liver transplant. Abbreviations: NASH, non-alcoholic steatohepatitis. *Image obtained from Pellicoro et al. Nat Rev Immunol (2014) (4).*

Etiologies of CLD are diverse: chronic viral hepatitis (mostly after hepatitis B, C or D virus infections), alcoholic liver disease, metabolic dysfunction-associated steatohepatitis (MASH), autoimmune disorders (such as primary biliary cirrhosis (PBC), autoimmune hepatitis, and primary sclerosing cholangitis), and genetic disorder-related liver disease (such as haemochromatosis or Wilson's disease) (2) **(Figure 1)**. Inflammation is a key driver of liver disease progression and is closely related to the appearance of clinical complications such as advanced liver fibrosis, decompensated cirrhosis, and tumor propagation (6–8). Major clinical complications of cirrhosis include variceal bleeding, renal failure, ascites, and hepatic encephalopathy (3).

The elimination of the underlying cause of the disease has shown to reverse liver fibrosis (4). However, the morbidity and mortality related to CLD remains challenging and identifying an effective treatment is a major medical need. Indeed, there are currently no effective treatments for cirrhosis except for organ transplantation, which requires extensive surgery and continuous immunosuppression (9). However, only the 50% of eligible patients receive a liver transplant and around the 20% of patients die while being enrolled on the waiting list (10). Thus, alternative strategies to treat cirrhosis and stimulate hepatic regeneration are being investigated, including nanotherapeutics.

1.2. Liver fibrosis

Liver fibrosis is a common pathological trait in CLD (11). Liver fibrosis is the result of the wound-healing response of the liver to repeated injury and is characterized by the excessive production and deposition of extracellular matrix (ECM) proteins, including collagens (I, III, and V), fibronectin, undulin, elastin, laminin, hyaluronan, and proteoglycans (3).

Both the composition and the quantity of ECM are altered in the liver of patients with CLD. Interestingly, in advanced stages, the liver can contain approximately 6 times more ECM than in physiological conditions (3).

Liver fibrosis is inevitably coexisting with a sustained inflammatory response (3,11). Initial acute liver injury (such as viral infection) leads to an inflammatory response and a limited deposition of ECM. In this situation, parenchymal cells (hepatocytes) can regenerate and replace the necrotic or apoptotic cells (3). If the hepatic injury persists and becomes chronic (such as long-term alcohol consumption), liver regeneration fails, and the functional parenchymal tissue of the liver is partially substituted with abundant ECM (3). The distribution of these ECM components depends on the etiology of the liver injury (12). For instance, fibrotic tissue first appears around portal tracts in chronic viral hepatitis and chronic cholestasis, but it locates in pericentral and perisinusoidal regions in alcohol-induced liver disease (3,12). The histological determination of fibrosis in liver biopsies has been traditionally used and remains the gold standard for the diagnosis and staging of patients with CLD and experimental animal models with liver fibrosis (13). Other modern non-invasive diagnostic tools, such as Fibroscan, are also centered on evaluating the fibrous quantity in the liver of the patients (14), which highlights the importance of liver fibrosis as a prognostic factor in clinical settings.

The pathophysiology of liver fibrosis involves the crosstalk of several cell types, signaling pathways, and molecular mechanisms. Following liver injury, damaged hepatocytes secrete cytokines, chemokines, reactive oxygen species (ROS), damage-associated molecular patters (DAMPs), and extracellular vesicles (6,15). The resulting inflammatory response drives the activation of myofibroblasts,

which are the primary source of ECM in a fibrotic liver (6). Myofibroblast activation and the inflammatory response are two major cellular mechanisms involved in the pathophysiology of liver fibrosis.

1.2.1. Cellular and molecular mechanisms

To understand the cellular and molecular mechanisms of liver fibrosis, it is essential to comprehend the liver structure. The liver is the largest solid organ in the body that performs over 500 vital functions (16). In humans, the liver is anatomically shaped of two main lobes with eight well-defined segments as described by the Couinaud classification (16). In rodents, the liver is divided in four well-defined lobes (median, right, left, and caudate lobes) (16) **(Figure 2A)**. All lobes are formed by thousands of microscopic functional units, defined as the liver lobules **(Figure 2B)**. The microscopic architecture of the liver is generally similar in all mammals (16). The liver lobule is formed by a single central vein (which drains blood away from the liver lobule to the hepatic vein) and a portal triad consisting of three structures: a portal vein (which carries nutrient-rich blood from the intestines), an hepatic artery (which supplies oxygenated blood to the liver), and a bile duct (which drains bile, an excretory product) (16,17). Each lobule is made up of numerous cell types that interact together in the liver parenchyma, the sinusoids, and the space of Disse to maintain homeostasis **(Figure 2C)** (3). Indeed, liver homeostasis requires communication and collaboration between parenchymal cells (hepatocytes) and non-parenchymal cells (Kupffer cells (KCs), liver sinusoidal endothelial cells (LSECs), and hepatic stellate cells (HSCs)). This collaboration is disturbed when physiological equilibrium is altered due to liver injury (3).

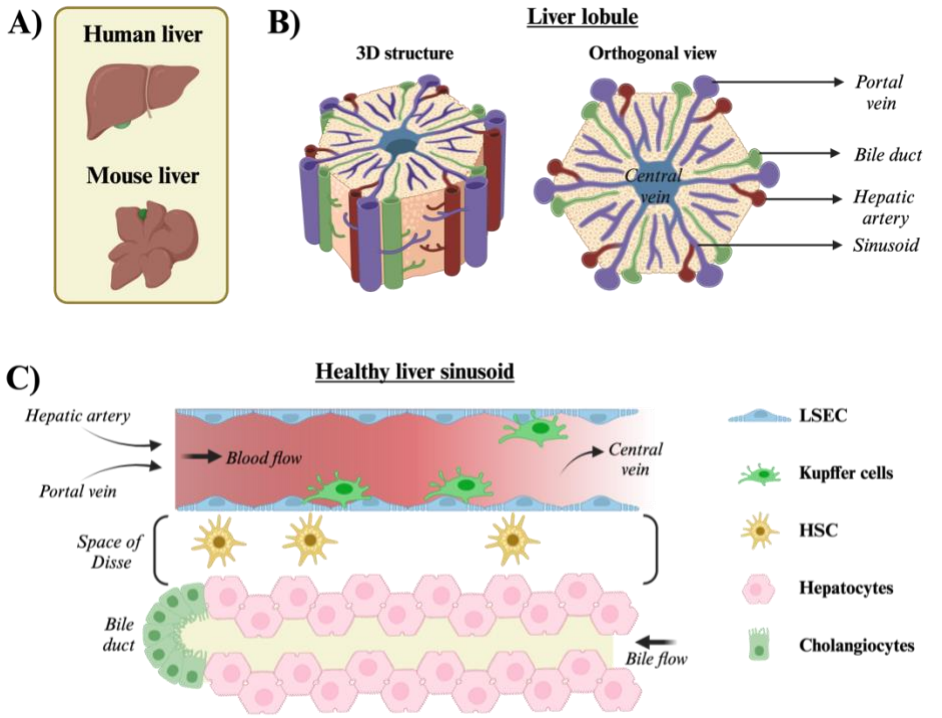

Figure 2: Macroscopic and microscopic structure of the liver. A) Human liver has two main lobes whereas mouse liver has anatomically well-defined four lobes. **B)** The liver lobule is the basic functional unit of the liver. This hexagonal area of the tissue receives blood flow from both the hepatic artery and the portal vein. It contains a single central vein that drains blood away from the liver sinusoid. **C)** The liver lobule contains parenchymal (hepatocytes) and non-parenchymal cells, each of them performing essential functions to maintain homeostasis. Abbreviations: LSEC, liver sinusoidal endothelial cells; HSC, hepatic stellate cells. *Original image created with Biorender.*

Following liver injury, damaged and dying cells release soluble mediators, such as DAMPs or alarmins, to alert surrounding cells such as KCs about the tissue damage (6). Then, KCs release an array of cytokines that activate HSCs, which in homeostatic conditions reside in the space of Disse and are the major storage sites of vitamin A, and transdifferentiate into myofibroblasts (3,6,18). Myofibroblastic HSCs acquire contractile, pro-inflammatory and fibrogenic properties (19). They also upregulate alpha-smooth muscle actin (α-SMA) and produce and secrete collagen I and tissue inhibitor metalloproteinases (TIMPs). HSC activation and

transdifferentiation is mainly mediated via KCs-secreted platelet-derived growth factor (PDGF-BB) and transforming growth factor-beta (TGF-β) (20,21). Indeed, PDGF-BB and TGF-β are considered predominant mitogens for the activation of HSC (20,21). Both KCs and myofibroblastic HSCs secrete pro-inflammatory chemokines that recruit circulating monocytes to the site of injury. These chemokines include CCL2, CCL3, CCL5, CXCL9, and CXCL10, which attract circulating monocytes primarily via CCR2 and CCR5 (6). Recruited monocyte-derived macrophages (MDMs) release inflammatory mediators such as TGFβ, PDGF-BB, oncostatin M (OSM), and interleukin-17 (IL-17) to further perpetuate myofibroblastic HSC activation and pro-inflammatory response (6,22). Myofibroblastic HSCs deposit ECM components to isolate injured areas (3) (**Figure 3)**.

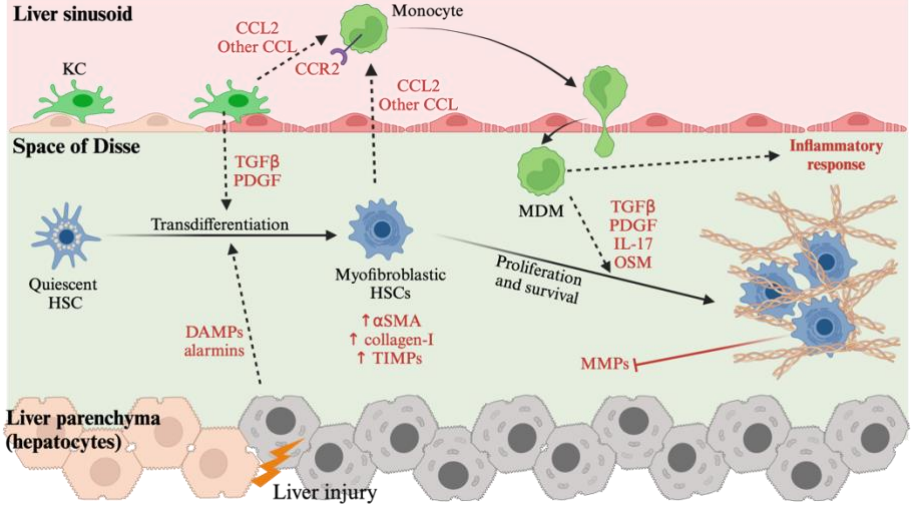

Figure 3: Major molecular and cellular mechanisms modulating fibrogenesis. Diverse type of non-parenchymal cells have essential functions in the modulation of fibrogenesis following liver injury. Myofibroblastic HSCs are the major source of extracellular matrix proteins. Abbreviations: KC, Kupffer cells; HSC, hepatic stellate cells; DAMPs, damage-associated molecular patterns; TGF-β, transforming growth factor-beta; PDGF, platelet-derived growth factor; α-SMA, alpha-smooth muscle actin; TIMPs, tissue inhibitor metalloproteinases; OSM, oncostatin M; MMPs, metalloproteinases. *Original image created with Biorender.*

Fibrogenesis is a tightly regulated process that initially aids to limit liver injury to avoid the loss of liver homeostasis. However, when the parenchymal injury is chronic, the hepatic overproduction and deposition of ECM from myofibroblasts, together with the inhibition of matrix metalloproteinases (MMPs) via TIMPs and the perpetuation of liver inflammation, eventually results in advanced fibrosis (3). During fibrosis progression, although HSCs are largely known as the main source of hepatic myofibroblasts, other cell linages such as portal fibroblasts, circulating fibrocytes, mesenchymal stem cells, and mesothelial cells may contribute to the myofibroblast population, which is not present in a healthy liver (18). Deep phenotyping and cell fate mapping have shown that activated HSCs and activated portal fibroblasts contribute to more than 95% of the myofibroblast population following liver injury (23). The origin of myofibroblasts in clinical liver disease and experimental animal models depends on the etiology of the pathology (18,23). For example, in animal models, HSCs are the major source of myofibroblasts (>87%) in carbon tetrachloride (CCl_4)-induced liver injury, whereas activated portal fibroblast are the major source of myofibroblasts in cholestatic liver injury (>70%) (23).

1.2.2. Fibrosis regression

Two key cellular events have been established at the cellular level for fibrosis regression: 1) hepatic myofibroblasts should undergo senescence and apoptosis; and 2) macrophages need to switch to an anti-inflammatory phenotype (18). Myofibroblastic HSCs may undergo apoptosis or return to an inactivated state (with a similar phenotype to quiescent HSC) during liver fibrosis regression (18) **(Figure 4)**. Macrophages can also support the regression of fibrosis through the promotion of an anti-inflammatory response and the secretion of matrix

remodeling enzymes that degrade fibrous scars (18). Indeed, fibrosis resolution is mostly associated to elevated collagenolytic activity (3,18). During fibrosis resolution, metalloproteinase (MMP) activity increases owing to a significant decline in TIMP expression in myofibroblasts. Fibrillar collagen is degraded, and the modified interaction between activated myofibroblasts and ECM can also promote myofibroblast apoptosis (3,18,19).

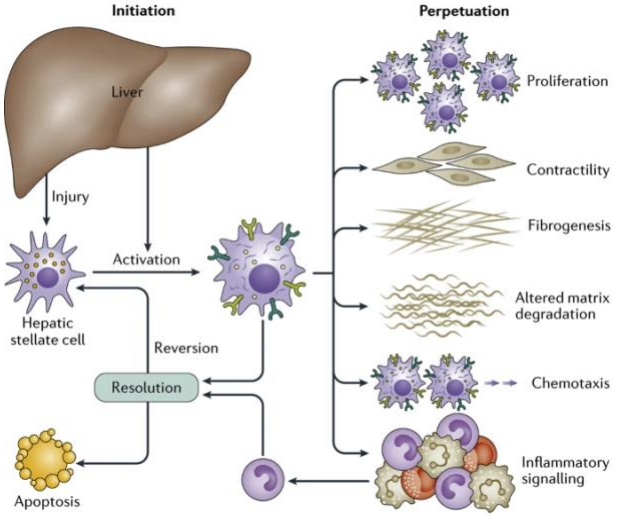

Figure 4: Functions, features, and phenotypes of HSCs in fibrosis perpetuation and resolution. Quiescent hepatic stellate cells (HSCs) begin to transdifferentiate into their active phenotype in response to liver damage. Activated HCSs are characterized by specific phenotypic changes including proliferation, contractility, fibrogenesis, altered matrix degradation, chemotaxis, and the induction of pro-inflammatory signaling. Activated HSCs can be cleared by apoptosis or be reverted to an inactivated phenotype due to anti-inflammatory macrophage activity, enabling fibrosis resolution. *Image obtained from Tsuchida et al. Nat Rev Gastroenterol Hepatol (2017) (19).*

Possible full recovery of the liver architecture in advanced fibrosis or cirrhosis remains controversial. It is known that, depending on the etiology, hepatic fibrosis may be halted or partially reversed after the cause of injury has been removed (3). For example, spontaneous resolution of liver fibrosis has been observed after the successful treatment and full response against hepatitis viral infections (3,24). This fibrosis

resolution correlates with an improved clinical outcome (25). However, significant fibrosis regression may only be noticeable after several years since the cause of the disease is removed. This time varies depending on the severity and the underlying cause of the liver disease (3). Thus, there is a crucial medical need to develop efficient anti-fibrotic therapeutic strategies to accelerate and promote fibrosis regression in patients with CLD even after removing the cause of the disease. Recent investigations suggest that even advanced fibrosis may be reversible, contrary to the traditional view that advanced liver disease is an irreversible condition (3,6,26–29). These studies have shown substantial improvement in hepatic structure and function (26–28). Despite many preclinical and clinical trials have demonstrated the potential of novel anti-fibrotic therapies, to date there is no anti-fibrotic drug approved by the European Medicines Agency or the Food and Drug Administration, since they have shown limited efficacy and considerable side effects. As we continue deepening our knowledge on cellular and molecular events associated with liver fibrosis progression and regression, we can investigate new efficient pharmaceutical approaches with reduced side effects for patients with CLD.

1.3. Liver regeneration

Liver regeneration is the process by which the liver can restore lost or damaged liver tissue (30). The liver is the unique visceral organ with the capacity to fully regenerate. Liver regeneration occurs after partial hepatectomy or liver injury due to hepatotoxic agents such as certain medications, toxins, chemicals, or infections (31). In mammals, the liver mostly regenerates through compensatory growth or hyperplasia (31). During compensatory hyperplasia, the remaining liver tissue becomes larger, allowing the organ to maintain functions, without returning to its

original shape (31). There is no formation of new liver lobes. In healthy patients, the liver can regenerate up to half of its mass within 30 days and a complete restoration of the liver residual size can be observed within 3 to 6 months (32). In rodents, most of the liver mass is restored within 7–8 days after a typical two-third partial hepatectomy (33).

Liver regeneration following partial hepatectomy, for example after the removal of benign tumors or cysts, is a very complex and well-orchestrated phenomenon (34). Hepatocytes are in G_0 phase in normal histological conditions. Following partial hepatectomy, they re-enter the cell cycle and proliferate until they meet the minimum liver weight required for survival (35). Liver regeneration involves several types of mature liver cells and comprises cytokines and growth factors involved in signaling pathways related to hepatocyte proliferation and matrix remodeling (33–35). The liver regeneration process is divided in three stages: initiation, progression, and termination. Relevant signaling pathways involved in these phases include IL-6, tumor necrosis factor alpha (TNF-α), Hippo, Wingless-related integration site (Wnt), hepatocyte growth factor (HGF), epidermal growth factor (EGF), and TGF-β pathways (35). These signaling pathways interact together to regulate the process of liver regeneration. Some pathways are more relevant in different stages; for instance, the HGF pathway is related mostly to the initiation and progression of liver regeneration (35).

Liver regeneration is usually characterized by phenotypic fidelity, meaning that hepatic epithelial cells (hepatocytes and cholangiocytes) proliferate to form epithelial cells, and same applies to other non-epithelial cells (HSCs, LSEC, KCs, and others) (33). In addition to local cell proliferation, precursor cells migrating from the bone marrow also participate in liver regeneration, such as circulating monocytes (33). Some

studies have demonstrated that circulating monocytes are selectively recruited to certain regions of regenerating livers after hepatectomy, particularly around sprouting points (36,37). Indeed, direct vascular interactions between endothelial cells and recruited circulating monocytes are essential for an ordered vascular growth during liver regeneration (36).

Liver regeneration also occurs in response to acute or chronic insults that induce inflammation, hepatocyte damage and subsequent tissue remodeling, such as those involved in CLD (33). However, loss of functional hepatocytes and changes in the ECM impose limits to the regenerative capacity of the liver (33,34). Moreover, the effects of free radicals and ROS on proliferative hepatocytes exposes them to genotoxic damage, which may lead to neoplasia (33). Thus, liver regeneration may be compromised in patients with CLD, and the restoration of homeostatic conditions is essential to prevent aberrant liver regeneration.

2. MACROPHAGES

Macrophages are a type of white blood cell from the innate immune system with essential functions in the body: 1) they act as professional phagocytes, highly specialized in the clearance of dying or dead cells and cellular debris (38), 2) they participate in the innate immune system through the phagocytosis of foreign substances and microbes, and the secretion of pro-inflammatory cytokines that induce inflammation and recruitment of other immune cells to the site of infection (39), and 3) they act as antigen-presenting cells for the adaptative immune system and help to initiate specific defense mechanisms (40). Apart from stimulating inflammation, macrophages can also play an anti-inflammatory role by releasing cytokines that reduce or modulate immune responses (41). Macrophages are very heterogenous and plastic cells found in almost all

tissues in the body and are part of the mononuclear phagocyte system (41). Depending on the location throughout the body, they have different nomenclatures; for example, KCs in the liver, alveolar macrophages in the lungs, osteoclasts in the bones, and microglia in the brain (41). Macrophages found in adult healthy tissues are derived either from circulating monocytes or have embryonic origin. By contrast, circulating monocytes are the major source of macrophages in disease or injury conditions (38,41).

2.1. Macrophages as key players in the liver

The liver is a central immunological organ in the body (6). Diverse types of immune cells are distributed throughout the liver parenchyma but enriched in periportal regions and play significant roles both in homeostasis and disease conditions, such as CLD (6) **(Table 1)**. The liver immune system is influenced by both intrahepatic and extrahepatic signals. Hepatic signals associated with hepatocyte homeostasis and endothelial cell signaling have an important impact on liver immunology (6). Moreover, the liver is in a strategic gatekeeper position to detect antigens and microbial substances, either from the intestines (via gut-liver axis) or arterial blood flow and eliminate them by phagocytes. Indeed, the liver harbors the largest number of phagocytes in any solid organ in the body (42). Under physiological conditions, most of the liver immune cells are tissue-resident KCs, comprising the largest population of resident macrophages in the body (around the 80–90% of total resident macrophages) and approximately the 35% of the liver non-parenchymal cells (43). KCs serve as intravascular sentinels that detect hepatocyte stress and damage signals from other cells (or from extrahepatic origins), phagocyte cellular debris, and activate inflammatory signals (6). Upon liver injury, the pool of hepatic macrophages expands significantly by the

infiltration of bone narrow-derived monocytes that give rise to MDMs (6,42). MDMs are functionally and phenotypically distinct to KCs and play essential roles in all stages of CLD, orchestrating pivotal functions in promoting inflammation and fibrogenesis, but also triggering anti-inflammatory responses and promoting ECM remodeling (6,42).

Table 1: Classification and characteristics of the main liver immune cells in homeostasis and hepatic inflammation and fibrosis. *Information obtained and summarized from Hammerick et al. Nat Rev Gastroenterol Hepatol (2023) (6).*

Hepatic immune cells	Homeostasis	Inflammation and fibrosis
Macrophages		
- **KCs**	Intravascular sentinels.	Initiation of fibrogenesis: recruitment of monocytes and secretion of inflammatory signals.
- **MDMs**	Negligible.	Expanded in fibrotic livers. Fundamental role in inflammation and the progression of liver fibrosis, but also in the resolution (secretion of proteolytic enzymes and induction of anti-inflammatory response).
Dendritic cells	APCs.	Expanded in fibrotic livers. Complex and controversial role in fibrogenesis.
Neutrophils	Negligible. Routinely patrol liver sinusoids.	Contribution to hepatic inflammation but seems not to contribute to fibrogenesis directly. Critical during the resolution.
B and T lymphocytes	Adaptive immune system.	Infiltration of parenchyma during inflammation and major role in antigen-driven liver diseases (viral infections). B cells: mainly pro-fibrotic role. T cells: both pro-fibrotic and pro-resolutive.
Natural killer cells	Substantial proportion of intrahepatic innate lymphocytes.	Associated with protective functions during fibrogenesis.

Abbreviations: KCs, Kupffer cells; MDMs, monocyte-derived macrophages, APCs, antigen-presenting cells.

MDMs are recruited to the liver after sensing cytokines released from KCs (6). CCL2 is one of the best-known cytokines released from

KCs that binds to monocyte CCR2 and regulates macrophage recruitment during inflammation (44). Recruited MDMs perform a major role in promoting pro-inflammatory immune response by the secretion of pro-inflammatory cytokines such as interleukin 1 beta (IL-1β) and TNF-α (6,45). Indeed, TNF-α is one of the most prominent cytokines driving inflammation in the context of CLD (46,47). Pro-inflammatory macrophages express genes related with inflammatory mediators, including nitric oxide synthase 2 (NOS2) and cyclooxygenase 2 (COX2) (48,49) and are characterized by being positive for the Ly-6C surface marker (50). These inflammatory mediators and cytokines perpetuate the inflammatory landscape. Moreover, pro-inflammatory MDMs facilitate Th1 adaptative immune response triggering the production and secretion of interferon gamma (IFN-γ), IL-2, and TNF-α (51). MDM-derived inflammatory response is initially a mechanism to fight against the insult of liver injury, including pathogens or toxic substances (52). When liver injury is prolonged, MDMs play a major role in the progression of the disease through the perpetuation of HSC activity and subsequent ECM deposition by the secretion of pro-fibrogenic factors, such as OSM, PDGF-BB y TGF-β (6).

Anti-inflammatory macrophages may influence the response of HSCs, endothelial cells, and other immune cells to liver injury, potentially altering the course of liver inflammation and fibrosis (53,54). Anti-inflammatory macrophages are characterized by efficient phagocytic activity and high expression of scavenger receptors, resistin-like alpha (RETNLA), arginase-1 (ARG1) and mannose receptor (MRC) (55,56). Anti-inflammatory macrophages release cytokines such as IL-4 and IL-10 that can eventually promote the transformation of infiltrated MDMs in fibrotic tracts towards an anti-inflammatory phenotype (45,56). This fact

is essential to boost the resolution of liver inflammation and fibrosis. Moreover, anti-inflammatory MDMs also secrete ECM remodeling MMPs, such as gelatinase MMP-2 and MMP-9, that participate in the degradation of the most abundant types of collagen in liver fibrosis (collagen type I, III and V) (6,42,57,58). The role of MDMs in the initiation, progression and resolution of liver inflammation and fibrosis in the context of CLD is summarized in **Figure 5**.

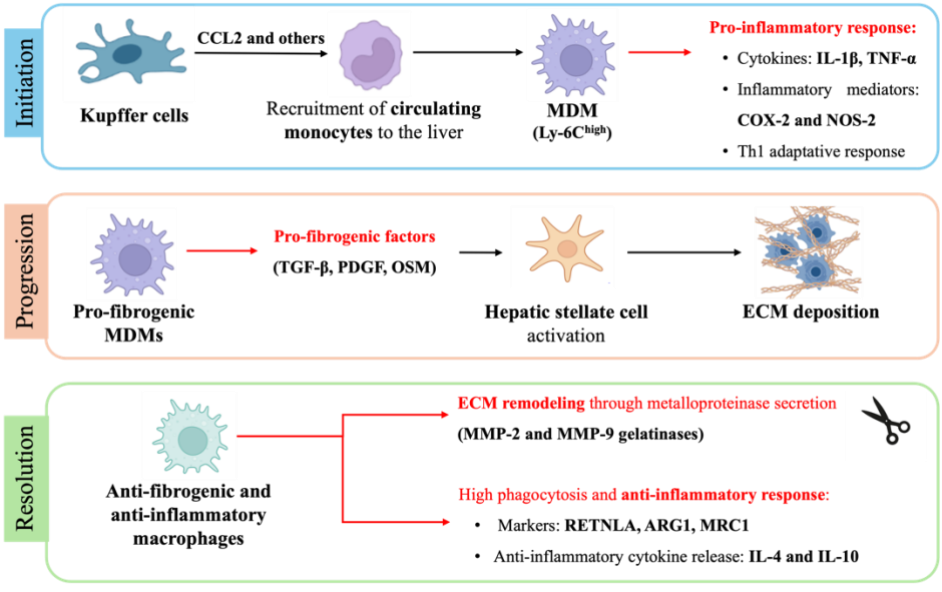

Figure 5: Role of monocyte-derived macrophages in the initiation, progression and resolution of liver inflammation and fibrosis. Upon liver injury, newly recruited MDMs promote pro-inflammatory immune response. During the progression of liver disease, MDMs support fibrogenesis through the secretion of pro-fibrogenic factors that activate hepatic stellate cells. Macrophages also have essential roles in the resolution of liver inflammation and fibrosis, promoting an anti-inflammatory response and secreting ECM remodeling metalloproteinases. Abbreviations: MDM, monocyte-derived macrophages; IL-1β, interleukin 1 beta; TNF-α, tumor necrosis factor alpha; OSM, oncostatin M; PDGF, platelet-derived growth factor; TGF-β, transforming growth factor beta; ECM, extracellular matrix; MMP-2, metalloproteinase 2; MMP-9, metalloproteinase 9; RETNLA, resistin-like 1 alpha, ARG, arginase-1; MRC, mannose receptor. *Original image created with Biorender.*

Anti-inflammatory macrophages have also been recognized as one of the most significant contributors to liver regeneration (59).

Macrophages with pro-resolutive and anti-inflammatory phenotype secrete major trophic factors that may directly drive the proliferation of hepatocytes or other cell linages in fibrotic and/or hepatectomized livers (59,60). Some of these pro-regenerative factors include HGF, insulin-like growth factor 1 (IGF-1) and vascular endothelial growth factor (VEGF). HGF is known to be the main hepatocyte proliferative factor (61), IGF-1 is also related to hepatocyte proliferation and HSC inactivation (62,63), and VEGF has been linked to the proliferation of certain pro-resolutive macrophage populations in fibrotic livers, named as scar-associated macrophages (64,65). Thus, macrophages from monocyte origin display essential functions during fibrogenesis and regeneration. In special, monocyte-endothelial cell interactions play a major role in the recruitment of circulating monocytes to the liver (36,37). Monocytes interact with endothelial cells under physiological or pathophysiological conditions to coordinate inflammation, tissue remodeling, and regeneration (66). Monocyte trafficking and the interaction with endothelial cells is orchestrated and controlled by chemoattractant and adhesion molecules, named as integrins (37). CD11b, also known as macrophage-1 antigen, is a highly expressed integrin in macrophages and modulates the inflammatory signaling in different myeloid cell types (22,67). CD11b plays a fundamental role in the recruitment of monocytes to inflamed livers (37). Monocyte CD11b interacts with intracellular adhesion molecule 1 (ICAM-1) in endothelial cells, allowing vascular transmigration (68,69) **(Figure 6A)**. Interestingly, the suppression of CD11b gene reduces survival in mice following partial hepatectomy and reduces the infiltration of circulating monocytes into the hepatic vascular network, hampering vascular and liver mass regeneration (36) **(Figure 6B)**.

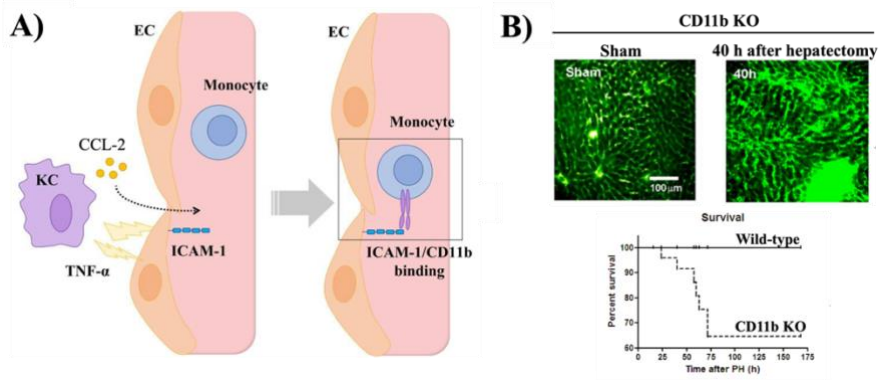

Figure 6: Monocyte-endothelial cell interaction. A) Cd11b in monocytes interacts with endothelial cells for their recruitment to the liver. **B)** Angiography images obtained with multiphoton microscopy of the liver of hepatectomized mice lacking cd11b and survival curves. Mice lacking cd11b display impaired liver regeneration and a decrease in survival after partial hepatectomy. Abbreviations: KC, Kupffer cells; EC, endothelial cells; TNF-α, tumor necrosis factor alpha; ICAM-1, intercellular adhesion molecule 1; KO, knock out; PH, partial hepatectomy. *Images obtained and adapted from A) Medrano-Bosch et al. Front. Immunol (2023) (37), and B) Melgar-Lesmes et al. J Hepatol (2015) (36).*

In summary, macrophages are essential cellular regulators during all stages of CLD, including the initiation and progression of liver inflammation and fibrosis, and also in the resolution of inflammation and fibrosis and in the promotion of liver regeneration. Indeed, macrophage activation has been linked to variceal bleeding and clinical decompensation in patients with CLD and has been proposed as a prognostic parameter for survival in cirrhotic patients (70–72). These facts highlights the relevance of macrophages in clinical settings. In fact, macrophages have emerged as master targets for novel therapeutic strategies for the treatment of CLD (11). Specifically, macrophage polarization towards an anti-inflammatory and pro-resolutive phenotype arises as a promising approach for the management of liver inflammation, fibrosis, and regeneration.

2.2. Macrophage polarization

Macrophage polarization refers to the process by which macrophages undergo distinct functional phenotypes in response to specific microenvironmental signals and stimuli (73). Historically, tissue macrophages have been divided into two main categories based on their biomarkers, activation signals, and cytokine production: classically activated macrophages with pro-inflammatory phenotype and alternatively activated macrophages with tissue remodeling and anti-inflammatory phenotype (42); however, macrophages are extremely plastic cells with the ability to transition between these polarization states. Macrophage polarization is mainly governed by the activation of certain transcription factors that will lead to different signaling pathways and the transcription of genes related with pro-inflammatory or anti-inflammatory phenotype (73). In addition, other molecular players such as immunomodulatory ubiquitin ligases have emerged as essential factors for the regulation of macrophage polarization (74).

2.2.1. Inflammation-related signaling pathways

Macrophage pro-inflammatory polarization can be driven by diverse cytokines including interleukins, lipopolysaccharide (LPS), IFN-γ, and TNF-α (73). These cytokines activate receptors in macrophage cell surface to activate inflammation-related signaling pathways. These receptors include Toll-like receptor 2 and 4 (TLR-2 and TLR-4), TNF receptors (TNFR1 and TNFR2) and type 1 cytokine receptors, also known as hematopoietin receptors (73,75,76). The most common pro-inflammatory signaling pathways are nuclear factor kappa-B (NF-κB), mitogen-activated protein kinase (MAPK), and Janus kinase (JAK)-signal transducer and activator of transcription (STAT) (76–78). All three signaling pathways lead to the gene expression and release of pro-

inflammatory cytokines and mediators, such as IL-1β, IL-6, TNF-α, IFN-γ, NOS2, and COX2. These cytokines and inflammatory mediators mediate positive feedback on unpolarized macrophages to perpetuate inflammation (73).

NF-κB is a highly ubiquitous family of transcription factors involved in cell survival, proliferation, and differentiation, but their main role is to regulate inflammation and autoimmune responses (79). In basal conditions, the inhibitor of NF-κB (IκB) retains NF-κB in the cytoplasm. Following the inflammatory stimuli, the IκB kinase (IKK) phosphorylates and inhibits IκB (canonical pathway) or phosphorylates and activates the NF-κB inducing kinase (NIK) (non-canonical pathway). Functionally, canonical NF-κB is involved in almost all aspects of the immune response, whereas the non-canonical NF-κB pathway seems to be involved in the supplementary signaling axis that cooperates with the canonical pathway in the regulation of the adaptive immune system. Both, IκB inhibition or NIK activation, trigger NF-κB nuclear translocation and expression of pro-inflammatory genes (79).

MAPKs are an extensive family of serine/threonine kinases involved in critical cellular functions such as cell cycle progression, cell adherence, cell metabolism, or inflammatory cytokine expression (80). MAPK signaling pathway consists of, at least, three components: a MAPK, a MAPK kinase (MAPKK), and a MAPKK kinase (MAPKKK). In subsequential phosphorylation, MAPKKK activates MAPKK, which in turn activates MAPK, and this phosphorylates and activates a MAPK-activated protein kinase (MAPKAPK) (80). MAPKAPKs are responsible for transmitting the signal by phosphorylating other substrates at different

molecular levels, such as extracellular signal-regulated kinases (ERKs), to mediate signal transduction during cellular stress or inflammation (81).

JAK/STAT is a phylogenetically highly conserved signaling pathway (78). The activation of JAK-associate receptors triggers a conformational change that brings the associated JAKs closer. This fact allows them to phosphorylate each other at the intracellular region of the receptor (82). This phosphorylation creates docking sites for the cytoplasmic latent STATs, which undergo further phosphorylation by the JAKs. STAT phosphorylation leads to their dimerization, and the subsequent DNA binding after nuclear translocation to regulate gene expression (82). Different combinations of JAKs and STATs (depending on the stimulus) lead to different response patterns (82). Therefore, the JAK/STAT signaling pathway provides direct and specific responses to a wide range of extracellular factors.

Macrophage anti-inflammatory polarization occurs in response to downstream signals of cytokines such as IL-4, IL-13, IL-10, and TGF-β (73). These signals are recognized by macrophages through their associated receptors (83), both to directly induce anti-inflammatory macrophage activation or to amplify anti-inflammatory response by stimulating Th2-derived cytokine production (84). The expression and subsequent up-regulation of cytokines and chemokines, such as IL-10, TGF-β, CCL1, CCL17, CCL18, CCL22, and CCL24 also modulate unpolarized macrophages towards an anti-inflammatory phenotype (85). Anti-inflammatory macrophages can be identified by the expression of the following surface markers: CD206 (also known as MRC), CD163, CD209, Fizz-1 (also known as RETNLA) and, Ym1/2 (73). Key signaling pathways involved in macrophage anti-inflammatory polarization and the expression of anti-inflammatory genes are cyclic adenosine

monophosphate (cAMP) response element-binding C (CREB-C) / CCAAT enhancer-binding protein beta (C/EBPβ) (86) and peroxisome proliferator-activated receptor gamma (PPARγ) (87).

C/EBPβ belongs to the basic leucine zipper (bZIP) family of transcription factors (86,88). During macrophage activation, C/EBPβ expression is transcriptionally induced by CREB-C transcription factor, which also belongs to bZIP family (89). CREB-mediated C/EBPβ upregulation has been described as a mechanism by which activated macrophages can coordinate anti-inflammatory gene induction programs. Indeed, CREB-C/EBPβ cascade is involved in macrophage anti-inflammatory polarization and muscle injury repair (86). Interestingly, the levels of active C/EBP are critical to determine which transcriptional programs are activated (pro-inflammatory or anti-inflammatory) (86). Moreover, C/EBPβ is known to activate the expression of C/EBPα and PPARγ, which are two genes associated with anti-inflammatory effects (89,90).

2.2.1.1. PPARγ

PPARγ is a ligand-activated type II nuclear receptor that acts as a transcription factor regulating the expression of a variety of genes (91). PPARγ has pleiotropic cellular effects, including adipocyte differentiation, lipid and glucose metabolism, cell cycle control, and inflammation (87). PPARγ has traditionally been associated with an anti-inflammatory phenotype in macrophages (87). Upon ligand activation, PPARγ heterodimerizes with the retinoid X receptor (RXR). The PPARγ–RXR complex translocates to the cell nucleus and recruits diverse co-activators or co-repressors to regulate gene expression (**Figure 7**). The complex binds to DNA binding sequences to regulate the expression of

target genes mainly related to inflammation and lipid and glucose metabolism (92). Some of the target genes for PPARγ are IL-10 and CD36 (93–95). IL-10 is a potent driver of macrophage anti-inflammatory response. CD36 is a class B scavenger receptor expressed on the surface of several cell types, including macrophages, that binds and phagocytoses oxidized lipids and apoptotic cells.

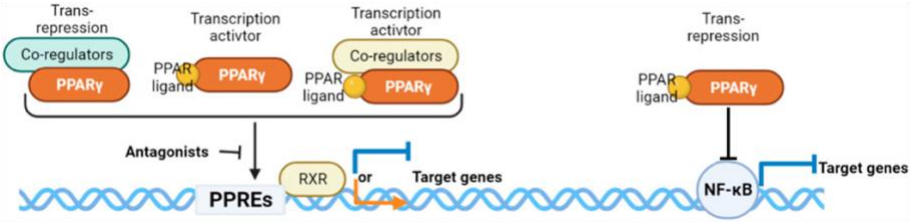

Figure 7: Molecular mechanisms of PPARγ. Upon activation, PPARγ–RXR complex translocates to the nucleus, recruits co-activators or co-repressors, and regulates the expression of target genes by its union to the DNA. PPARγ also interacts with NF-κB to determine macrophage polarization. Abbreviations: PPARγ, peroxisome proliferator activated receptor gamma; PPAR, peroxisome proliferator activated receptor; PPRE, peroxisome proliferator responsive element; RXR, retinoid X receptor; NF-κB, nuclear factor kappa-B. *Image adapted from Yu et al. Front. Pharmacol. (2023)* (96).

PPARγ interacts with other macrophage polarization-related signaling pathways, such as NF-κB and JAK2/STAT1, to tightly regulate the gene expression programs that govern and determine macrophage phenotype. For example, it is known that activation of PPARγ inhibits NF-κB-dependent pro-inflammatory signals in macrophages (96,97) (**Figure 7**). Moreover, PPARγ also phosphorylates and inactivates MAPK (97). In the absence of PPARγ activity, macrophages increase the secretion of pro-inflammatory cytokines and reduce the gene expression of anti-inflammatory mediators (87,98). Thus, PPARγ is a key nuclear receptor to induce a phenotypic change from pro-inflammatory to anti-inflammatory phenotype in macrophages (99).

PPARγ can bind to a large variety of natural and synthetic ligands. Natural ligands of PPARγ mainly include unsaturated fatty acids and their metabolites (100). Synthetic ligands for PPARγ are divided into thiazolidinediones (TZD) and non-TZD, and they differ on their chemical configuration. TZD basic structure is composed of a 2,4-thiazolidinedione moiety, whereas non-TZD present a large variety of chemical structures (100). Both TZDs (troglitazone, rosiglitazone, ciglitazone, and pioglitazone) and non-TZDs are insulin-sensitizing, potent anti-diabetic drugs with anti-inflammatory effects (96,101–104).

Diverse PPARγ agonists have been proposed to induce an anti-inflammatory phenotype in macrophages (105). Namely, GW1929 (N-(2-benzoylphenyl)-O-[2-(methyl-2-pyridinylamino)ethyl]-l-tyrosine) is a potent tyrosine-based non-TZD PPARγ agonist (106), with a well-established efficacy for macrophage anti-inflammatory polarization. GW1929 has shown to promote an anti-inflammatory phenotype in human monocytes via PPARγ selective activation, illustrated by an increase in MRC expression (99). Moreover, PPARγ activation with GW1929 has also been described to inhibit the expression of NOS2 (107) and the production of TNF-α and IL-6 in LPS-activated macrophages (108). The efficacy of GW1929 has also been tested in animal models. Kaundal et al. demonstrated the neuroprotective effect of GW1929 in a gerbil model of cerebral ischemia-reperfusion, and the beneficial effects were attributed to a reduction in inflammation (109). However, the use of many PPAR agonists is greatly restricted in conventional therapy due to their wide and severe side effects, which include obesity, cardiovascular risk, loss of bone mineral density, edema, hepatotoxicity, and fluid retention (101,110–112). Macrophage-selective drug delivery with novel

engineered nanoscale therapies could overcome the translational barriers associated with adverse side effects regarding the use of PPARγ agonists.

2.2.2. Ubiquitin ligases

Ubiquitination is the process by which ubiquitin (Ub), a small and highly conserved cytoplasmic protein of 76 amino acids, in transferred to target proteins to regulate various cellular processes, including macrophage polarization (113–115). Post-translational ubiquitin modifications are involved in almost all biological activities in eukaryotes (116). Ubiquitination involves a three-enzyme cascade (117) **(Figure 8)**. Ub is activated for transfer by the E1 Ub-activating enzyme. E1 enzyme uses ATP to activate Ub for its conjugation and transfer to E2 Ub-conjugating enzyme. The E2-Ub next interacts with an E3 Ub ligase, which finally transfers Ub from E2-Ub to the target substrate. Monoubiquitinated substrates either dissociate from E3 or acquire additional Ub modifications to form an Ub chain. Monoubiquitination mainly alters the function of a target protein, whereas polyubiquitin chains are signals for the proteasomal degradation of proteins (117). The biological outcome of ubiquitination (both degradation or signaling) is normally dictated by ubiquitin receptors (UbR) that bind and interpret the ubiquitin signal.

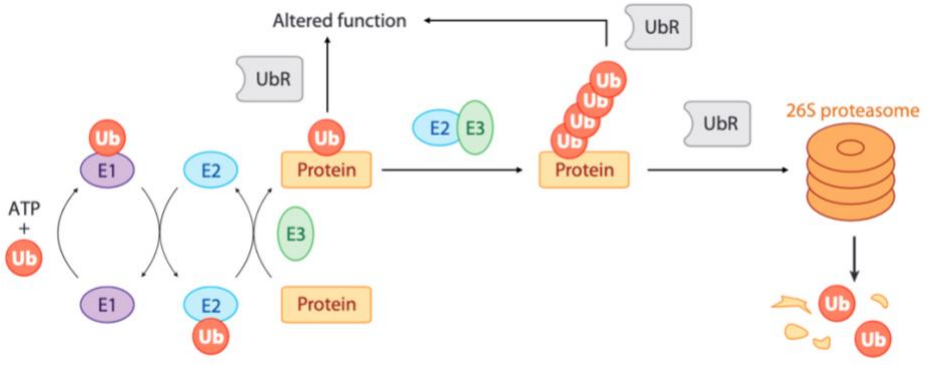

Figure 8: The ubiquitin system. The ubiquitination process involves a three-enzyme cascade, including the action of E1 Ub-activation enzyme, E2 Ub-conjugating enzyme

and E3 Ub ligases. The biological outcome of ubiquitination can be divided in protein degradation or molecular signaling with a variety of cellular responses. Abbreviations: Ub, ubiquitin; UbR, ubiquitin receptor. *Image obtained and adapted from Deshaies et al. Annu. Rev. Biochem. (2009)* (117).

E3 Ub ligases, which are usually a multi-protein complex, are responsible for targeting ubiquitination to specific substrate proteins (117). The human genome encodes over 600 E3 ligases with great diversity in specific substrates. The E3s have been historically grouped in two classes depending on their catalytic domain: really interesting new gene (RING)–type E3s and the (homologous to the E6AP carboxyl terminus (HECT)–type E3s. The HECT-type ubiquitination involves an obligate thioester intermediate, with a non-direct Ub transfer from E2 to the substrate (118). However, the vast majority of E3 ligases are RING-type ligases, which are characterized by containing a RING or U-box fold catalytic domain that promotes direct Ub transfer from an E2 to a substrate (116). The RING finger (RNF) family of proteins belong to RING-type E3 Ub ligases and are classified into five subfamilies that share a common N-terminal RING domain among other various unique domains (119). The function of non-RING domains remains unclear in most E3 ligases (117,119). The RNF family is the largest E3 Ub ligase family with 340 validated human members (119). E3 Ub ligases in macrophages can promote both anti-inflammatory and pro-inflammatory polarization (113–115). Moreover, some E3 Ub ligases has also been identified as regulators of fibrogenic processes in macrophages (120).

2.2.2.1. RNF41

RNF41, also known as neuregulin receptor degradation protein 1 (NRDP1) or fetal liver ring finger (FLRF), belongs to RING-type E3 Ub ligases and has been identified as an immunoregulatory E3 Ub ligase in macrophages, since it is involved in various inflammation-related cellular

processes. RNF41 is involved in the degradation of pro-inflammatory cytokine receptors (121). These receptors lead to the activation of JAK/STAT signaling pathway (122). Wauman et al. demonstrated that RNF41 interacts with JAK2-associated type 1 pro-inflammatory cytokine receptors and promotes their proteolytic cleavage resulting in degradation and inactivation (121). The inhibition of JAK2/STAT3 signaling in macrophages has been associated to a reduction in inflammation (123). RNF41 also inhibits the production of pro-inflammatory cytokines (124). Wang et al. demonstrated that RNF41 suppresses the signaling of various TLRs in macrophages via the polyubiquitination and degradation of Myd88, which is a TLR adaptor, and the activation of TANK-binding kinase 1 (TBK1) (124). The absence of MyD88-dependent pathway upon TLR activation ultimately leads to NF-κB inhibition and a subsequent reduction in the expression of pro-inflammatory mediators (124). In the same study, the activation of RNF41 was also associated to the inactivation of pro-inflammatory MAPK signaling and an increased production of anti-inflammatory IFN-γ. Indeed, the activation of RNF41 conferred resistance to LPS-induced sepsis in mice (124). RNF41 has also been involved in macrophage anti-inflammatory polarization. Wu et al. demonstrated that RNF41 can ubiquitinate and activate C/EBPβ. This C/EBPβ activation promoted an increase in the expression levels of anti-inflammatory ARG1 (125). Moreover, the activation of CREB-C/EBPβ cascade has shown to induce macrophage anti-inflammatory polarization and muscle injury repair (86), which suggests that RNF41 may also be involved in the regulation of regenerative processes.

3. NANOPARTICLES

Nanoparticles (NPs) are nanomaterials with three external nanoscale dimensions and typically range from 1 to 1000 nm (126). Over

the past years, the interest in the use of NPs for medical applications has been constantly increasing (127). Indeed, the Food and Drug Administration approval for the use of lipid NP-based carriers for mRNA vaccines against COVID-19 has powered even greater interest in nanotechnology (128). NPs are widely used in medicine and biomedicine due to their unique physicochemical properties including their size range, their large ratio between the surface area and the volume, hydrophilic properties, and charge characteristics (126). NPs are used as carriers for imaging contrast agents, antigens, nucleic acids, and therapeutic drugs for the diagnosis or therapy of a multitude of diseases at the cellular and molecular level (126). NPs used for biomedical applications must be non-toxic, biocompatible, water dispensable, non-immunogenic and stable in physiological media, and can be classified as follows: organic NPs, carbon-based NPs, and inorganic NPs (129). Organic NPs are built using proteins, carbohydrates, lipids, polymers, dendrimers, and DNA complexes, among others (129). Carbon-based NPs are exclusively formed by carbon atoms (129). Inorganic NPs comprise NPs that are not formed by organic materials or carbon (129). Examples of inorganic NPs are pure metals (especially NPs based on gold or silver), metal oxides (such as solid or mesoporous silica or iron NPs), semiconductor materials (such as quantum dots), and calcium phosphate NPs (130).

One of the most exploited applications in nanomedicine is the use of NPs as drug and nucleic acid delivery systems (131,132). NPs have various unique properties that make them ideal delivery systems (126): 1) Most NPs are synthesized from biocompatible materials with low toxicity and can efficiently encapsulate drugs or nucleic acids; 2) NPs may cross physiological barriers and remain stable in the bloodstream (133); 3) NP optimal size, shape, and surface can be tuned to improve their biodistribution, solubility, degradation, immune system evasion, and to

increase circulation time. This fact also permits NPs to prolong drug presence at the target tissue, allowing a reduction in the dosage (133,134); and 4) NPs can be modified by the addition of surface ligands to achieve specific tissue or cell targeting.

3.1. Nanoparticles in liver diseases

The liver shows a unique ability to capture NPs, avoiding accumulation in other organs, and facilitating the therapeutic landscape of the use of drug and gene delivery systems for the treatment of liver diseases (135). Indeed, it is estimated that 30-99% of intravenously administered NPs accumulate in the liver following their administration into the bloodstream (136). The liver also acts as the main detector organ for most intravenously administered NPs. NPs lower than 6 nm may be directly eliminated through the kidney, whereas NPs over 6 nm tend to be retained by the liver and the spleen, and excreted through the hepatobiliary systems (136). Moreover, the fact that the blood flow in the hepatic sinusoid is lower than in systemic circulation also favors NP hepatic retention (137). Despite the majority of cells in the liver are parenchymal hepatocytes, most NPs are typically sequestered by non-parenchymal cells residing in the surroundings of the hepatic sinusoids and the space of Disse (135,136).

The use of NPs as novel drug and gene therapy delivery systems has been proposed to treat liver inflammation and fibrosis, and to boost liver regeneration (26,27,138). However, most *in vivo* studies are focused on the accumulation of NPs at the organ level, and do not consider how the unique architecture and position of cells within the liver affects their interaction (135,136). Thus, specific and selective cell-targeted NPs are essential to efficiently treat pathological processes governing liver

diseases at the cellular and molecular level. Indeed, recent studies have proposed the use of selective agents included in NPs to treat specific cell lineages in the liver, such as HSC (139–141), LSEC (142,143) and macrophages (144). Interestingly, macrophages display unique ability to capture and process NPs mainly because they are the major exponent of the mononuclear phagocyte system, which is responsible for the rapid detection and blood and tissue clearance of NPs (126). Thus, macrophages have emerged as one of the main cellular targets for the design of cell-directed NPs.

NPs can selectively target liver macrophage subsets, potentially altering their polarization and subsequent interactions with other parenchymal and non-parenchymal cells in the liver. Moreover, pro-inflammatory macrophages exhibit higher NP capture ability, as they are more reactive in detecting foreign substances (26,145). Since pro-inflammatory macrophages are key players in the initiation and progression of liver inflammation and fibrosis, novel engineered NPs designed to deliver small therapeutic molecules or gene therapy to promote macrophage polarization arise as a promising nanotherapeutic strategy for the treatment of liver diseases. Diverse types of NPs have been proposed to selectively alter the polarization state of liver macrophages, including organic lipid-based NPs (144,146), polymeric NPs (147), biomimetic NPs (148), and carbon-based NPs (26).

3.2. Carbon-based nanoparticles

Carbon-based NPs are particularly non-toxic by injection, ingestion, or skin-absorption in quantities that might be used for imaging, research, or delivery purposes (149,150). Moreover, carbon is one of the most abundant elements in the known universe (151). Due to their unique and

excellent physicochemical properties, carbon-based NPs have attracted significant interest in diverse areas, including medicine (149). Indeed, carbon-based NPs have been traditionally used as a specific stain for macrophages avoiding their incorporation in dendritic cells (152). Carbon-based nanomaterials include fullerenes, carbon black NPs, and graphene and its derivatives, such as graphene nanotubes, graphene nanohorns and graphite NPs (153).

Graphene is an allotrope of carbon constituted of a single layer of carbon atoms arranged in a hexagonal nanostructure (154) **(Figure 9)**, and is part of the basic structure of the NPs used in this thesis: graphene nanostars (GNS) and graphite NPs (GNP). GNSs are formed of clusters of graphene-based single-walled carbon nanohorns (SWCNH), which are nanostructures with a diameter of 2-5 nm and a length of 40-50 nm. SWCNH aggregate to form spherical nanostars of about 100 nm in diameter (155) **(Figure 9)**. GNP are composed of many layers of graphene shits stacked together through van der Waals and π–π interactions, forming a spherical structure (156,157) **(Figure 9)**. Both GNS and GNP have been previously used for biomedical applications (155,156).

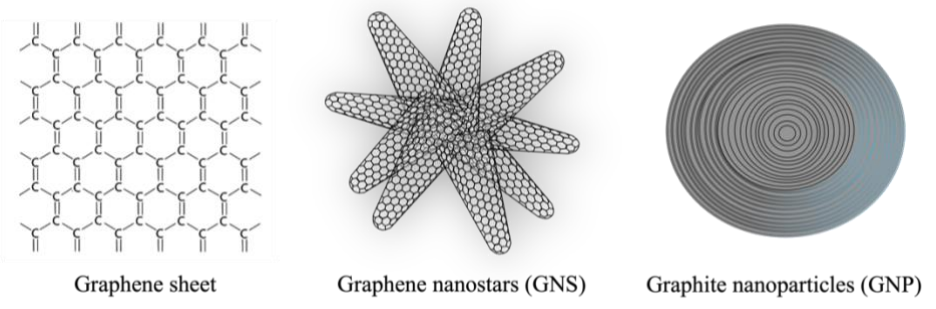

Figure 9: Schematic representation of graphene, graphene nanostar, and graphite nanoparticle structure. Graphene sheets are solely formed by carbon atoms forming a hexagonal nanoconstruct. Graphene nanostars are clusters of graphene nanohorns and graphite nanoparticles are formed to many layers of graphene sheets forming a spherical nanostructure. Abbreviations: GNS, graphene nanostars; GNP, graphite nanoparticles. *Original image.*

GNS and GNP are relatively easy to functionalize. Surface functionalization of oxidized GNS and GNP with polyamidoamine (PAMAM) dendrimers permits the incorporation of nucleic acids (26,145) or small molecule therapeutics to the final nanoconstruct **(Figure 10)**. PAMAM dendrimers are hyperbranched and ordered polymers with high molecular uniformity, narrow molecular weight distribution, and a multifunctional terminal surface (158). PAMAMs consist of an ethylenediamine core, a repetitive amidoamine branching internal structure and a primary amine terminal surface (158). PAMAM dendrimers are synthetized in an iterative manufacturing process from the central core and each amidoamine branch represents a new generation of dendrimer. For example, a generation 5 dendrimer (G5 PAMAM) consists of 5 amidoamine branches (158). Oxidized GNS or GNP can be covalently linked to PAMAM dendrimers to obtain dendrimer-graphene nanostars (DGNS) or dendrimer-graphite nanoparticles (DGNP), respectively (**Figure 10**). DGNSs and DGNPs can then be functionalized via electrostatic interactions with negatively charged plasmid DNAs (pDNA) or covalently linked to small therapeutic molecules (**Figure 10**).

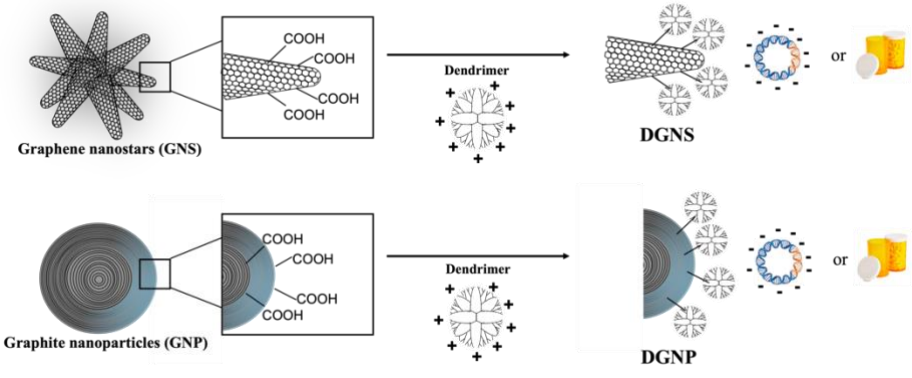

Figure 10: Functionalization of oxidized graphene nanostars (GNS) and graphene nanoparticles (GNP) with PAMAM dendrimers. Oxidized GNS and GNP can be covalently linked to positively charged dendrimers to form DGNS and DGNP, respectively. DGNS or DGNP can then be linked to pDNA or small therapeutic molecules. Abbreviations: DGNS, dendrimer-graphene nanostars; DGNP, dendrimer-graphite nanoparticles. *Original image.*

The binding of GNS or GNP to PAMAM dendrimers combine both macrophage selective targeting and nucleic acid or drug delivery for the therapeutic polarization of macrophages. Indeed, in a previous study from our lab, DGNS functionalized with G5 PAMAM dendrimers were used to selectively deliver a MMP9-expressing pDNA in the liver macrophages of fibrotic mice (26) **(Figure 11)**. The expression of the pDNA was controlled under a CD11b promoter, to ensure that only CD11b^{high} pro-inflammatory macrophages would express this protein. DGNS efficiently delivered MMP9-expressing pDNA into liver macrophages, inducing the synthesis and secretion of MMP-9 to digest adjacent collagen fibers. The therapy also promoted macrophage switch from pro-inflammatory to pro-regenerative phenotype (26) **(Figure 11)**.

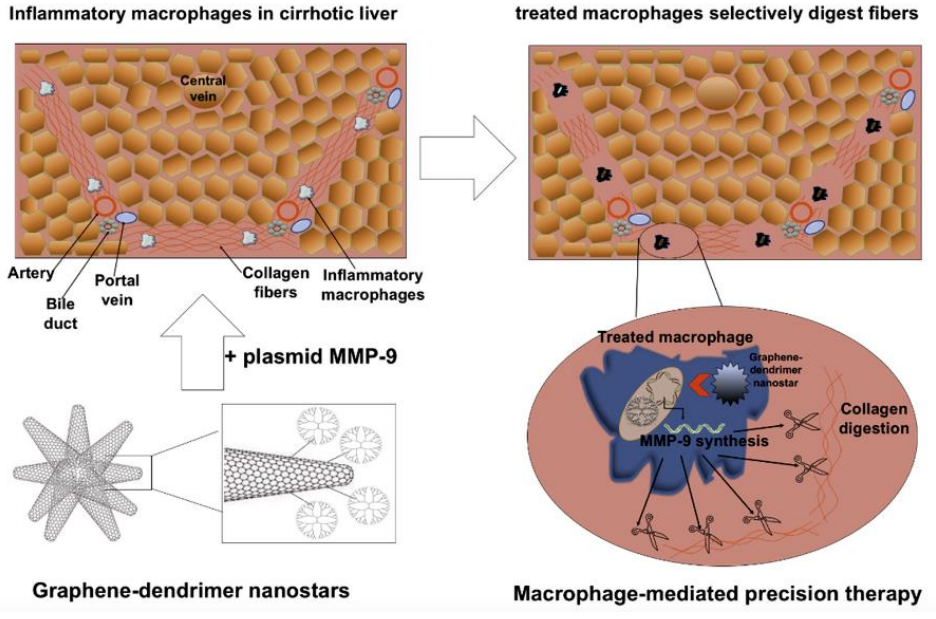

Figure 11: Schematic representation of the therapeutic effects of a pDNA expressing MMP9 selectively delivered with dendrimer-graphene nanostars to liver macrophages in fibrotic mice. Abbreviations: MMP9, metalloproteinase-9. *Image obtained from Melgar-Lesmes et al. Nano Lett. (2018) (26).*

HYPOTHESIS

The incidence of CLD is increasing worldwide and the development of novel therapeutic strategies is a major medical need. Sustained inflammation and fibrosis are key pathological features governing the progression of CLD. Liver MDMs play essential roles in all stages of CLD promoting both liver inflammation and fibrosis. Indeed, macrophage activation is a predictive parameter for survival in patients with CLD. Macrophages are also essential for the resolution of liver fibrosis, as they can promote an anti-inflammatory response, secrete enzymes for ECM remodeling and promote liver regeneration. However, sustained liver injury in CLD may perpetuate infiltration of MDMs and the release of pro-inflammatory and pro-fibrogenic signals. In this scenario, PPARγ and RNF41 are two molecules that have been associated to macrophage anti-inflammatory polarization. Therefore, macrophage-selective PPARγ and RNF41 modulation using carbon-based NPs could reprogram MDMs towards an anti-inflammatory phenotype.

Considering all this evidence, the hypothesis of this thesis was that **the selective activation of the PPARγ and RNF41 anti-inflammatory pathways in liver macrophages using macrophage-targeted carbon-based nanotools may stimulate a pro-resolutive phenotype in these immune cells resulting in a reduction of liver inflammation and fibrosis and stimulation of hepatic regeneration in CLD.**

OBJECTIVES

To test the hypothesis of the thesis, the following two main objectives and specific objectives were proposed:

The **first objective** of the thesis was to analyze the effects that a macrophage-selective activation of peroxisome proliferator-activated receptor gamma (PPARγ) promotes in the liver of fibrotic mice using dendrimer-graphene nanostars linked to the PPARγ agonist GW1929. The specific objectives were:

a) To synthetize and characterize dendrimer-graphene nanostars linked to the PPARγ agonist GW1929 (DGNS-GW).

b) To investigate DGNS-GW uptake, PPARγ activation, and macrophage polarization in tumor necrosis factor alpha-stimulated macrophages.

c) To evaluate the therapeutic potential of macrophage-selective PPARγ activation with DGNS-GW in liver inflammation, fibrosis, and regeneration.

The **second objective** of the thesis was to investigate the role of the E3 ubiquitin ligase RING finger 41 (RNF41) on hepatic macrophage regulation in chronic liver disease, and to study the effects of a macrophage-selective modulation of RNF41 on liver inflammation, fibrosis, and regeneration in mouse models of chronic liver disease using dendrimer-graphite nanoparticles. The specific objectives were:

a) To analyze the RNF41 expression in $CD11b^{high}$ monocyte-derived macrophages isolated from the liver of cirrhotic patients, fibrotic

mice, and healthy biopsies, and to evaluate the effects of sustained inflammation on macrophage RNF41 *in vitro*.

b) To synthetize and characterize dendrimer-graphite nanoparticles linked to a plasmid DNA expressing RNF41 under a CD11b promoter (pRNF41-DGNP) and to assess its efficacy as a macrophage-selective gene delivery system.

c) To evaluate the therapeutic implications of the macrophage-selective induction of RNF41 expression using pRNF41-DGNP on liver inflammation, fibrosis, and regeneration in fibrotic mice with or without hepatectomy.

d) To analyze *in vitro* the effects of the secretome from macrophages stimulated with pRNF41-DGNP on hepatic stellate cell activation and hepatocyte proliferation.

e) To explore the effects of macrophage-selective RNF41 expression blockade on inflammation, fibrosis, and survival in fibrotic mice.

MATERIAL, METHODS, AND RESULTS

Article 1:

PPAR-γ agonist GW1929 targeted to macrophages with dendrimer–graphene nanostars reduces liver fibrosis and inflammation

***Moreno-Lanceta A**, Medrano-Bosch M, Simón-Codina B, Barber-González M, Jiménez W and Melgar-Lesmes P. PPAR-γ agonist GW1929 targeted to macrophages with dendrimer–graphene nanostars reduces liver fibrosis and inflammation. Pharmaceutics. 2023;* 15*(5), 1452.*

This article corresponds to the **first objective** of the thesis. The **first objective** of the thesis was to analyze the effects that a macrophage-selective activation of peroxisome proliferator-activated receptor gamma (PPARγ) promotes in the liver of fibrotic mice using dendrimer-graphene nanostars linked to the PPARγ agonist GW1929.

pharmaceutics

MDPI

Article

PPAR-γ Agonist GW1929 Targeted to Macrophages with Dendrimer–Graphene Nanostars Reduces Liver Fibrosis and Inflammation

Alazne Moreno-Lanceta [1,2], Mireia Medrano-Bosch [1], Blanca Simón-Codina [1], Montserrat Barber-González [1], Wladimiro Jiménez [1,2] and Pedro Melgar-Lesmes [1,2,3,*]

[1] Department of Biomedicine, School of Medicine, University of Barcelona, 08036 Barcelona, Spain; amorenol@recerca.clinic.cat (A.M.-L.)
[2] Biochemistry and Molecular Genetics Service, Hospital Clínic Universitari, Instituto de Investigaciones Biomédicas August Pi i Sunyer (IDIBAPS), Centro de Investigación Biomédica en Red de Enfermedades Hepáticas y Digestivas (CIBERehd), 08036 Barcelona, Spain
[3] Institute for Medical Engineering and Science, Massachusetts Institute of Technology, Cambridge, MA 02139, USA
* Correspondence: pmelgar@ub.edu; Tel.: +34-934020294

Abstract: Macrophages play essential roles during the progression of chronic liver disease. They actively participate in the response to liver damage and in the balance between fibrogenesis and regression. The activation of the PPARγ nuclear receptor in macrophages has traditionally been associated with an anti-inflammatory phenotype. However, there are no PPARγ agonists with high selectivity for macrophages, and the use of full agonists is generally discouraged due to severe side effects. We designed dendrimer–graphene nanostars linked to a low dose of the GW1929 PPARγ agonist (DGNS-GW) for the selective activation of PPARγ in macrophages in fibrotic livers. DGNS-GW preferentially accumulated in inflammatory macrophages in vitro and attenuated macrophage pro-inflammatory phenotype. The treatment with DGNS-GW in fibrotic mice efficiently activated liver PPARγ signaling and promoted a macrophage switch from pro-inflammatory M1 to anti-inflammatory M2 phenotype. The reduction of hepatic inflammation was associated with a significant reduction in hepatic fibrosis but did not alter liver function or hepatic stellate cell activation. The therapeutic antifibrotic utility of DGNS-GW was attributed to an increased expression of hepatic metalloproteinases that allowed extracellular matrix remodeling. In conclusion, the selective activation of PPARγ in hepatic macrophages with DGNS-GW significantly reduced hepatic inflammation and stimulated extracellular matrix remodeling in experimental liver fibrosis.

Keywords: liver; inflammation; fibrosis; graphene nanostars

Citation: Moreno-Lanceta, A.; Medrano-Bosch, M.; Simón-Codina, B.; Barber-González, M.; Jiménez, W.; Melgar-Lesmes, P. PPAR-γ Agonist GW1929 Targeted to Macrophages with Dendrimer–Graphene Nanostars Reduces Liver Fibrosis and Inflammation. *Pharmaceutics* **2023**, *15*, 1452. https://doi.org/10.3390/pharmaceutics15051452

Academic Editor: Tomáš Etrych

Received: 29 March 2023
Revised: 3 May 2023
Accepted: 9 May 2023
Published: 10 May 2023

1. Introduction

Liver fibrosis is characterized by the excessive production and deposition of extracellular matrix (ECM) proteins, such as collagen, and its occurrence inevitably coexists with a sustained inflammatory response [1,2]. Advanced liver fibrosis may result in cirrhosis and ultimately in liver failure and death [1]. Cirrhosis accounts for 4% of all deaths worldwide [3], and there are no specific anti-fibrotic therapeutic options available in clinic yet [4]. The pathophysiology of liver fibrosis involves the crosstalk of several parenchymal and nonparenchymal cells, including hepatocytes, hepatic stellate cells (HSCs), Kupffer cells (KCs), and liver sinusoidal endothelial cells (LSECs). Throughout the last decade, diverse anti-fibrotic pharmacological strategies have been proposed to inhibit the proliferation and activation of HSCs, to reduce the production and the deposition of the ECM, to reduce inflammation, or to promote liver protection [5,6]. However, these therapeutic approaches have shown limited efficacy and considerable side effects. Recently, different

novel nanoscale therapeutic strategies have been suggested to treat liver fibrosis, overcoming the limitations of conventional pharmacological therapies by either protecting the liver from inflammation and oxidative stress or by targeting and treating macrophages [7,8].

Macrophages play essential roles during all stages of chronic liver disease, including fibrosis initiation, progression, and resolution [9,10]. In the initial phase, hepatocyte injury activates KCs, which secrete chemokines, such as CCL_2, to attract monocytes from the bloodstream to the liver. During fibrosis progression, monocytes recruited to the liver differentiate into macrophages and secrete an array of pro-inflammatory and pro-fibrogenic factors that activate HSCs, which produce collagen and other fibers to restrict tissue damage propagation. Macrophages also contribute to fibrosis resolution mainly through the secretion of metalloproteinases and the stimulation of an anti-inflammatory and regenerative response [10]. The role of macrophages on fibrosis resolution may be dysregulated due to iterative and prolonged inflammatory stimuli occurring in chronic liver disease [2]. This hepatic milieu stimulates an uncontrolled production of inflammatory mediators by macrophages. This results in a defective formation of anti-inflammatory macrophages and an unpaired interplay between macrophages and HSCs, hepatocytes, or LSECs that may impair physiological liver regeneration [11,12]. Macrophages with anti-inflammatory, anti-fibrogenic, and pro-resolving capabilities are essential to restore physiological liver functions and homeostasis. For this reason, macrophage polarization to an anti-inflammatory phenotype has emerged as a potential therapeutic strategy to treat chronic liver disease [13,14].

Graphene nanostars linked to polyamidoamine (PAMAM) dendrimers have demonstrated excellent efficiency to target and treat macrophages with gene therapy in liver fibrosis [7]. Graphene nanostars (GNS) are formed by clusters of graphene-based single-walled carbon nanohorns (SWCNH) [15]. SWCNHs are nanostructures with a diameter of 2–5 nm and a length of 40–50 nm. SWCNHs aggregate to form spherical nanostars of around 100 nm in diameter [7,15,16]. PAMAM dendrimers are highly ordered and hyperbranched polymeric nanostructures formed by an ethylenediamine core, a repetitive branching amidoamine internal structure, and a primary amine terminal surface, which is easily modifiable to bind either peptides, nucleic acids, or other molecules [17].

Peroxisome proliferator-activated receptor γ (PPARγ) activation in macrophages has traditionally been associated with an anti-inflammatory phenotype [18]. PPARγ is a ligand-activated transcription factor included in the superfamily of nuclear receptors [19]. It has pleiotropic cellular effects, including lipid and glucose metabolism, adipocyte differentiation, cell growth control, and inflammation [19]. PPARγ heterodimerizes with the retinoid X receptor (RXR), and the PPARγ–RXR complex translocates to the cell nucleus to recruit diverse gene expression co-activators or co-repressors. The complex binds to DNA binding sequences and regulates the expression of target genes mainly related to inflammation and lipid and glucose metabolism [20]. In the absence of PPARγ activity, macrophages secrete high levels of pro-inflammatory cytokines and reduce the gene expression of anti-inflammatory mediators [18]. PPARγ activation and interaction with other signaling pathways, such as NF-kB and JAK2/STAT1, regulates macrophage polarization [21] and induces a phenotypic change from pro-inflammatory M1 to anti-inflammatory M2 macrophages [22]. In this context, diverse PPARγ agonists have been proposed to induce an anti-inflammatory response [23]. GW1929 is a potent tyrosine-based non-thiazolidinedione PPARγ agonist [19] with a well-established efficacy for macrophage M2 polarization [22,24–26]. However, the use of most PPARγ full agonists is greatly restricted in conventional therapy due to their wide and severe side effects, which include increased cardiovascular risk, bone loss, edema, and fluid retention [27–29]. Therefore, an ideal nanoscale delivery system for GW1929 should selectively target macrophages and transport a reduced drug dose to avoid possible side effects and to overcome the limitations of conventional dosage forms. Here, we sought to selectively activate PPARγ in liver macrophages with a low dose of the GW1929 agonist linked to dendrimer–graphene

nanostars to selectively stimulate a M2 anti-inflammatory macrophage phenotype and to boost macrophage-driven liver fibrosis resolution.

2. Materials and Methods

2.1. Synthesis of Dendrimer–Graphene Nanostars Linked to GW1929 (DGNS-GW) or Mannitol (DGNS-Man)

Carbon graphene oxide nanohorns, GW1929 PPARγ agonists, and mannitol were supplied by Sigma (St. Louis, MO, USA). Generation 5 (G5) poly (amidoamine) (PAMAM) dendrimer was purchased from Dendritech Inc. (Midland, MI, USA). Oxidized GNS were dispersed in dimethyl sulfoxide (DMSO) (500 μg/mL) and separated via the incubation of the dispersion in an ultrasound bath (Selecta, Barcelona, Spain) at a frequency of 50 kHz and potency 360 W for 15 min as previously described [7]. A total of 100 μL of carbon nanohorns was mixed with 900 μL of 1 mg/mL of free access crosslinking agents 1-Ethyl-3-(3-dimethylaminopropyl)-carbodiimide (EDC)/N-Hydroxysuccinimide (NHS) 1:1 with 30 μL of PAMAM dendrimer 25% *v*/*v*. GNS, EDC/NHS, and G5 PAMAM were incubated for 2 h in the ultrasound bath to have the nanohorns separated for the reaction, with constant temperature at 25 ± 2 °C with ice. Dispersions were centrifuged at 21,000 Gs for 10 min and washed three times with DMSO. A total of 200 μL of DMSO-dispersed DGNS (50 μg/mL) were mixed with 800 μL of DMSO; 10, 2, 1, or 0.5 mg of DMSO-soluble GW1929 or mannitol; and 1 mg/mL of EDC/NHS for a second reaction with crosslinking agents in constant agitation in a magnetic stirrer at 25 °C for two hours. Dispersions were centrifuged at 21,000 Gs for 10 min and washed one time with DMSO and four times with phosphate-buffered saline (PBS) for further analysis. An adequate GW1929 concentration for maintaining a negative nanoparticle surface was established using the variations in Zeta potential from positive (DGNS) to negative (DGNS-GW or DGNS-Man).

2.2. Physicochemical Characterization of Nanoparticles

Nanoparticle hydrodynamic size properties were determined by Dynamic Light Scattering (DLS), using a Zetasizer nano ZS (Malvern Instruments Ltd., Worcestershire, UK). Size measurements were carried out at 25 °C and at fixed angle of 173° by analyzing the intensity of the scattered light supplied by a helium–neon laser (maximum output power = 4 mW, beam wavelength = 633 nm). DLS data were calculated from the autocorrelation function of scattered light by means of two mathematical methods—the method of cumulants and Dispersion Technology Software nano v. 5.10 (Malvern Instruments Ltd.). Two important parameters were obtained through the cumulants analysis: the mean of particle hydrodynamic diameter (Z-average) and the width of the particle size distribution (polydispersity index—PDI). Samples for measurements were prepared as follows: 50 μL of GNS, DGNS, DGNS-GW, and DGNS-Man suspension was dispersed in 950 μL of PBS in an ordinary cuvette. The reported values of Z-Average and PDI corresponded to the average of approximately 40 measurement runs from three different dispersions. A total of 50 μL of GNS, DGNS, DGNS-GW, and DGNS-Man dispersed in 950 μL of PBS was used to perform Zeta-potential measurements using disposable folded capillary cells (DTS1070, Malvern Instruments Ltd., Worcestershire, UK) in a Zetasizer nano ZS.

2.3. Cell Culture

Mouse RAW 264.7 macrophages (ATCC, Manassas, VA, USA) were cultured with Dulbecco's modified Eagle's medium (DMEM) supplemented with 10% fetal bovine serum (FBS) and 50 U/mL penicillin/streptomycin. Cells were grown at 37 °C and 5% CO_2 in a water-jacketed incubator. For macrophage polarization and nanoparticle uptake experiment, cells were seeded in six-well plates at a density of 2×10^4 cell/cm^2 supplemented with low FBS (1%). At 16 h after seeding, cells were treated with or without DGNS-GW or DGNS-Man (100 ng/mL) and with TNF-α (5 ng/mL, Life Technologies, Carlsbad, CA, USA) for three days with the daily renewal of culture media. After three days, cells were harvested with a 1 mL of TRIZOL reagent (Gibco-Invitrogen, Paisley, UK) for RNA isolation.

Nanoparticle uptake post-TNF-α stimulation and DGNS-GW treatment was determined using black aggregate quantification. Black aggregates of DGNS-GW were visualized at high magnification to establish the number of cells incorporating the nanostars. The percentage of cells incorporating DGNS-GW was calculated as follows: the number of cells with black aggregates/total number of cells per field × 100. At least 30 different fields were used to calculate the uptake percentage per condition.

2.4. Animal Studies

Male Balb/c mice were purchased from Charles River Laboratories (Charles River, Saint Aubin les Elseuf, France). The study was performed according to the criteria of the Investigation and Ethics Committees of the Hospital Clínic Universitari of Barcelona. Animals were maintained in a temperature-controlled room (22 °C) on a 12 h light–dark cycle. After arrival, mice were continuously fed ad libitum until euthanasia (endpoint). For liver fibrosis induction, mice were injected with intraperitoneal CCl_4 diluted 1:8 v/v in corn oil twice a week for 10 weeks. After fibrosis induction, dispersions of DGNS-Man or DGNS-GW in PBS were intravenously injected (50 μg/Kg DGNS and 2.5 mg/Kg GW1929 or mannitol) every 3 days for 10 days (4 injections in total). Animals were euthanized the day after the last intravenous injection (at day 11). Liver samples and serum were collected and frozen for further analysis. Serum alanine aminotransferase (ALT), aspartate aminotransferase (AST), albumin and total protein were measured using a BS-200E Chemistry Analyzer (Mindray Medical international Ltd., Shenzhen, China). Liver weight/body weight ratio was calculated as follows: liver weight/body weight × 100 g.

2.5. Gene Expression Assay

Total RNA from liver was extracted using commercially available RNeasy RNA extraction kit (Qiagen, Germantown, MD, USA). RNA from cells was extracted using TRIzol™ kit (Gibco-Invitrogen, Paisley, UK). A 1 μg aliquot of total RNA was reverse transcribed using a complementary DNA synthesis kit following the manufacturer's instructions (High-Capacity cDNA Reverse Transcription Kit, Applied Biosystems, Foster City, CA, USA). Gene expression assays were designed using the Taqman Gene Expression assay software (Applied Biosystems). Probes and primers for gene expression assays (Applied Biosystems) were selected as follows: IL-10 (Taqman assay reference from Applied Biosystems: Mm00439614_m1), NOS2 (Mm00440502_m1), COX-2 (Mm00478374_m1), MRC1 (Mm00485148_m1), ARG-1 (Mm00475988_m1), Col1A1 (Mm00801666_g1), α-SMA (Mm01204962_gH), TIMP-1 (Mm01341360_g1), MMP-9 Mm00442991_m1), TIMP-2 (Mm00442991_m1), MMP-2 (Mm00439498_m1), HGF (Mm01135184_m1), IGF-1 (Mm00439560_m1), VEGF (Mm00437306_m1), and hypoxanthine phosphoribosyltransferase (HPRT) (Mm03024075_m1) used as an endogenous standard. Real-time quantitative PCR was analyzed in duplicate and performed with a Lightcycler-480 II (Roche Diagnostics). For each PCR reaction, a 10 μL aliquot of the total volume reaction of Taqman probes and primers, the FastStart TaqMan Master (Applied Biosystems), and 1:8 diluted complementary DNA were used. The TaqMan probe fluorescence signal was captured during each of the 45 cycles (denaturing 10 s at 95 °C, annealing 15 s at 60 °C, and extending 20 s at 72 °C). The relative gene expression was quantified using the comparative threshold cycle (CT), which was inversely related to the abundance of mRNA transcripts in the initial sample. The mean CT of the duplicate measurements was used to calculate ΔCT (difference in CT between the target and endogenous standard gene for each sample). ΔΔCT was obtained from the normalization of ΔCT values per each sample with the mean ΔCT of control samples. The relative expression of a gene was expressed as the fold induction of the target gene compared with the control primers, according to the formula $2^{-\Delta\Delta CT}$.

2.6. Fibrosis Quantification

For fibrosis quantification, the liver was excised, washed with PBS, and fixed with 10% buffered formaldehyde solution for 24 h. Afterwards, the liver tissue was embedded in

paraffin and 6 µm liver sections were obtained. Before staining, paraffin was removed using xylene, xylene/ethanol 1:1, ethanol, ethanol/deionized water 1:1, and deionized water (5 min in each solution). Liver sections were stained in 0.1% Sirius Red F3B (Sigma) with saturated picric acid (Sigma). The relative fibrosis area (expressed as a percentage of total liver area) was analysed in 10 fields of Sirius red-stained liver sections per animal using the morphometry software ImageJ. To evaluate the relative fibrosis area, the measured collagen area was divided by the net field total liver area and then multiplied by 100. From each animal analysed, the percentage of fibrosis area was calculated and the average value presented.

2.7. Immunofluorescence and Imaging in Liver Tissues

For proliferating cell nuclear antigen (PCNA), pro-inflammatory M1-like marker (nitric oxide synthase 2: NOS2, cyclooxygenase-2: COX-2), and anti-inflammatory M2-like marker (mannose receptor 1: MRC1, arginase 1: ARG1) immunostaining, the liver was excised, washed with PBS, and fixed with 10% buffered formaldehyde solution for 24 h. Afterwards, the liver tissue was cryo-protected with 30% sucrose solution (in PBS) for another 24 h, embedded using Tissue-Tek OCT compound (Sakura Fineteck USA, Torrance, CA, USA), and frozen. For immunostaining, 6 µm liver sections were obtained using a cryostat (Leica Biosystems, Wetzlar, Germany). Liver sections underwent 1% SDS solution antigen retrieval for 5 min at room temperature and then were blocked with 5% normal goat serum in PBS for another hour. Liver sections were incubated with rabbit polyclonal anti-PCNA antibody (1:100, Abcam, Cambridge, MA, USA), rabbit anti-NOS2 polyclonal antibody (1:100, Thermofisher Scientific, Waltham, MA, USA), rabbit anti-COX-2 polyclonal antibody (1:100, Proteintech), rabbit anti-ARG1 polyclonal (1:100, Thermofisher Scientific), or rabbit polyclonal anti-MRC1 (1:100, Abcam, Cambridge, MA, USA) for 16 h at 4 °C. Primary antibodies were revealed using donkey-anti-rabbit IgG Alexa Fluor 594 (1:500, Jackson ImmunoResearch Laboratories, West Grove, PA, USA) or Cy3-conjugated donkey-anti-rabbit IgG (1:500, Jackson ImmunoResearch Laboratories, West Grove, PA, USA) incubated for 2 h at room temperature. The presence of PCNA, COX-2, NOS2, ARG1, and MRC1 was visualized with an epifluorescence microscope. DAPI (Vectashield, Vector laboratories, Burlingame, CA, USA) was used to counterstain cell nuclei. The percentage of positive PCNA cells was calculated as follows: PCNA positive nuclei/total number of cells defined by DAPI nuclei per field $\times$ 100. PCNA positive cells were analysed in 10 fields per animal and the average values are presented.

2.8. Statistical Analysis

All data were expressed as mean $\pm$ standard error of mean (S.E.M). The number of replicates per each experiment is detailed in figure legends. The statistical analysis of the results was performed through Student's *t*-tests with GraphPad Prism v6.0a. Differences were considered statistically significant when the *p*-value ≤ 0.05.

3. Results

3.1. Synthesis and Physicochemical Characterization of Dendrimer–Graphene Nanostars Linked to GW1929 PPARγ Agonist

We used a synthesis method modified from a previous design of dendrimer–graphene nanostars (DGNS) [7] to obtain DGNS linked to a low dose of the GW1929 PPARγ agonist (DGNS-GW) to induce macrophage M2 polarization for the treatment of liver fibrosis. GW1929 (Figure 1a) has a carboxylic group on its chemical structure that can react with the primary amines in G5 PAMAM dendrimers in the presence of EDC/NHS crosslinking agents. DGNS-GW were synthetized in two consecutive chemical reactions. First, the crosslinking agents EDC/NHS and G5 PAMAM dendrimers were incubated with carboxylated GNS using continuous ultrasonic agitation for two hours at a constant temperature of 25 °C. Then, GW1929 was covalently linked to DGNS through a second reaction with

EDC/NHS under constant magnetic stirring and temperature (25 °C) for two hours in order to obtain DGNS-GW (Figure 1b).

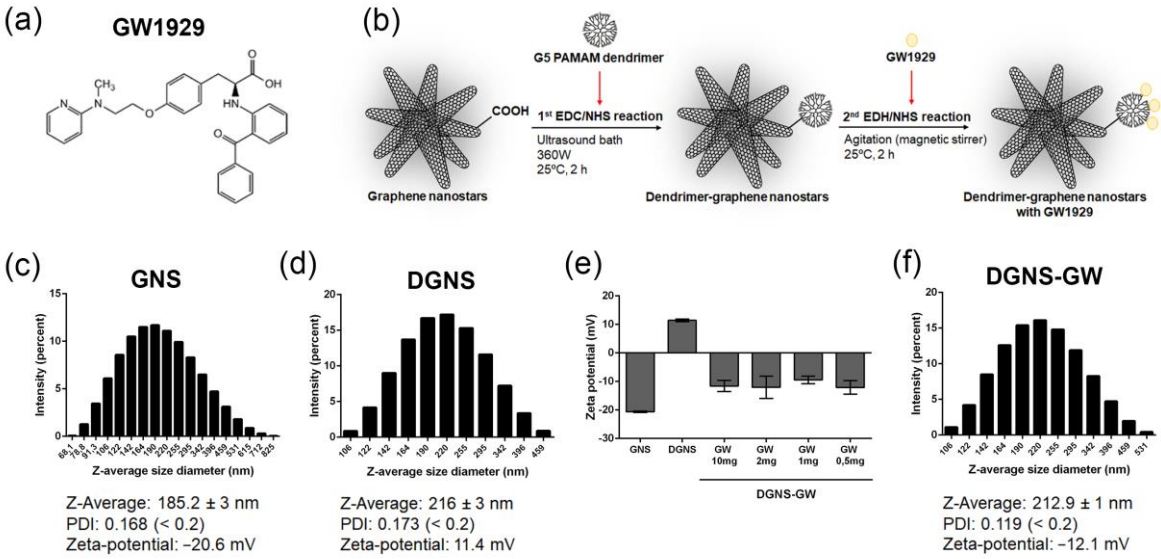

Figure 1. Synthesis and physicochemical characterization of dendrimer–graphene nanostars linked to the GW1929 agonist. (**a**) Chemical structure of GW1929. (**b**) Schematic representation of the chemical synthesis process of dendrimer–graphene nanostars linked to GW1929. (**c**) Representative particle hydrodynamic size histogram of graphene nanostars (GNS) obtained through dynamic light scattering (DLS) showing the values of the Z-average, polydispersity index (PDI), and Zeta-potential. (**d**) Representative particle hydrodynamic size histogram of dendrimer–graphene nanostars (DGNS) obtained via DLS showing the Z-average, PDI, and Zeta-potential values. (**e**) Zeta-potential of GNS, DGNS, and DGNS dispersed in PBS linked to different quantities of GW1929 (10 mg, 2 mg, 1 mg, and 0.5 mg) per milliliter of DGNS suspension. (**f**) Representative particle hydrodynamic size histogram of DGNS linked to GW1929 (DGNS-GW) obtained via DLS showing the Z-average, PDI, and Zeta-potential values. N = 3 different measurements. For (**e**), data are shown as mean ± S.E.M.

The measurements of the hydrodynamic diameter via DLS revealed a Z-average of 185.2 ± 3 nm in carboxylated GNS and a negative Zeta-potential (−20.6 mV) due to the presence of carboxylic groups (Figure 1c). The Z-average rose to 216 ± 3 nm when PAMAM dendrimers were covalently incorporated (Figure 1d). The Zeta-potential of DGNS switched to positive (11.4 mV), resulting in a hyperosmotic nanoparticle dispersion (Figure 1d). Different concentrations of GW1929 were incubated with DGNS (10 µg/mL) to determine the minimum drug quantity required to obtain biologically compatible nanostars with a negative Zeta-potential surface. DGNS switched to negative Zeta-potential when they were linked with 10 mg of GW1929 (Figure 1e). DGNS demonstrated similar negative Zeta-potential when incubated with 20-fold less of the free drug (0.5 mg) (Figure 1e). We used this formulation with a low drug levels of GW1929 linked to DGNS for subsequent experiments. DLS measurements revealed a Z-average size of DGNS-GW of 212.9 ± 1 nm, indicating no significant change in the hydrodynamic diameter of drug-linked particles compared to DGNS, and a Zeta-potential of −12.1 mV (Figure 1f). All GNS, DGNS, and DGNS-GW preparations demonstrated a uniform particle size distribution and a low polydispersity index (PDI < 0.2) (Figure 1c,d,f).

3.2. In Vitro Evaluation of the Activity of DGNS-GW to Stimulate Macrophage Polarization

We then investigated the potential of DGNS-GW in macrophage polarization in vitro. We first synthetized DGNS linked to mannitol (DNGS-Man) (Figure 2a) as control nanoparticles. Mannitol has previously been used as a standard control in macrophage polarization experiments [30–32]. DLS measurements revealed a Z-average of DGNS-Man of 213.6 ± 1.9 nm, a uniform nanoparticle size distribution, and a low PDI (Figure 2b).

DGNS-Man also presented a Zeta-potential of −13.3 mV (Figure 2b), thus demonstrating no significant differences in terms of nanoparticle characteristics as compared to DGNS-GW. To confirm that the treatment with DGNS-Man had no impact on PPARγ activation, we measured the expression of the downstream PPARγ target interleukin 10 (IL-10) in mouse RAW 264.7 macrophages treated with DGNS-Man. We found no differences in IL-10 expression in macrophages treated with DGNS-Man compared to control macrophages without any stimulation (Figure 1c). To ensure that mannitol was not exerting any effect on macrophage polarization, we evaluated the expression of pro-inflammatory M1-like genes (nitric oxide synthase 2, NOS2; cyclooxygenase-2, COX-2) and anti-inflammatory M2-like genes (mannose receptor 1, MRC1; arginase 1, ARG1) in macrophages treated with DGNS-Man. We found no differences in the M1-like gene expression (Figure 2d) or M2-like gene expression (Figure 2e) in macrophages treated with DGNS-Man compared to non-stimulated macrophages, indicating the suitability of DGNS-Man as control nanoparticles for further experiments.

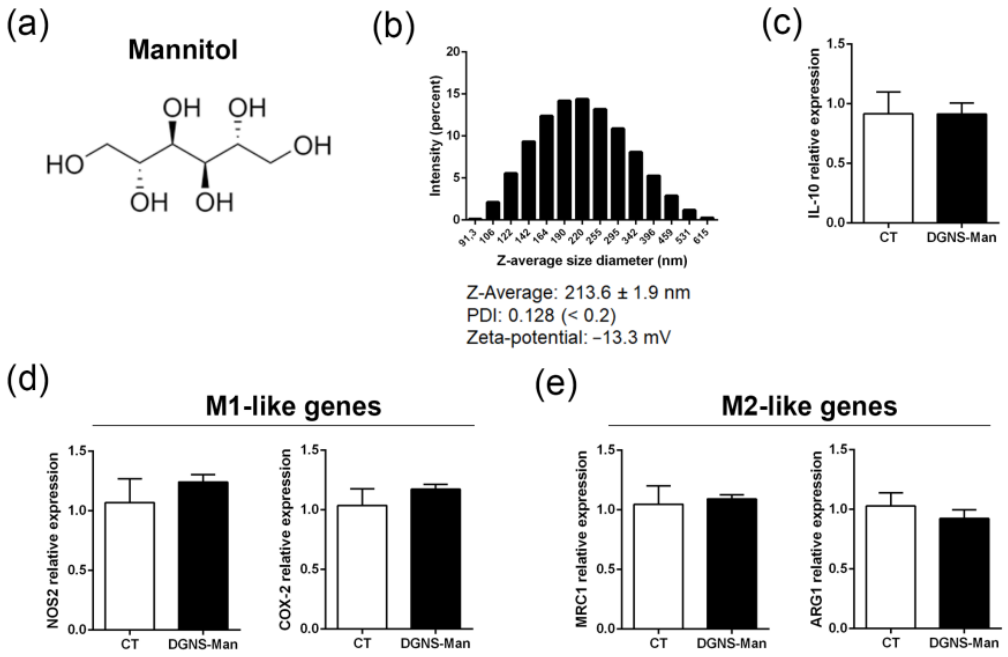

Figure 2. Physicochemical characterization and in vitro validation of dendrimer–graphene nanostars linked to mannitol as control nanoparticles. (**a**) Chemical structure of mannitol. (**b**) Representative particle hydrodynamic size histogram of dendrimer–graphene nanostars linked to mannitol (DGNS-Man) obtained via DLS, showing the values of Z-average, PDI, and Zeta-potential. (**c**) IL-10 expression in control mouse RAW 264.7 macrophages and macrophages stimulated with DGNS-Man for three days. (**d**) M1-like gene expression (NOS2 and COX-2) in control mouse RAW 264.7 macrophages and macrophages stimulated with DGNS-Man for three days. (**e**) M2-like gene expression (MRC1 and ARG1) in control mouse RAW 264.7 macrophages and macrophages stimulated with DGNS-Man for three days. For (**b**), N = 3 different measurements. For (**c**–**e**), experiments were performed in sextuplicate. Data are shown as mean ± S.E.M. No significant differences were observed using Student's *t*-test.

To investigate whether DGNS could be incorporated by macrophages and retained for long periods, we incubated macrophages with DGNS-GW for three days with or without TNF-α inflammatory stimulus. Approximately 40% of macrophages still conserved DGNS-GW after three days of treatment under TNF-α stimulation. In contrast, only 10% of non-stimulated macrophages conserved DGNS-GW after three days of nanoparticle treatment (Figure 3a). These results reinforce the fact that DGNS-GW could be selectively incorporated and retained by pro-inflammatory macrophages in livers undergoing chronic

inflammation, where they could act as drug delivery systems for efficient macrophage-targeted nanotherapeutics.

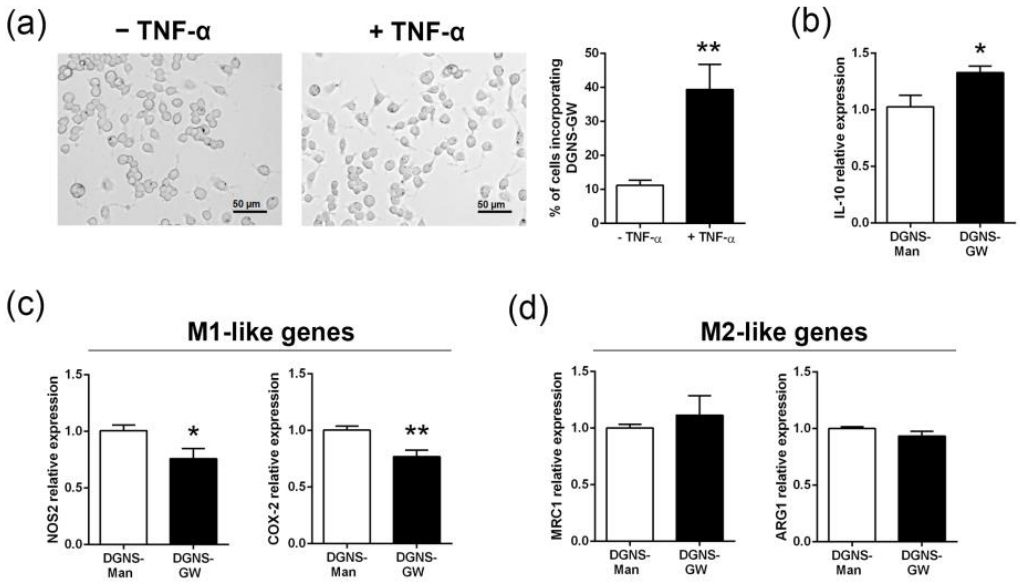

Figure 3. In vitro nanoparticle uptake and macrophage polarization following the treatment with dendrimer–graphene nanostars linked to GW1929. (**a**) Uptake experiment using RAW 264.7 macrophages incubated with dendrimer–graphene nanostars linked to GW1929 (DGNS-GW) for 3 days in the presence or absence of TNF-α (5 ng/mL), showing representative images and percentages of cells incorporating nanoparticles. (**b**) IL-10 expression in mouse RAW 264.7 macrophages in the presence of TNF-α and treated with dendrimer–graphene nanostars linked to mannitol or GW1929 for three days. (**c**) M1-like gene expression (NOS2 and COX-2) in mouse RAW 264.7 macrophages in the presence of TNF-α and treated with dendrimer–graphene nanostars linked to mannitol or GW1929 for three days. (**d**) M2-like gene expression (MRC1 and ARG1) in mouse RAW 264.7 macrophages in the presence of TNF-α and treated with dendrimer–graphene nanostars linked to mannitol or GW1929 for three days. Experiments were performed in sextuplicate. Data are shown as mean ± S.E.M. * indicates $p < 0.05$ and ** indicates $p < 0.01$ using Student's *t*-test.

We then investigated the pharmacological effectivity of DGNS-GW on the activation of PPARγ downstream signals via the evaluation of IL-10 gene expression. IL-10 expression was higher in mouse macrophages stimulated in vitro with TNF-α and treated with DGNS-GW compared to macrophages treated with DGNS-Man stimulated with TNF-α (Figure 3b). Moreover, the expression of M1-like genes (NOS2 and COX-2) decreased in macrophages treated with DGNS-GW compared to macrophages treated with DGNS-Man (Figure 3c), without affecting the expression of M2-like genes (MRC1 and ARG1) (Figure 3d).

3.3. Evaluation of the Therapeutic Utility of DGNS-GW in Mice with Liver Fibrosis

We then evaluated the therapeutic utility of DGNS-GW in a mouse model of liver fibrosis. The conventional dosage form of the systemic treatment of GW1929 is between 5 mg/kg and 20 mg/kg in mice [33–35]. We wondered whether the selective activation of PPARγ in liver macrophages with a low dose (1/4 of conventional dose) of GW1929 that was linked to DGNS could be effective in stimulating a selective M2 anti-inflammatory macrophage phenotype and boosting macrophage-driven liver fibrosis resolution.

Liver fibrosis was induced in twelve male Balb/c mice via intraperitoneal injections of the hepatotoxic molecule CCl_4 twice a week for 10 weeks. We intravenously administered DGNS-GW or DGNS-Man every 3 days for 10 days (four injections in total) to fibrotic mice (Figure 4a). To ensure that DGNS-GW with low drug dose levels were efficient for PPARγ signaling activation, we quantified IL-10 gene expression in the liver of fibrotic mice

treated with DGNS-GW. The IL-10 expression was approximately four times higher in the liver of fibrotic mice treated with DGNS-GW compared to mice treated with DGNS-Man (Figure 4b). These results indicated that DGNS could be an adequate nanoscale delivery system for transporting a low dose of GW1929 agonist to macrophages in order to overcome the side effects and limitations of conventional dosages and formulations.

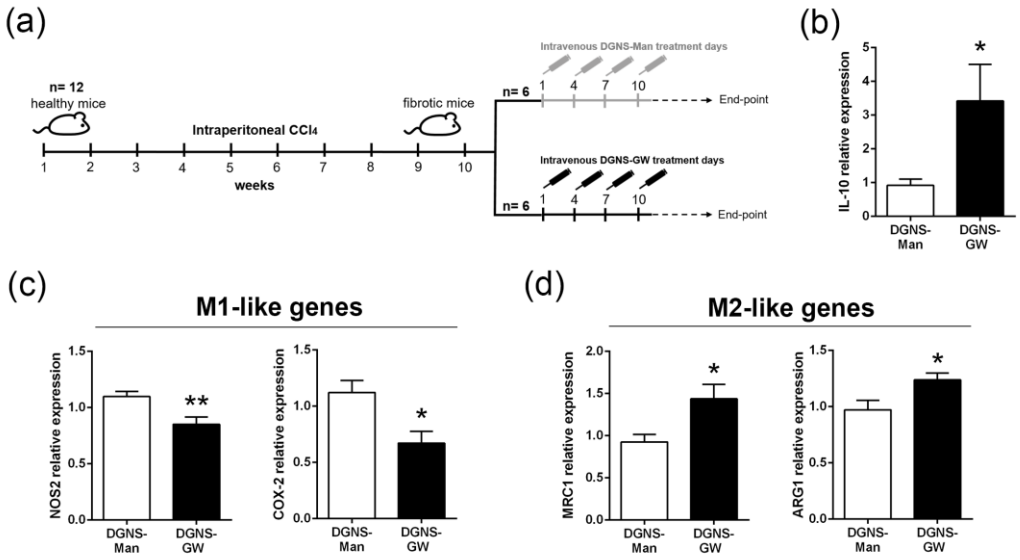

Figure 4. Hepatic immunomodulation of macrophage gene expression profile in mice with liver fibrosis treated with DGNS-GW. (**a**) Schematic illustration indicating the time points of fibrosis induction with CCl_4 and the administration schedule of dendrimer–graphene nanostars linked to mannitol (DGNS-Man) or GW1929 (DGNS-GW). (**b**) IL-10 expression in the livers of fibrotic mice treated with DGNS-Man or DGNS-GW. (**c**) M1-like gene expression (NOS2 and COX-2) in the livers of fibrotic mice treated with DGNS-Man or DGNS-GW. (**d**) M2-like gene expression (MRC1 and ARG1) in the livers of fibrotic mice treated with DGNS-Man or DGNS-GW. N = six mice per group. Data are shown as mean ± S.E.M. * indicates $p < 0.05$ and ** indicates $p < 0.01$ using Student's *t*-test.

In accordance with our in vitro results, the selective activation of PPARγ in macrophages from fibrotic livers reduced the expression and synthesis of M1-like pro-inflammatory genes (NOS2 and COX-2) in the liver of fibrotic animals (Figures 4c and S1). Moreover, treatment with DGNS-GW increased the expression and synthesis of anti-inflammatory M2-like genes (MRC1 and ARG1) in the liver of fibrotic mice treated with DGNS-GW compared to DGNS-Man (Figures 4d and S1). These results suggest that the selective activation of PPARγ in hepatic macrophages with DGNS-GW could exert hepatic immunomodulatory activity via the re-education of macrophages on an anti-inflammatory phenotype.

Since macrophages play essential roles in the balance between fibrogenesis and regression and PPARγ agonists have been proven to reduce experimental liver fibrosis [23,36,37], we then evaluated the potential therapeutic utility of macrophage-targeted DGNS-GW in ECM remodeling in liver fibrosis. We stained collagen fibers in the livers of fibrotic mice treated with DGNS-GW or DGNS-Man. Fibrotic mice treated with DGNS-GW showed approximately 60% less fibrotic area compared to mice treated with DGNS-Man, illustrated through Sirius Red staining (Figure 5a). This reduction in liver fibrosis did not affect the serum markers of liver damage (ALT and AST) or serum markers of hepatic function (albumin and total protein) (Table S1). The reduction in liver fibrosis was associated with a decrease in the liver expression of alpha smooth muscle actin (α-SMA), without altering the expression of collagen 1 (Figure 5b). Since macrophages modulate hepatic fibrosis regression through the secretion of matrix metalloproteinases (MMPs) [10,14] but activated HSCs produce tissue inhibitor metalloproteinases (TIMPs) suppressing MMPs activity in late stages of liver fibrosis [2], we wondered whether the selective activation of PPARγ

in hepatic macrophages could modulate the liver expression of MMPs and TIMPs. The treatment with DGNS-GW in fibrotic mice increased the expression of the gelatinases MMP-2 and MMP-9 but did not affect the hepatic expression of the associated TIMPs (TIMP-1 and TIMP-2) (Figure 5c), suggesting that the selective activation of PPARγ in hepatic macrophages with DGNS-GW impairs liver fibrosis and modulates macrophage fate towards a pro-resolutive phenotype via the induction of the expression of these extracellular matrix metalloproteinases.

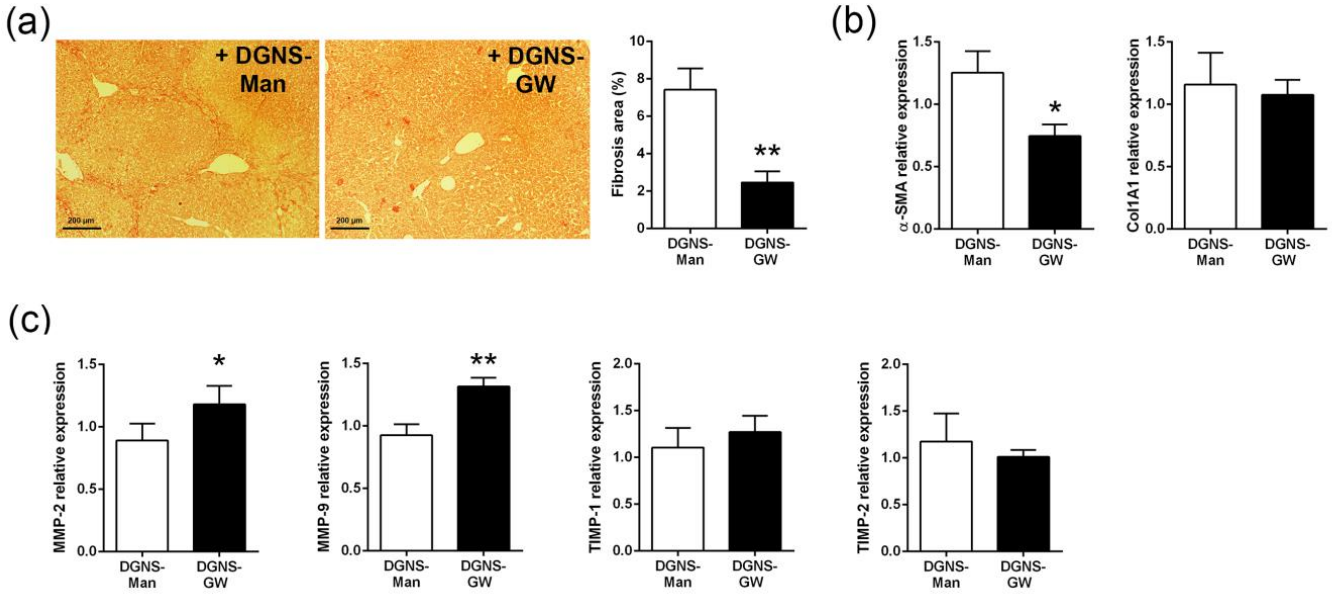

Figure 5. Effect of macrophage-targeted DGNS-GW therapy on liver fibrosis and the expression of extracellular matrix-related genes. (**a**) Representative images and quantification of Sirius Red staining in the livers of fibrotic mice treated with dendrimer–graphene nanostars linked to mannitol (DGNS-Man) or GW1929 (DGNS-GW). (**b**) Alpha smooth muscle actin (α-SMA) and collagen I (Col1A1) expression in the livers of fibrotic mice treated with DGNS-Man or DGNS-GW. (**c**) Tissue inhibitor metalloproteinases (TIMP-1 and TIMP-2) and gelatinase metalloproteinases (MMP-9 and MMP-2) expression in the livers of fibrotic mice treated with DGNS-Man or DGNS-GW. N = six mice per group. Data are shown as mean ± S.E.M. * indicates $p < 0.05$ and ** indicates $p < 0.01$ using Student's *t*-test.

Fibrotic mice treated with DGNS-GW displayed a significant increase in liver mass compared to fibrotic mice treated with DGNS-Man (Figure 6a). We speculated whether the selective activation of PPARγ in hepatic macrophages could favor hepatic regeneration in the context of liver fibrosis. We evaluated the abundance of the proliferating cellular nuclear antigen (PCNA) by immunohistochemistry in the livers of fibrotic mice treated with DGNS-Man or DGNS-GW. Fibrotic mice treated with DGNS-GW displayed an increase in the number of PCNA-positive cells, indicating an augmented hepatic cellular proliferation (Figure 6b). Then, we evaluated the hepatic expression of hepatocyte growth factor (HGF), insulin-like growth factor-1 (IGF-1), and vascular endothelial growth factor (VEGF), since the pro-resolutive macrophage phenotype is characterized by the secretion of these growth factors, which promote liver cell proliferation and blood vessel development [12]. We did not find significant differences in the hepatic expression of HGF and IGF-1 (Figure 6c). In contrast, fibrotic mice treated with DGNS-GW showed a significant increase in the hepatic expression of VEGF compared to fibrotic mice treated with DGNS-Man (Figure 6c), indicating that PPARγ-activated liver macrophages stimulate hepatic proliferation in part via the synthesis of VEGF.

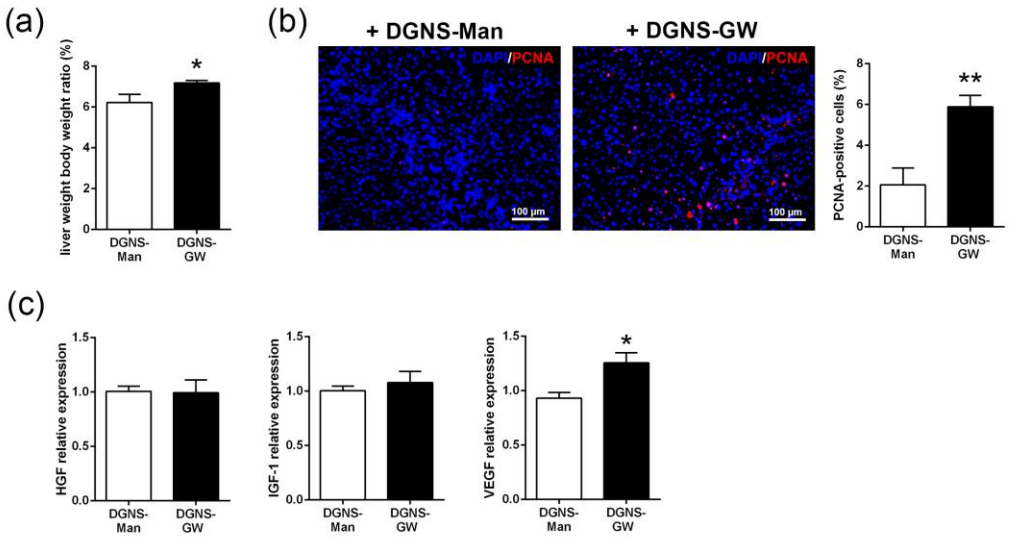

Figure 6. Effect of macrophage-targeted DGNS-GW therapy on liver regeneration. (**a**) Liver restoration rate in fibrotic mice treated with dendrimer–graphene nanostars linked to mannitol (DGNS-Man) or GW1929 (DGNS-GW). (**b**) Proliferating cell nuclear antigen (PCNA) immunofluorescence staining representative images and quantification (percentage of PCNA positive cells) in the livers of fibrotic mice treated with DGNS-Man or DGNS-GW. (**c**) Hepatocyte growth factor (HGF), Insulin-like growth factor-1 (IGF-1), and vascular endothelial growth factor (VEGF) expression in the livers of fibrotic mice treated with DGNS-Man or DGNS-GW. N = six mice per group. Data are shown as mean ± S.E.M. * indicates $p < 0.05$ and ** indicates $p < 0.01$ using Student's *t*-test.

4. Discussion

PPARγ agonists have traditionally been used for the treatment of diabetes mellitus and other metabolic disorders [38]. Diverse PPARγ full agonists have also been proposed to stimulate macrophage anti-inflammatory responses [22,23]. However, the use of full agonists in biological systems is greatly limited due to side effects [27–29]. Some polymeric nanoparticles have already been suggested for the delivery of low dose PPARγ agonists to overcome toxicity-related limitations [39–41]. Here, we sought to design a macrophage-selective treatment with a low dose of GW1929 PPARγ agonist linked to carbon-based nanoparticles (DGNS-GW) as drug delivery systems for the treatment of liver fibrosis.

We first characterized nanoparticle surface charge and hydrodynamic diameter via dynamic light scattering. Cationic carbon nanoparticles (with positive surface charge) have been associated with toxicity in macrophages and cells from epithelial origin [42]. Chemical linkage between GW1929 and DGNS solved this potential biocompatibility problem, exhibiting a negative surface charge. Indeed, we have previously demonstrated that anionic pDNA-DGNS presented no harmful effects on human endothelial cells, which are the primary cells in blood vessels and the first biological barrier for intravenously administered formulations [7]. The hydrodynamic size of DGNS-GW resulted in 212.9 nm. Since most nanoparticles administered in vivo that are over 200 nm are supposed to be primarily incorporated by macrophages [13,43], DGNS appear as a suitable nanoscale system for GW1929 agonist delivery to macrophages. Indeed, macrophages are more efficient in incorporating functionalized anionic DGNS under TNF-α inflammatory stimulation [7]. In a previous report, approximately 80% of macrophages incorporated these nanoparticles as fast as three hours after TNF-α stimulation and only 20% of macrophages without TNF-α stimulation were able to engulf them [7]. Here, we observed that 40% of macrophages still conserved DGNS-GW after three days of treatment under TNF-α stimulation. We also synthetized and characterized DGNS linked to mannitol as control nanoparticles for subsequent in vitro and in vivo experiments. Mannitol has previously been used as a standard control in macrophage polarization experiments [30–32]. We further confirmed that DGNS-Man had no impact on macrophage polarization. Both DGNS linked to mannitol or

GW1929 presented no significant differences according to nanoparticle hydrodynamic size and Zeta-potential, illustrating the suitability of DGNS-Man as control nanoparticles for our study.

Liver fibrosis is associated with a sustained inflammatory milieu [1,2]. TNF-α is a prominent cytokine driving inflammation in chronic liver disease [44,45]. Moreover, TNF-α has been associated with the inhibition of PPARγ both at pre-translational and post-translational levels [46]. Heming et al. demonstrated that macrophages display sustained immune responses in the absence of PPARγ signaling, impairing their ability to reprogram towards a pro-resolving phenotype [47]. Since PPARγ activation has been linked to macrophage anti-inflammatory phenotypes [18], we tested the functional ability of DGNS-GW on macrophage polarization in cells under TNF-α stimulation and in the liver of mice with liver fibrosis induced by the i.p. administration of CCl_4 as an in vivo inflammatory niche. The chronic administration of CCl_4 has been classically used to promote chronic liver injury in animal models. CCl_4 induces the formation of hepatic regenerative nodules surrounded by fibrotic tracts and the infiltration of pro-inflammatory macrophages that sustain the inflammatory response [48]. We have previously demonstrated the selectivity of anionic DGNS linked to plasmids to target and treat inflammatory macrophages with gene therapy in the liver of fibrotic mice [7]. Here, livers of fibrotic mice treated with anionic DGNS-GW displayed a reduction in the gene and protein expression of M1 pro-inflammatory factors. PPARγ activation has been linked to the inhibition of the molecular signaling of the nuclear factor NF-kB [49], which can ultimately result in the downregulation of pro-inflammatory genes. This fact may explain the observed effects on the decreased expression of COX-2 and NOS2 in both in vitro and in vivo experiments under a constant inflammatory stimulus.

The expression of M2 anti-inflammatory genes and proteins increased in the livers of fibrotic mice following macrophage-selective PPARγ activation with DGNS-GW. Anti-inflammatory M2 polarization has been classically associated with the activation of macrophages with IL-4 and IL-13 interleukin signals [50]. The anti-inflammatory IL-4 or IL-13 initiates a cytoplasmic signaling cascade that culminates in the activation of STAT6 transcription factor [50]. Phosphorylated STAT6 dimerizes and translocates to the nucleus to induce the expression of its target genes, including M2 macrophage markers (MRC1 and ARG1) and other regulators of PPARγ [50]. While the instructions for M2 macrophage polarization may not be directly linked to PPARγ activation, the acquisition and long-term maintenance of this phenotype requires PPARγ activity [50]. This may explain the upregulation of the expression of M2 anti-inflammatory genes observed in the livers of mice treated with DGNS-GW for ten days. Altogether, our results reinforce the fact that PPARγ acts as a nuclear regulator of inflammation in macrophages. In the context of chronic liver disease, the macrophage-selective activation of PPARγ may be a promising therapeutic strategy for promoting macrophage polarization from pro-inflammatory to anti-inflammatory phenotypes.

Since chronic liver inflammation and fibrosis are two phenomena that are tightly associated [51], we evaluated the anti-fibrotic utility of DGNS-GW on mice with liver fibrosis. The modulation of PPARγ has been proven to attenuate HSC activation and to reduce liver fibrosis [36]. Our results revealed a reduction in the liver fibrotic area and a decreased expression of liver α-SMA in mice treated with DGNS-GW. IL-10 expression is regulated by PPARγ and has been directly linked to α-SMA reduction [52]. Interestingly, we did not observe a significant reduction in collagen I and TIMPs gene expression following selective macrophage PPARγ activation with DGNS-GW. This fact illustrated that DGNS-GW treatment may not directly modulate HSC activity. Macrophages play an essential role in extracellular matrix remodeling through the secretion of MMPs [10]. Indeed, DGNS-GW treatment in fibrotic mice increased the expression of liver gelatinase MMPs (MMP-2 and MMP-9). Therefore, the anti-fibrotic effect of DGNS-GW treatment may be associated with the increase in macrophage MMPs secretion rather than the inhibition of HSC activity. We finally observed a significant hepatic regeneration and an increase in PCNA-positive cells

along fibrotic tracts in the liver of fibrotic mice treated with DGNS-GW. This correlated with an augmented liver VEGF expression. PPARγ activation has been associated with VEGF production in macrophage cell lines [53]. Moreover, VEGF has been linked to fibrosis resolution through the stimulation of scar-associated macrophages [54]. Taken together, DGNS-GW treatment may induce liver macrophage VEGF secretion to stimulate the proliferation of pro-resolutive liver cells, such as scar-associated macrophages. However, we cannot exclude other cellular or molecular components involved in the anti-fibrotic effect of DGNS-GW treatment. Overall, our results indicate that macrophage-selective PPARγ activation with DGNS-GW may polarize liver macrophages towards a pro-resolutive phenotype to stimulate extracellular matrix remodeling in liver fibrosis.

5. Conclusions

We designed dendrimer–graphene nanostars linked to a low dose of the GW1929 PPARγ agonist (DGNS-GW) to induce a selective activation of PPARγ in macrophages in fibrotic liver. The treatment with DGNS-GW effectively activated PPARγ signaling in macrophages in in vitro and in vivo experiments, illustrated by the increase in IL-10 expression. DGNS-GW accumulated in macrophages stimulated with TNF-α and attenuated their pro-inflammatory phenotype. Accordingly, the treatment with DGNS-GW in fibrotic mice promoted a macrophage switch from pro-inflammatory M1 to anti-inflammatory M2 phenotypes. The reduction of hepatic inflammation correlated with a reduction in liver fibrosis and an increase in gelatinase MMPs (MMP-2 and MMP-9). Moreover, the treatment with DGNS-GW induced liver regeneration and augmented liver VEGF expression. In conclusion, the selective activation of PPARγ in hepatic macrophages using DGNS-GW reduces hepatic inflammation and fibrosis. This study gives new insights into the relationship between PPARγ activation in hepatic macrophages and fibrosis resolution and highlights that DGNS-GW is a promising macrophage-targeted nanoscale therapy for chronic liver disease.

Supplementary Materials: The following supporting information can be downloaded at: https://www.mdpi.com/article/10.3390/pharmaceutics15051452/s1, Table S1: Serum parameters of liver damage (alanine aminotransferase (ALT) and aspartate aminotransferase (AST)) and liver function (albumin and total protein) in fibrotic mice treated with dendrimer–graphene nanostars linked to mannitol (DGNS-Man) or GW1929 (DGNS-GW); Figure S1: Immunofluorescent staining of pro-inflammatory M1-like markers (NOS2 and COX-2) and anti-inflam-matory M2-like markers (MRC1 and ARG1) in the liver of in fibrotic mice treated with dendrimer-graphene nanos-tars linked to mannitol (DGNS-Man) or GW1929 (DGNS-GW). Scale bar: 250 μm.

Author Contributions: Conceptualization, A.M.-L. and P.M.-L.; methodology, A.M.-L., M.M.-B., B.S.-C. and M.B.-G.; formal analysis, A.M.-L. and P.M.-L.; investigation, A.M.-L. and P.M.-L.; resources, P.M.-L. and W.J.; data curation, A.M.-L. and P.M.-L.; writing—original draft preparation, A.M.-L.; writing—review and editing, P.M.-L.; supervision, P.M.-L. and W.J.; project administration, A.M.-L. and P.M.-L.; funding acquisition, P.M.-L. and W.J. All authors have read and agreed to the published version of the manuscript.

Funding: This research was funded by grants from the Ministerio de Ciencia e Innovación (MCIN/AEI/10.13039/501100011033 (RTI2018-094734-B-C21 and PID2021-123426OB-I00) and, as appropriate, by "ERDF A way of making Europe") to P.M.-L., W.J. and P.M.-L. was additionally supported by a fellowship from the Ramon y Cajal Program (RYC2018-0Z23971-I) from the Spanish Ministerio de Ciencia, Innovación y Universidades. A.M.-L. received a Formación de Personal Investigador (FPI) grant from the Ministerio de Ciencia, Innovación y Universidades (Reference: PRE2019-088097). M.M.-B. received a Formación de Profesorado Universitario (FPU) grant from Ministerio de Ciencia, Innovación y Universidades (Reference: FPU19/03323). The Centro de Investigación Biomédica en Red de Enfermedades Hepáticas y Digestivas (CIBERehd) is supported by the Instituto de Salud Carlos III. RedFibro (RED2022-134485-T) of the 2022 call for aid to «RESEARCH NETWORKS», within the framework of the Programa Estatal del Plan Estatal de Investigación Científica, Técnica y de Innovación 2021–2023, and Consolidated Research Group of the Generalitat de Catalunya AGAUR (2021 SGR 00881).

Institutional Review Board Statement: The animal study protocol was approved by the Investigation and Ethics Committees of the Hospital Clínic Universitari of Barcelona (approval codes: 49/17 and 339/22, with approval date March 2017 and February 2023, respectively).

Informed Consent Statement: Not applicable.

Data Availability Statement: All data are available in the main manuscript text and Supplementary Material.

Conflicts of Interest: The authors declare no conflict of interest.

References

1. Bataller, R.; Brenner, D.A. Liver fibrosis. *J. Clin. Investig.* **2005**, *115*, 209–218. [CrossRef] [PubMed]
2. Wynn, T.A.; Ramalingam, T.R. Mechanisms of fibrosis: Therapeutic translation for fibrotic disease. *Nat. Med.* **2012**, *18*, 1028–1040. [CrossRef] [PubMed]
3. Sepanlou, S.G.; Safiri, S.; Bisignano, C.; Ikuta, K.S.; Merat, S.; Saberifiroozi, M.; Poustchi, H.; Tsoi, D.; Colombara, D.V.; Abdoli, A.; et al. The global, regional, and national burden of cirrhosis by cause in 195 countries and territories, 1990–2017: A systematic analysis for the Global Burden of Disease Study 2017. *Lancet Gastroenterol. Hepatol.* **2020**, *5*, 245–266. [CrossRef] [PubMed]
4. Wynn, T.A. Cellular and molecular mechanisms of fibrosis. *J. Pathol.* **2008**, *214*, 199–210. [CrossRef] [PubMed]
5. Perramón, M.; Carvajal, S.; Reichenbach, V.; Fernández-Varo, G.; Boix, L.; Macias-Muñoz, L.; Melgar-Lesmes, P.; Bruix, J.; Melmed, S.; Lamas, S.; et al. The pituitary tumour-transforming gene 1/delta-like homologue 1 pathway plays a key role in liver fibrogenesis. *Liver Int.* **2022**, *42*, 651–662. [CrossRef] [PubMed]
6. Tan, Z.; Sun, H.; Xue, T.; Gan, C.; Liu, H.; Xie, Y.; Yao, Y.; Ye, T. Liver Fibrosis: Therapeutic Targets and Advances in Drug Therapy. *Front. Cell Dev. Biol.* **2021**, *9*, 730176. [CrossRef]
7. Melgar-Lesmes, P.; Luquero, A.; Parra-Robert, M.; Mora, A.; Ribera, J.; Edelman, E.R.; Jiménez, W. Graphene–Dendrimer Nanostars for Targeted Macrophage Overexpression of Metalloproteinase 9 and Hepatic Fibrosis Precision Therapy. *Nano Lett.* **2018**, *18*, 5839–5845. [CrossRef]
8. Carvajal, S.; Perramón, M.; Casals, G.; Oró, D.; Ribera, J.; Morales-Ruiz, M.; Casals, E.; Casado, P.; Melgar-Lesmes, P.; Fernández-Varo, G.; et al. Cerium Oxide Nanoparticles Protect against Oxidant Injury and Interfere with Oxidative Mediated Kinase Signaling in Human-Derived Hepatocytes. *Int. J. Mol. Sci.* **2019**, *20*, 5959. [CrossRef]
9. Wen, Y.; Lambrecht, J.; Ju, C.; Tacke, F. Hepatic macrophages in liver homeostasis and diseases-diversity, plasticity and therapeutic opportunities. *Cell. Mol. Immunol.* **2021**, *18*, 45–56. [CrossRef]
10. Tacke, F.; Zimmermann, H.W. Macrophage heterogeneity in liver injury and fibrosis. *J. Hepatol.* **2014**, *60*, 1090–1096. [CrossRef]
11. Melgar-Lesmes, P.; Edelman, E.R. Monocyte-endothelial cell interactions in the regulation of vascular sprouting and liver regeneration in mouse. *J. Hepatol.* **2015**, *63*, 917–925. [CrossRef] [PubMed]
12. Wynn, T.A.; Vannella, K.M. Macrophages in Tissue Repair, Regeneration, and Fibrosis. *Immunity* **2016**, *44*, 450–462. [CrossRef] [PubMed]
13. Medrano-Bosch, M.; Moreno-Lanceta, A.; Melgar-Lesmes, P. Nanoparticles to target and treat macrophages: The ockham's concept? *Pharmaceutics* **2021**, *13*, 1340. [CrossRef] [PubMed]
14. Tacke, F. Targeting hepatic macrophages to treat liver diseases. *J. Hepatol.* **2017**, *66*, 1300–1312. [CrossRef] [PubMed]
15. Moreno-Lanceta, A.; Medrano-Bosch, M.; Melgar-Lesmes, P. Single-Walled Carbon Nanohorns as Promising Nanotube-Derived Delivery Systems to Treat Cancer. *Pharmaceutics* **2020**, *12*, 850. [CrossRef]
16. Karousis, N.; Suarez-Martinez, I.; Ewels, C.P.; Tagmatarchis, N. Structure, Properties, Functionalization, and Applications of Carbon Nanohorns. *Chem. Rev.* **2016**, *116*, 4850–4883. [CrossRef]
17. Abedi-Gaballu, F.; Dehghan, G.; Ghaffari, M.; Yekta, R.; Abbaspour-Ravasjani, S.; Baradaran, B.; Ezzati Nazhad Dolatabadi, J.; Hamblin, M.R. PAMAM dendrimers as efficient drug and gene delivery nanosystems for cancer therapy. *Appl. Mater. Today* **2018**, *12*, 177–190. [CrossRef]
18. Moore, K.J.; Rosen, E.D.; Fitzgerald, M.L.; Randow, F.; Andersson, L.P.; Altshuler, D.; Milstone, D.S.; Mortensen, R.M.; Spiegelman, B.M.; Freeman, M.W. The role of PPAR-γ in macrophage differentiation and cholesterol uptake. *Nat. Med.* **2001**, *7*, 41–47. [CrossRef]
19. Willson, T.M.; Brown, P.J.; Sternbach, D.D.; Henke, B.R. The PPARs: From Orphan Receptors to Drug Discovery. *J. Med. Chem.* **2000**, *43*, 527–550. [CrossRef]
20. Chandra, V.; Huang, P.; Hamuro, Y.; Raghuram, S.; Wang, Y.; Burris, T.P.; Rastinejad, F. Structure of the intact PPAR-γ–RXR-α nuclear receptor complex on DNA. *Nature* **2009**, *456*, 350–356. [CrossRef]
21. Wang, C.; Ma, C.; Gong, L.; Guo, Y.; Fu, K.; Zhang, Y.; Zhou, H.; Li, Y. Macrophage Polarization and Its Role in Liver Disease. *Front. Immunol.* **2021**, *12*, 803037. [CrossRef]
22. Bouhlel, M.A.; Derudas, B.; Rigamonti, E.; Dièvart, R.; Brozek, J.; Haulon, S.; Zawadzki, C.; Jude, B.; Torpier, G.; Marx, N.; et al. PPARγ Activation Primes Human Monocytes into Alternative M2 Macrophages with Anti-inflammatory Properties. *Cell Metab.* **2007**, *6*, 137–143. [CrossRef] [PubMed]

23. Li, J.; Guo, C.; Wu, J. The agonists of peroxisome proliferator-activated receptor-γ for liver fibrosis. *Drug Des Devel Ther.* **2021**, *15*, 2619–2628. [CrossRef] [PubMed]
24. Tsoyi, K.; Ha, Y.M.; Kim, Y.M.; Lee, Y.S.; Kim, H.J.; Kim, H.J.; Seo, H.G.; Lee, J.H.; Chang, K.C. Activation of PPAR-γ by Carbon Monoxide from CORM-2 Leads to the Inhibition of iNOS but not COX-2 Expression in LPS-Stimulated Macrophages. *Inflammation* **2009**, *32*, 364–371. [CrossRef] [PubMed]
25. Kaundal, R.K.; Sharma, S.S. GW1929: A nonthiazolidinedione PPARγ agonist, ameliorates neurological damage in global cerebral ischemic-reperfusion injury through reduction in inflammation and DNA fragmentation. *Behav. Brain Res.* **2011**, *216*, 606–612. [CrossRef]
26. Paukkeri, E.-L.; Leppänen, T.; Lindholm, M.; Yam, M.F.; Asmawi, M.Z.; Kolmonen, A.; Aulaskari, P.H.; Moilanen, E. Anti-inflammatory properties of a dual PPARgamma/alpha agonist muraglitazar in in vitro and in vivo models. *Arthritis Res. Ther.* **2013**, *15*, R51. [CrossRef]
27. Wright, M.B.; Bortolini, M.; Tadayyon, M.; Bopst, M. Minireview: Challenges and Opportunities in Development of PPAR Agonists. *Mol. Endocrinol.* **2014**, *28*, 1756–1768. [CrossRef]
28. Xi, Y.; Zhang, Y.; Zhu, S.; Luo, Y.; Xu, P.; Huang, Z. PPAR-Mediated Toxicology and Applied Pharmacology. *Cells* **2020**, *9*, 352. [CrossRef]
29. Bortolini, M.; Wright, M.B.; Bopst, M.; Balas, B. Examining the safety of PPAR agonists—Current trends and future prospects. *Expert Opin. Drug Saf.* **2013**, *12*, 65–79. [CrossRef]
30. Torres-Castro, I.; Arroyo-Camarena, D.; Martínez-Reyes, C.P.; Gómez-Arauz, A.Y.; Dueñas-Andrade, Y.; Hernández-Ruiz, J.; Béjar, Y.L.; Zaga-Clavellina, V.; Morales-Montor, J.; Terrazas, L.I.; et al. Human monocytes and macrophages undergo M1-type inflammatory polarization in response to high levels of glucose. *Immunol. Lett.* **2016**, *176*, 81–89. [CrossRef]
31. Grosick, R.; Alvarado-Vazquez, P.A.; Messersmith, A.R.; Romero-Sandoval, E.A. High glucose induces a priming effect in macrophages and exacerbates the production of pro-inflammatory cytokines after a challenge. *J. Pain Res.* **2018**, *11*, 1769–1778. [CrossRef] [PubMed]
32. Pavlou, S.; Lindsay, J.; Ingram, R.; Xu, H.; Chen, M. Sustained high glucose exposure sensitizes macrophage responses to cytokine stimuli but reduces their phagocytic activity. *BMC Immunol.* **2018**, *19*, 24. [CrossRef] [PubMed]
33. Moore-Carrasco, R.; Figueras, M.; Ametller, E.; López-Soriano, F.J.; Argiles, J.M.; Busquets, S. Effects of the PPARγ agonist GW1929 on muscle wasting in tumour-bearing mice. *Oncol. Rep.* **2008**, *19*, 253–256. [CrossRef] [PubMed]
34. Tickner, J.; Fan, L.M.; Du, J.; Meijles, D.; Li, J.-M. Nox2-derived ROS in PPARγ signaling and cell-cycle progression of lung alveolar epithelial cells. *Free. Radic. Biol. Med.* **2011**, *51*, 763–772. [CrossRef]
35. Li, Z.; Liu, T.; Feng, Y.; Tong, Y.; Jia, Y.; Wang, C.; Cui, R.; Qu, K.; Liu, C.; Zhang, J. PPAR γ Alleviates Sepsis-Induced Liver Injury by Inhibiting Hepatocyte Pyroptosis via Inhibition of the ROS/TXNIP/NLRP3 Signaling Pathway. *Oxidative Med. Cell. Longev.* **2022**, *2022*, 1269747. [CrossRef]
36. Alatas, F.S.; Matsuura, T.; Pudjiadi, A.H.; Wijaya, S.; Taguchi, T. Peroxisome Proliferator-Activated Receptor Gamma Agonist Attenuates Liver Fibrosis by Several Fibrogenic Pathways in an Animal Model of Cholestatic Fibrosis. *Pediatr. Gastroenterol. Hepatol. Nutr.* **2020**, *23*, 346–355. [CrossRef]
37. Yang, L.; Stimpson, S.A.; Chen, L.; Harrington, W.W.; Rockey, D.C. Effectiveness of the PPARγ agonist, GW570, in liver fibrosis. *Inflamm. Res.* **2010**, *59*, 1061–1071. [CrossRef]
38. Chiarelli, F.; Di Marzio, D. Peroxisome proliferator-activated receptor-γ agonists and diabetes: Current evidence and future perspectives. *Vasc. Health Risk Manag.* **2008**, *4*, 297–304. [CrossRef]
39. Laddha, U.D.; Kshirsagar, S.J. Formulation of PPAR-gamma agonist as surface modified PLGA nanoparticles for non-invasive treatment of diabetic retinopathy: In vitro and in vivo evidences. *Heliyon* **2020**, *6*, e04589. [CrossRef]
40. Wei, S.; Xu, C.; Zhang, Y.; Shi, Z.; Wu, M.; Yang, B. Ultrasound Assisted a Peroxisome Proliferator-Activated Receptor (PPAR)γ Agonist-Loaded Nanoparticle-Microbubble Complex to Attenuate Renal Interstitial Fibrosis. *Int. J. Nanomed.* **2020**, *15*, 7315–7327. [CrossRef]
41. Alves, C.; de Melo, N.; Fraceto, L.; Araújo, D.; Napimoga, M. Effects of 15d-PGJ2-loaded poly(D,L-lactide-co-glycolide) nanocapsules on inflammation. *Br. J. Pharmacol.* **2011**, *162*, 623–632. [CrossRef] [PubMed]
42. Weiss, M.; Fan, J.; Claudel, M.; Sonntag, T.; Didier, P.; Ronzani, C.; Lebeau, L.; Pons, F. Density of surface charge is a more predictive factor of the toxicity of cationic carbon nanoparticles than zeta potential. *J. Nanobiotechnology* **2021**, *19*, 5. [CrossRef] [PubMed]
43. Gustafson, H.H.; Holt-Casper, D.; Grainger, D.W.; Ghandehari, H. Nanoparticle uptake: The phagocyte problem. *Nano Today* **2015**, *10*, 487–510. [CrossRef] [PubMed]
44. Yang, Y.M.; Seki, E. TNFα in liver fibrosis. *Curr. Pathobiol. Rep.* **2015**, *3*, 253–261. [CrossRef]
45. Connolly, M.K.; Bedrosian, A.S.; Clair, J.M.-S.; Mitchell, A.P.; Ibrahim, J.; Stroud, A.; Pachter, H.L.; Bar-Sagi, D.; Frey, A.B.; Miller, G. In liver fibrosis, dendritic cells govern hepatic inflammation in mice via TNF-α. *J. Clin. Investig.* **2009**, *119*, 3213–3225. [CrossRef]
46. Ye, J. Regulation of PPARγ function by TNF-α. *Biochem Biophys Res Commun.* **2008**, *374*, 405–408. [CrossRef]
47. Heming, M.; Gran, S.; Jauch, S.-L.; Fischer-Riepe, L.; Russo, A.; Klotz, L.; Hermann, S.; Schäfers, M.; Roth, J.; Barczyk-Kahlert, K. Peroxisome Proliferator-Activated Receptor-γ Modulates the Response of Macrophages to Lipopolysaccharide and Glucocorticoids. *Front. Immunol.* **2018**, *9*, 893. [CrossRef]

48. Muñoz-Luque, J.; Ros, J.; Fern´ández-Varo, G.; Tugues, S.; Morales-Ruiz, M.; Alvarez, C.E.; Friedman, S.L.; Arroyo, V.; Jiménez, W. Regression of Fibrosis after Chronic Stimulation of Cannabinoid CB2 Receptor in Cirrhotic Rats. *J. Pharmacol. Exp. Ther.* **2008**, *324*, 475–483. [CrossRef]
49. Scirpo, R.; Fiorotto, R.; Villani, A.; Amenduni, M.; Spirili, C.; Strazzabosco, M. Stimulation of nuclear receptor PPAR-γ limits NF-kB-dependent inflammation in mouse cystic fibrosis biliary epithelium. *Hepatology.* **2015**, *62*, 1551–1562. [CrossRef]
50. Chawla, A. Control of Macrophage Activation and Function by PPARs. *Circ. Res.* **2010**, *106*, 1559–1569. [CrossRef]
51. Koyama, Y.; Brenner, D.A. Liver inflammation and fibrosis. *J. Clin. Investig.* **2017**, *127*, 55–64. [CrossRef] [PubMed]
52. Zhu, H.; Qu, X.; Zhang, C.; Yu, Y. Interleukin-10 promotes proliferation of vascular smooth muscle cells by inhibiting inflammation in rabbit abdominal aortic aneurysm. *Int. J. Clin. Exp. Pathol.* **2019**, *12*, 1260–1271. [PubMed]
53. Jozkowicz, A.; Dulak, J.; Piatkowska, E.; Placha, W.; Dembinska-Kiec, A. Ligands of peroxisome proliferator-activated receptor- g increase the generation of vascular endothelial growth factor in vascular smooth muscle cells and in macrophages. *Acta Biochim Pol.* **2000**, *47*, 1147–1157. [CrossRef] [PubMed]
54. Yang, L.; Kwon, J.; Popov, Y.V.; Gajdos, G.B.; Ordog, T.; Brekken, R.A.; Mukhopadhyay, D.; Schuppan, D.; Bi, Y.; Simonetto, D.; et al. Vascular Endothelial Growth Factor Promotes Fibrosis Resolution and Repair in Mice. *Gastroenterology* **2014**, *146*, 1339–1350e1. [CrossRef]

pharmaceutics

MDPI

Article

PPAR-γ Agonist GW1929 Targeted to Macrophages with Dendrimer–Graphene Nanostars Reduces Liver Fibrosis and Inflammation

Alazne Moreno-Lanceta [1,2], Mireia Medrano-Bosch [1], Blanca Simón-Codina [1], Montserrat Barber-Gonzá lez[1], Wladimiro Jiménez [1,2] and Pedro Melgar-Lesmes [1,2,3,*]

[1] Department of Biomedicine, School of Medicine, University of Barcelona, 08036 Barcelona, Spain; amorenol@recerca.clinic.cat (A.M.-L.)
[2] Biochemistry and Molecular Genetics Service, Hospital Clínic Universitari, Instituto de Investigaciones Biomédicas August Pi i Sunyer (IDIBAPS), Centro de Investigación Biomédica en Red de Enfermedades Hepáticas y Digestivas (CIBERehd), 08036 Barcelona, Spain
[3] Institute for Medical Engineering and Science, Massachusetts Institute of Technology, Cambridge, MA 02139, USA
* Correspondence: pmelgar@ub.edu; Tel.: +34-934020294

Table S1. Serum parameters of liver damage (alanine aminotransferase (ALT) and aspartate aminotransferase (AST)) and liver function (albumin and total protein) in fibrotic mice treated with dendrimer-graphene nanostars linked to mannitol (DGNS-Man) or GW1929 (DGNS-GW).

Serum parameter	DGNS-Man (N=6)	DGNS-GW (N=6)
ALT (U/L)	37.13 ± 9.12	40.46 ± 5.46
AST (U/L)	277.8 ± 155	332.4 ± 66.87
Albumin (g/L)	27.05 ± 0.22	27.19 ± 0.37
Total protein (g/L)	49.53 ± 0.77	47.65 ± 0.89

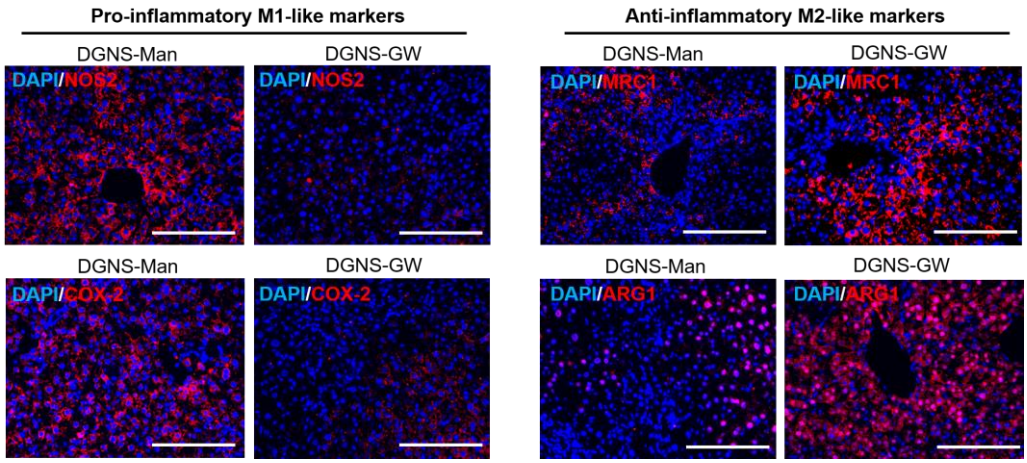

Figure S1. Immunofluorescent staining of pro-inflammatory M1-like markers (NOS2 and COX-2) and anti-inflammatory M2-like markers (MRC1 and ARG1) in the liver of in fibrotic mice treated with dendrimer-graphene nanostars linked to mannitol (DGNS-Man) or GW1929 (DGNS-GW). Scale bar: 250 μm.

Article 2:

RNF41 orchestrates macrophage-driven fibrosis resolution and hepatic regeneration

Moreno-Lanceta A, *Medrano-Bosch M, Fundora Y, Perramón M, Aspas J, Parra-Robert M, Baena S, Fondevila C, Edelman ER, Jiménez W, Melgar-Lesmes P. RNF41 orchestrates macrophage-driven fibrosis resolution and hepatic regeneration. Science Translational Medicine. 2023;* 15*(704): eabq6225.*

This article corresponds to the **second objective** of the thesis. The **second objective** of the thesis was to investigate the role of the E3 ubiquitin ligase RING finger 41 (RNF41) on hepatic macrophage regulation in chronic liver disease, and to study the effects of a macrophage-selective modulation of RNF41 on liver inflammation, fibrosis, and regeneration in mouse models of chronic liver disease using dendrimer-graphite nanoparticles.

LIVER FIBROSIS

RNF41 orchestrates macrophage-driven fibrosis resolution and hepatic regeneration

Alazne Moreno-Lanceta[1,2], Mireia Medrano-Bosch[1], Yilliam Fundora[2,3], Meritxell Perramón[2,4], Jessica Aspas[3], Marina Parra-Robert[4], Sheila Baena[3], Constantino Fondevila[2,3], Elazer R. Edelman[5,6], Wladimiro Jiménez[1,2,4], Pedro Melgar-Lesmes[1,2,5]*

Hepatic inflammation is a common trigger of chronic liver disease. Macrophage activation is a predictive parameter for survival in patients with cirrhosis. Ring finger protein 41 (RNF41) negatively regulates proinflammatory cytokines and receptors; however, the precise involvement of macrophage RNF41 in liver cirrhosis remains unknown. Here, we sought to understand how RNF41 dictates macrophage fate in hepatic fibrosis and repair within the inflammatory milieu. We found that *RNF41* expression is down-regulated in CD11b$^+$ macrophages recruited to mouse fibrotic liver and to patient cirrhotic liver regardless of cirrhosis etiology. Prolonged inflammation with TNF-α progressively reduced macrophage *RNF41* expression. We designed a macrophage-selective gene therapy with dendrimer-graphite nanoparticles (DGNPs) to explore the influence of macrophage RNF41 restoration and depletion in liver fibrosis and regeneration. *RNF41* expression induced in CD11b$^+$ macrophages by DGNP-conjugated plasmids ameliorated liver fibrosis, reduced liver injury, and stimulated hepatic regeneration in fibrotic mice with or without hepatectomy. This therapeutic effect was mainly mediated by the induction of insulin-like growth factor 1. Conversely, depletion of macrophage *RNF41* worsened inflammation, fibrosis, hepatic damage, and survival. Our data reveal implications of macrophage RNF41 in the control of hepatic inflammation, fibrosis, and regeneration and provide a rationale for therapeutic strategies in chronic liver disease and potentially other diseases characterized by inflammation and fibrosis.

INTRODUCTION

Chronic liver disease accounts for nearly 2 million deaths per year worldwide. Cirrhosis is within the top 20 causes of disability-adjusted life years and years of life lost (*1*). No curative solutions exist for cirrhosis except for organ transplantation, which requires substantial surgery and lifelong immunosuppression. However, only 50% of eligible patients receive a liver transplant, which translates into a shortage of about 13,000 donors per year (*2*). Alternative strategies to treat cirrhosis and stimulate hepatic regeneration are thus being investigated, including nanotherapeutics and cell therapies (*3*–*5*).

Macrophages are cellular regulators involved in all stages of liver disease, from initial tissue injury to chronic inflammation, fibrosis, and repair (*6*). Resident hepatic macrophages release signals that promote local immune response and limit initial injury through the classic path of inflammatory cell recruitment and subsequent activation of hepatic stellate cells (HSCs) with production of a supporting extracellular matrix (ECM) (*7*–*9*). When injury abates, macrophages remodel fibrosis primarily by releasing matrix metalloproteinases (MMPs). MMPs then promote fibrotic ECM degradation and repair through elaboration of factors that reduce the inflammatory response and boost liver regeneration (*10*, *11*).

Ring finger protein 41 (*RNF41*), also known as neuregulin receptor degradation protein 1 (Nrdp1) or fetal liver ring finger, is an E3 ubiquitin protein ligase that plays an essential role in the degradation of various proinflammatory cytokine receptors, adaptors, and kinases (*12*). This ligase inhibits the production of proinflammatory cytokines in Toll-like receptor–triggered macrophages via suppression of MyD88 and nuclear factor κB (NF-κB) activation and confers resistance to lipopolysaccharide-induced endotoxin shock (*13*). RNF41 also promotes anti-inflammatory macrophage polarization by ubiquitination and activation of the transcription factor CCAAT/enhancer-binding protein β (C/EBPβ) (*14*), which has been associated with muscle injury repair (*15*). Collectively, these data induced our investigation of the roles of RNF41 on the control of macrophage behavior in the context of chronic liver injury and regeneration. To our knowledge, nothing is known about the regulation of macrophage *RNF41* expression in a prolonged tissue inflammatory environment or its pathophysiological roles in liver fibrosis and regeneration. Considering the crucial influence that macrophages exert on the modulation of the hepatic cellular response to injury, we further explored the use of a nanoscale gene therapy delivery system designed to modulate inflammatory macrophages for the harmonization of fibrosis resolution and hepatic regeneration. We recently reported that graphene-derived nanoparticles linked to polyamidoamine (PAMAM) dendrimers preferentially accumulate in inflammatory macrophages within the fibrotic liver, where they function as a precision gene therapy system (*16*). A modified version of this system was used in this investigation to explore the role of macrophage RNF41 in chronic liver disease.

Here, we investigated whether RNF41 is regulated by the sustained inflammatory milieu of the cirrhotic liver and how altered

[1]Department of Biomedicine, School of Medicine, University of Barcelona, Barcelona 08036, Spain. [2]Institut d'Investigacions Biomèdiques August Pi-Sunyer (IDIBAPS), Centro de Investigación Biomédica en Red de Enfermedades Hepáticas y Digestivas (CIBERehd), Barcelona 08036, Spain. [3]Liver Transplant Unit, Institut Clínic de Malalties Digestives I Metabòliques, Hospital Clínic, University of Barcelona, Barcelona 08036, Spain. [4]Biochemistry and Molecular Genetics Service, Hospital Clínic Universitari, Barcelona 08036, Spain. [5]Institute for Medical Engineering and Science, Massachusetts Institute of Technology, Cambridge, MA 02139, USA. [6]Cardiovascular Division, Brigham and Women's Hospital, Harvard Medical School, Boston, MA 02115, USA.
*Corresponding author. Email: pmelgar@ub.edu

RNF41 expression in macrophages from cirrhotic livers affects hepatic inflammation, damage, and survival. We used macrophage-selective nanoparticles linked to plasmids to study the effects that the modulation of macrophage *RNF41* expression exert on liver fibrosis and regeneration. We further explored the relationship between macrophage RNF41 and the synthesis of inflammatory and profibrogenic cytokines in different models of liver fibrosis and hepatic regeneration and the downstream molecular signals associated with these effects.

RESULTS

Macrophage *RNF41* decays in human cirrhotic and mouse fibrotic liver

To determine the *RNF41* gene expression in macrophages recruited to cirrhotic liver ($CD11b^{high}$), we isolated $CD11b^+$ macrophages from liver biopsy specimens of patients with liver cirrhosis and healthy participants. This cell surface marker is a selective macrophage marker in liver injury and regeneration (*2*). Twelve patients ($n = 3$ female and $n = 9$ males, 58.7 ± 6.1 years) with decompensated liver cirrhosis and MELD (Model for End-Stage Liver Disease) scores between 13 and 30 were selected from a single center (Hospital Clinic of Barcelona, Spain). Demographic and baseline characteristics of study participants are shown in table S1. Participants in the diseased group displayed a mean duration of cirrhosis of 4.3 ± 5.8 years. *RNF41* macrophage mRNA expression was notably lower in macrophages from cirrhotic than healthy liver (Fig. 1A) regardless of cirrhosis etiology (alcoholic, nonalcoholic, hepatitis C, or autoimmune). This also occurred with ubiquitin-specific peptidase 8 (*USP8*) expression, a known stabilizer of RNF41 activity (Fig. 1B) (*17*). We also evaluated macrophage *RNF41* expression in an animal model of CCl_4-induced chronic liver injury and fibrosis in the BALB/c mouse strain because these mice are most sensitive to induction of liver fibrosis (*18*). CCl_4 is a hepatotoxic molecule classically used to promote chronic liver injury, fibrosis, and infiltration of proinflammatory macrophages (*18*, *19*). Quantification of *RNF41* in $CD11b^+$ macrophages from liver specimens obtained from healthy and fibrotic mice mirrored what we saw in human specimens with down-regulated *RNF41* (Fig. 1C) and *USP8* (Fig. 1D). Although human and mouse $CD11b^+$ macrophages were isolated after removing other $CD11b^+$ cells such as neutrophils and dendritic cells, we cannot exclude that *RNF41* and *USP8* down-regulation is shared by different specific macrophage subpopulations with diverse abundances of CD11b, suggesting that these findings should be considered for all liver $CD11b^+$ macrophages. No changes in *RNF41* or *USP8* expression were found in hepatocytes isolated from hepatic specimens obtained from healthy participants, cirrhotic patients, or mice with liver fibrosis (fig. S1). Neither *RNF41* nor *USP8* expression was down-regulated in HSCs and up-regulated in liver sinusoidal endothelial cells (LSECs) from fibrotic mice (fig. S1).

We hypothesized that hepatic chronic inflammation could be behind the down-regulation of macrophage *RNF41* due to the known cross-talk between RNF41 and cytokine receptors (*12*) and some indications on the human and mouse gene expression atlas and bulk data (table S2). We used human THP-1 and mouse RAW 264.7 macrophages to design an in vitro model of prolonged inflammation (independent of infection and lipopolysaccharide) using tumor necrosis factor–α (TNF-α), a prominent cytokine driving inflammation in chronic liver disease (*20*). *RNF41* expression was up-regulated in human THP-1 and mouse RAW 264.7 macrophages during the first 24 hours of induction with TNF-α and then decreased from day 1 to day 5, becoming lower than that in untreated macrophages (Fig. 1, E and F). The same pattern of initial up-regulation and subsequent drop in expression of *RNF41* after day 1 was observed in primary mouse hepatic macrophage cultures (Fig. 1G). This pattern was also found with *USP8*, the RNF41 stabilizer (Fig. 1, H, I, and J). It is known that phospho-Akt (pAkt) phosphorylates USP8 and that the latter stabilizes RNF41 (*21*). To understand the connection between the inflammatory activity of TNF-α and RNF41, we analyzed downstream transduction pathways engaged by TNF-α, including Akt (*22*) and mitogen-activated protein kinases (MAPKs) [such as extracellular signal–regulated kinases (ERKs) (*23*)]. Phosphorylation of Erk1/2 and Akt increased during the first 6 hours after TNF-α stimulation, but only pAkt substantially dropped afterward (Fig. 1K), coinciding with the observed down-regulation pattern of *RNF41* and its stabilizer *USP8*.

Plasmid-dendrimer-graphite nanoparticles selectively induce *RNF41* in inflammatory macrophages

An expression plasmid for *RNF41* was designed with a CD11b promoter (to assure that only recruited inflammatory macrophages express this protein) and an enhanced green fluorescent protein (*EGFP*) gene reporter under the control of a cytomegalovirus (CMV) promoter (fig. S2). To synthesize the gene therapy nanosystem, we first oxidized graphite nanoparticles (GNPs) to obtain GNPs decorated with a carboxylated surface. Then, we chemically attached PAMAM generation 5 dendrimers, which are established to bind nucleic acids (*24*) (such as plasmids) by electrostatic forces (Fig. 2A). Transmission electron microscopy (TEM) images revealed GNPs with a diameter of 29.9 ± 2.9 nm (Fig. 2B) that rose to 36.8 ± 4.2 nm when PAMAM dendrimers were covalently incorporated (Fig. 2C). GNP diameters visualized by TEM were more than eight times smaller than the size of nanoparticles dispersed in phosphate-buffered saline (PBS) and measured by dynamic light scattering. The hydrodynamic diameter of GNPs resulted in a mean particle diameter (*Z* average) of 255.6 nm, denoting a highly hydrated corona and a high aggregation of GNPs in PBS with rather narrow particle size distributions [polydispersity index (PDI) < 0.20] (Fig. 2D). The *Z*-average of dendrimer-GNPs (DGNPs) increased to 280.3 nm, preserving a narrow particle size distribution (Fig. 2E). As expected, GNPs showed a negative zeta potential (−43.2 mV) because of their carboxylic groups and isotonic properties (Fig. 2F). The chemical binding of dendrimers to GNPs promoted a switch to a positive zeta potential (49.01 mV), resulting in hypertonic nanoparticle dispersions (Fig. 2F). The addition of a RNF41 plasmid to DGNPs (pRNF41-DGNPs) switched the zeta potential back to negative (−31.52 mV), returning the composition to physiological osmolality (Fig. 2F).

Isotonic dispersions of pRNF41-DGNPs were then tested for biocompatibility with human endothelial cells, the standard primary cell barrier in blood vessels. No harmful effects of the nanoparticles were found on human umbilical vein endothelial cells (fig. S3A). The uptake of nanoparticles over 200 nm is conceptually assumed to involve mainly macrophages, especially proinflammatory macrophages at diseased sites (*25*). The incorporation of pRNF41-DGNPs in RAW 264.7 macrophages activated by TNF-α increased over time

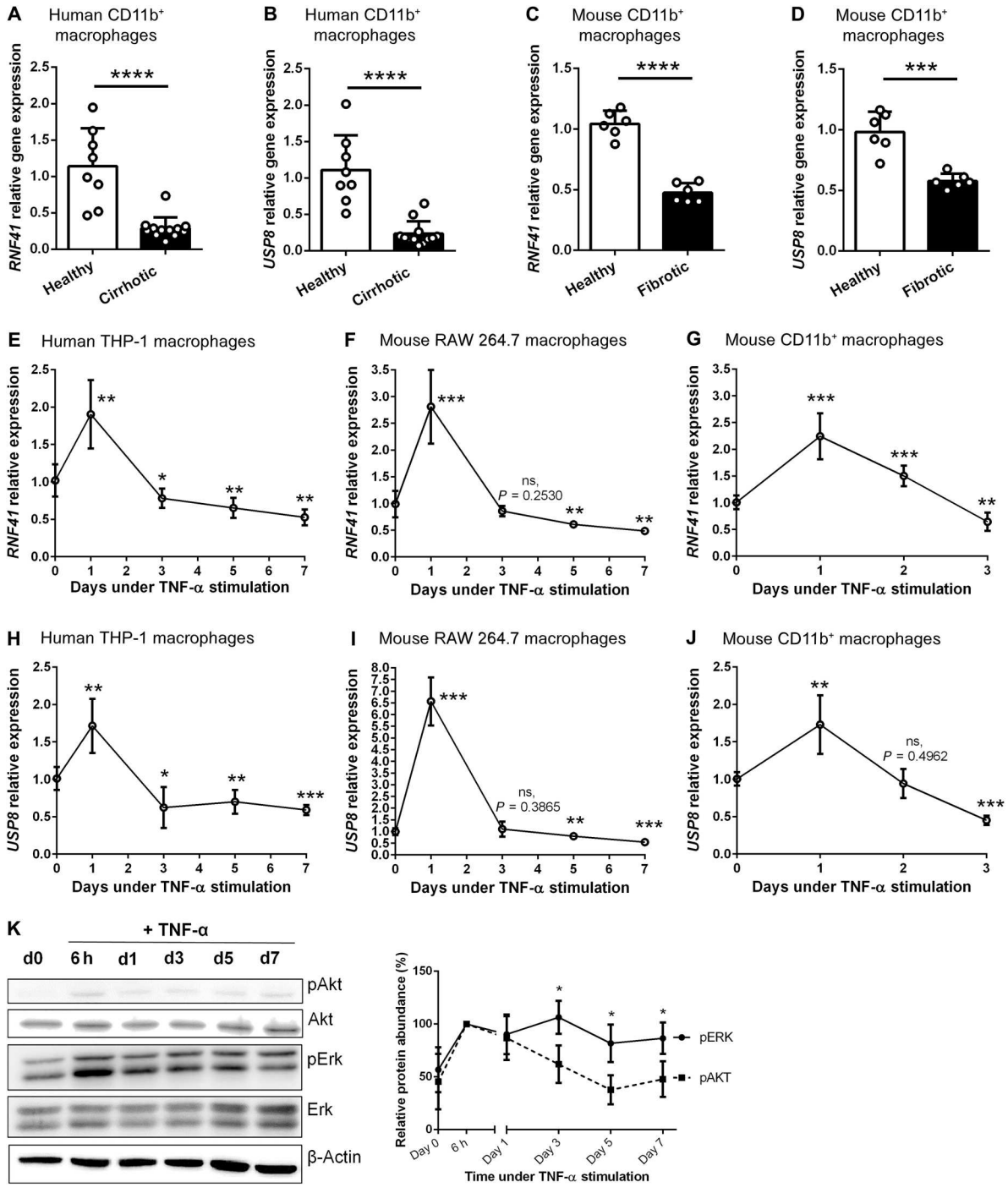

Fig. 1. Macrophage *RNF41* and its stabilizer *USP8* are down-regulated in cirrhotic liver in part due to chronic inflammation. (**A**) *RNF41* expression in CD11b$^+$ macrophages isolated from the livers of patients with liver cirrhosis (n = 12) and healthy participants (n = 8). (**B**) *USP8* expression in CD11b$^+$ macrophages isolated from the livers of patients with liver cirrhosis (n = 12) and healthy participants (n = 8). (**C**) *RNF41* expression in CD11b$^+$-macrophages isolated from the livers of healthy and fibrotic mice (n = 6 per group). (**D**) *USP8* expression in CD11b$^+$-macrophages isolated from the livers of healthy and fibrotic mice (n = 6 per group). (**E**) *RNF41* expression in THP-1 macrophages stimulated with TNF-α for 7 days. (**F**) *RNF41* expression in RAW 264.7 macrophages stimulated with TNF-α for 7 days. (**G**) *RNF41* expression in freshly isolated primary hepatic CD11b$^+$ macrophages stimulated with TNF-α for 3 days. (**H**) *USP8* expression in THP-1 macrophages stimulated with TNF-α for 7 days. (**I**) *USP8* expression in RAW 264.7 macrophages stimulated with TNF-α for 7 days. (**J**) *USP8* expression in freshly isolated primary hepatic CD11b$^+$ macrophages stimulated with TNF-α for 3 days. Experiments in (E) and (F) to (J) were performed in triplicates in two independent experiments. (**K**) Western blot analysis of phospho-Akt, total Akt, phospho-Erk, total Erk, and β-actin in RAW 264.7 macrophages stimulated with TNF-α for 7 days and relative protein abundance (%) of phospho-Akt and phospho-Erk relative to β-actin (n = 3). For (A) to (D), Student's t test. For (E) to (J), versus day 0 using Student's t test with Benjamini-Hochberg correction for multiple comparisons. For (K), comparison between pAKT protein abundance and pERK protein abundance in each time point using Student's t test. Data are shown as means ± SD. *$P \leq 0.05$, **$P \leq 0.01$, ***$P \leq 0.001$, and ****$P \leq 0.0001$. ns, not significant.

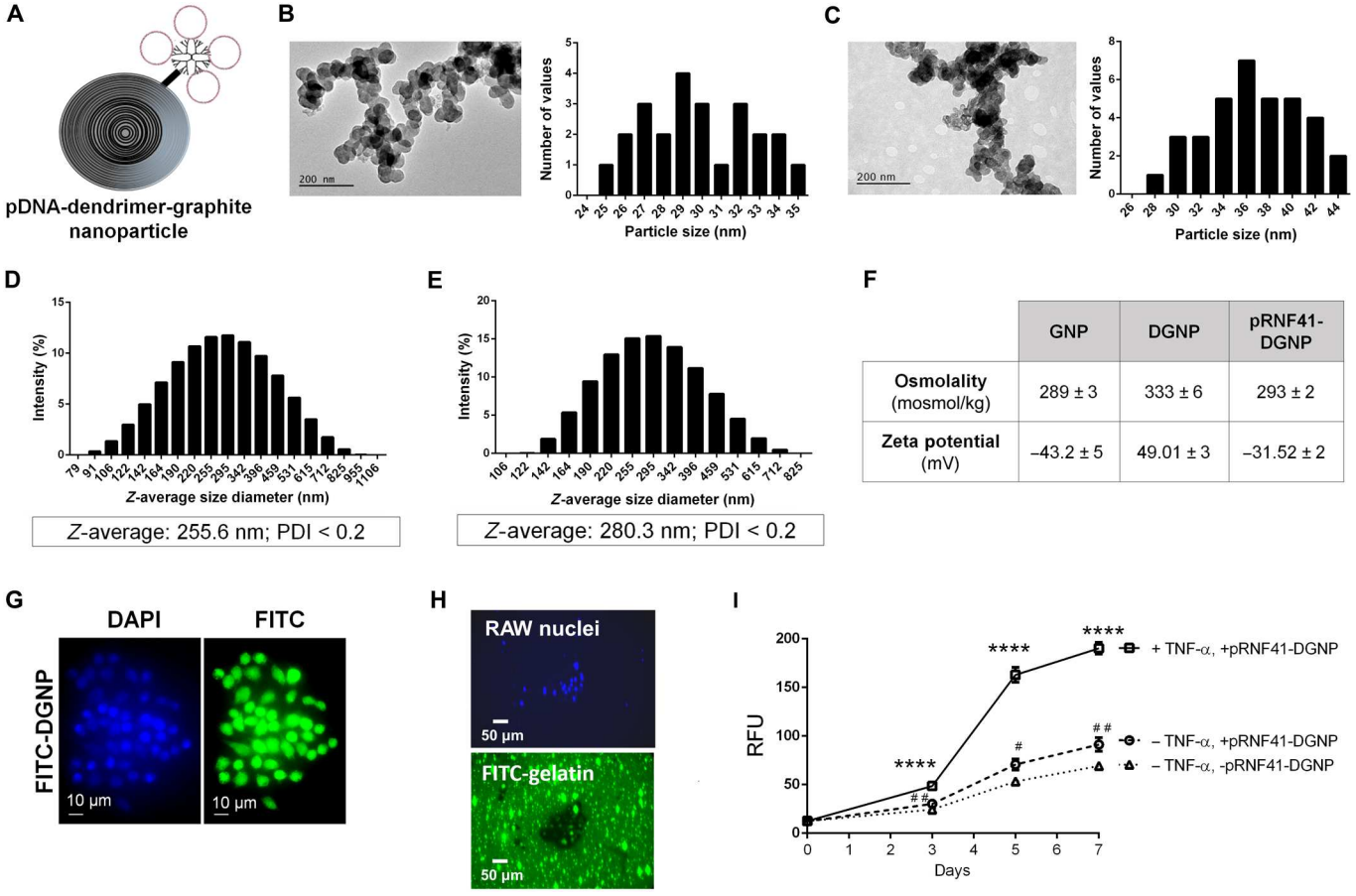

Fig. 2. Dendrimer-graphite nanoparticles are macrophage-selective plasmid-delivery vectors for effective gene therapy. (**A**) Structure of graphite nanoparticles linked to dendrimer and plasmid DNA. (**B**) Particle size (in nanometers) of graphite nanoparticles measured using TEM images. (**C**) Particle size (in nanometers) of dendrimer-graphite nanoparticles measured using TEM images. (**D**) *Z*-average size and polydispersity index (PDI) of graphite nanoparticles measured using dynamic light scattering. (**E**) *Z*-average size and PDI of dendrimer-graphite nanoparticles measured using dynamic light scattering. (**F**) Osmolality and zeta potential of every graphite nanoparticle composite. (**G**) RAW 264.7 macrophage intracellular distribution of FITC-dendrimer-graphite nanoparticles. (**H**) Fluorescence images of RAW 264.7 macrophages seeded on FITC-gelatin–coated plates and treated with dendrimer-graphite nanoparticles linked to pRNF41 (pRNF41-DGNP) for 5 days displaying a black halo indicating collagen digestion and green nuclear staining indicating *EGFP* expression. (**I**) Time-course quantitative analysis of FITC released to the medium in the gelatinase activity assay in the presence or absence of TNF-α or pRNF41-DGNP for 7 days ($n = 3$ to 5). For (I), ****$P \leq 0.0001$ versus macrophages without TNF-α and with or without pRNF41-DGNP, #$P \leq 0.05$ versus macrophages without TNF-α and pRNF41-DGNP, and ##$P \leq 0.01$ versus macrophages without TNF-α and pRNF41-DGNP at the same time point using a one-way analysis of variance (ANOVA) with posthoc Newman-Keuls test. RFU, relative fluorescence units. Data are shown as means ± SD.

up to 45 min and then only rose in the presence of TNF-α, reaching most of the cells after 180 min (fig. S3B) and lasting for at least 24 hours (fig. S3C). These results indicate that the GNP core is involved in selective macrophage uptake. Fluorescein isothiocyanate (FITC)–decorated DGNPs confirmed the intracellular fate of dendrimers after internalization in inflamed macrophages. FITC-DGNPs were internalized and degraded by macrophages, distributing the dendrimer-FITC molecules throughout the cell, including the cell nucleus (Fig. 2G). These results suggested that these nanoparticles could be useful for selective gene therapy to inflammatory macrophages in chronically inflamed livers. Certainly, dendrimers are known to escape from lysosomes by the proton sponge effect, opening pores in the nuclear membrane for pDNA or small interfering RNA gene therapy (*26*).

We next sought to confirm the effectiveness of plasmid-DGNPs for gene therapy in vitro. In line with the previous uptake outcomes, pRNF41-DGNPs were mainly phagocytized by macrophages stimulated with TNF-α, and plasmid expression efficiency was functionally highlighted by the high abundance of intracellular EGFP in most cells after 3 days of incubation (fig. S3D). Moreover, macrophages incubated with pRNF41-DGNP and TNF-α (a CD11b promoter activator) displayed a switch in macrophage morphology (fig. S4A) and phenotype, exemplified by elevated expression of CD206 (mannose receptor, an anti-inflammatory macrophage marker) (fig. S4B). Induced *RNF41* expression has previously been associated with anti-inflammatory macrophage polarization (*14*). Anti-inflammatory macrophages produce high amounts of MMPs to degrade ECM proteins such as collagen (*27*). Because this collagenase activity of anti-inflammatory macrophages might be beneficial for the treatment of liver fibrosis, we tested the capacity of macrophages treated with pRNF41-DGNPs to digest collagen using FITC-gelatin. RAW 264.7 macrophages seeded on FITC-gelatin–coated plates and treated with pRNF41-DGNPs for 5 days displayed a black halo and green nuclear staining due to collagen digestion

and *EGFP* expression, respectively (Fig. 2H). FITC released during the gelatinase assay revealed that collagen degradation rapidly increased because of pRNF41-DGNPs 3 days after incubation only when TNF-α was present, because collagen degradation was much lower in the absence of inflammatory stimulus (Fig. 2I). This functional experiment was the rationale for our administration schedule of 3 days for in vivo experiments in animals with liver fibrosis using pRNF41-DGNPs.

RNF41 restoration in macrophages orchestrates fibrosis regression and hepatocyte proliferation

We intravenously administered pRNF41-DGNPs or DGNPs with the same plasmid but with an RNF41 scrambled sequence (pSCR-DGNP) every 3 days for a total of 10 days to mice with CCl_4-induced liver fibrosis (Fig. 3A). To determine whether pDNA-DGNPs were incorporated into hepatic inflammatory macrophages, we isolated all hepatic cells from fibrotic mice 24 hours after receiving pSCR-DGNPs. We mainly found an intense fluorescence signal in $CD11b^+$ macrophages corresponding to the plasmid EGFP reporter and a negligible signal in hepatocytes, HSCs, and LSECs (Fig. 3B). This was confirmed via visualization of hepatic $EGFP^+$ cells in fibrotic mice treated with pSCR-DGNPs. We found high intracellular EGFP abundance specifically in Ly6c-stained inflammatory macrophages (an inflammatory surface marker of macrophages in transition from monocytes) (Fig. 3, C and D). These $EGFP^+$ inflammatory macrophages lacked CD206 all along the fibrotic tracts in fibrotic livers (Fig. 3, E and F). In contrast, we mainly observed macrophages expressing both EGFP and CD206 in liver fibrotic tracts from animals treated with pRNF41-DGNPs (Fig. 3, G and H). The presence of functional pSCR-DGNP was negligible in other organs such as the kidney (Fig. 3I) and low in the spleen (Fig. 3J) and the lung (Fig. 3K) from fibrotic animals, denoting the selectivity of these nanoparticles for inflammatory and scar-associated macrophages present in injured livers. Negative controls for these immunofluorescence stainings can be found in fig. S5.

Macrophage expression of *RNF41* was substantially reduced in animals with fibrosis treated with pSCR-DGNPs compared with control mice receiving corn oil and restored to physiological amounts after pRNF41-DGNP exposure (Fig. 4A). The first hepatic effect of macrophage *RNF41* recovery after plasmid administration was visually appreciated as a change in the macroscopic aspect of fibrotic liver from micronodular pathology to a nonfibrotic liver appearance (Fig. 4B). Rescue of *RNF41* expression in macrophages of fibrotic liver promoted an 86% reduction in the hepatic fibrosis area and a recovery of physiological parenchymal structure (Fig. 4C), along with a diminished abundance of hydroxyproline (Fig. 4D). This decrease in the collagen fibers in the fibrotic liver was associated with decreased *collagen-I* expression (fig. S6A) and mitigated HSC activity, as illustrated by reduced expression and presence of α–smooth muscle actin (α-SMA) (fig. S6B) and tissue inhibitor of metalloproteinases-1 (TIMP-1) (fig. S6C). These beneficial antifibrotic effects translated into substantially reduced liver injury (Fig. 4E and fig. S6D).

Inflammatory macrophages stimulate HSC activation and subsequent fiber production during liver fibrosis through the synthesis and release of agents such as oncostatin M (*OSM*), platelet-derived growth factor-BB (*PDGF-BB*), and transforming growth factor–β (*TGF-β*) (*28*, *29*). Accordingly, it is consistent that pRNF41-DGNPs promoted a substantial reduction in hepatic *OSM* (fig. S7A), *PDGF-BB* (fig. S7B), and *TGF-β* expression (fig. S7C), indicating that macrophage RNF41 hinders ECM excessive production in fibrosis though the down-regulation of major macrophage-derived signals involved in HSC activation. RNF41 not only promoted the synthesis of HSC-inhibitory factors in macrophages but also macrophage overproduction of the collagenase *MMP-9* to boost collagenous fiber digestion (fig. S8A). Fibrotic tracts spatially limit hepatocyte expansion. The reduction in these collagenous chains in the livers of fibrotic mice treated with pRNF41-DGNPs was associated with an increase in proliferating cell nuclear $antigen^+$ ($PCNA^+$) cells (Fig. 4F), most of which corresponded to proliferating hepatocytes (fig. S8B). This promoted the liver mass repair observed in scarred fibrotic livers from mice treated with pRNF41-DGNPs (fig. S8C).

We then wondered whether major trophic factors might be also directly involved in the hepatocyte proliferation induced by macrophage RNF41 recovery. Hepatocyte growth factor (*HGF*; the main hepatocyte proliferative factor) was not affected by pRNF41-DGNPs in fibrotic mice, but insulin-growth factor 1 (*IGF-1*) expression was up-regulated in the livers of these animals (Fig. 4G). IGF-1 is related to hepatocyte proliferation and HSC inactivation (*30*, *31*). For this reason, we hypothesized that IGF-1 synthesized by macrophages treated with pRNF41-DGNPs might be directly associated with the effects observed in hepatocyte proliferation and HSC activation. To test this hypothesis, we incubated hepatocytes isolated from mouse livers with conditioned medium from macrophages stimulated with pRNF41-DGNPs, pSCR-DGNPs, or DGNPs containing a plasmid with an inhibitory shRNF41 (shRNF41-DGNPs) in the presence or absence of a specific antibody against IGF-1. Only conditioned medium from macrophages treated with pRNF41-DGNPs stimulated hepatocyte proliferation similar to fetal bovine serum (FBS) (10%), and this proliferative induction was reduced with the addition of an antibody blocking IGF-1 effects (Fig. 4H). We also tested the possible effects of macrophage RNF41-induced IGF-1 production on LX-2 human HSC activation using the same conditioned medium and experimental conditions. Conditioned medium from macrophages treated with TNF-α and pSCR-DGNPs up-regulated HSC expression of *collagen I* (fig. S9A), α-*SMA* (fig. S9B), and *TIMP-1* (fig. S9C), which was abolished by the treatment with pRNF41-DGNPs and then recovered when IGF-1 was blocked with a specific antibody.

Anti-inflammatory macrophages may influence the response of HSCs, endothelial cells, and other immune cells to injury (*32*). To investigate whether *RNF41* restoration was related to the hepatic macrophage phenotype, we quantified gene expression of proinflammatory and anti-inflammatory macrophage markers in fibrotic livers from animals treated with either pSCR-DGNPs or pRNF41-DGNPs. We found a quantitative increase in anti-inflammatory markers *ARG1*, *MRC1*, and *RETNLA* and a decrease in proinflammatory markers *NOS2*, *COX-2*, and *IL-1β* in liver tissue and isolated $CD11b^+$ macrophages, which denoted that this *RNF41*-restorative gene therapy switched proinflammatory to anti-inflammatory macrophages in fibrotic livers (Fig. 4I and fig. S10D). It is known that peroxisome proliferator–activated receptor γ (PPAR-γ) activation triggers macrophages into an alternative anti-inflammatory phenotype (*33*). We quantified the expression of both downstream PPAR-γ target genes *IL-10* and *CD36* in fibrotic livers from animals treated with either pSCR-DGNPs or pRNF41-DGNPs. Induced macrophage *RNF41* expression stimulated the expression of *IL-10* (fig.

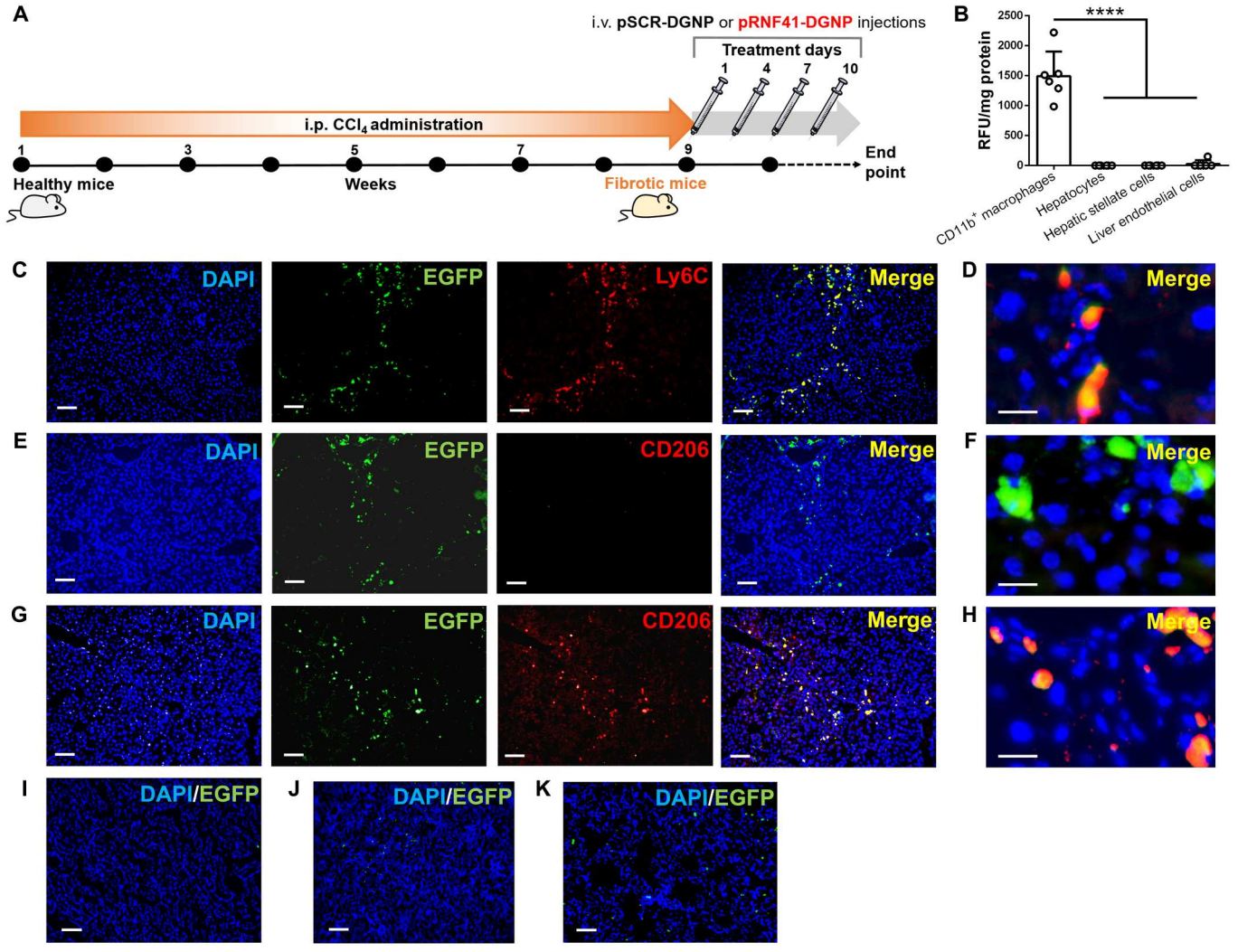

Fig. 3. Dendrimer-graphite nanoparticles efficiently and selectively transfect a *RNF41*-encoding plasmid into macrophages recruited to mouse fibrotic liver. (**A**) Schematic figure illustrating the time points of fibrosis induction with CCl_4 and the administration schedule of dendrimer-graphite nanoparticles linked to plasmid pRNF41 (pRNF41-DGNPs) or scrambled pSCR (pSCR-DGNPs). (**B**) Relative fluorescence units (RFU) of EGFP per milligram of protein of liver isolated $CD11b^+$ macrophages, hepatocytes, hepatic stellate cells, and liver endothelial cells from mice treated with pSCR-DGNPs ($n = 6$). (**C**) Immunofluorescence (IF) staining for Ly6C and simultaneous detection of EGFP fluorescence in the livers of fibrotic mice treated with pSCR-DGNPs. (**D**) High-power image for Ly6C and simultaneous detection of EGFP fluorescence in the livers of fibrotic mice treated with pSCR-DGNPs. (**E**) IF staining for CD206 and simultaneous detection of EGFP fluorescence in the livers of fibrotic mice treated with pSCR-DGNPs. (**F**) High-power image for CD206 and simultaneous detection of EGFP fluorescence in the liver of fibrotic mice treated with pSCR-DGNPs. (**G**) IF staining for CD206 and simultaneous detection of EGFP fluorescence in the livers of fibrotic mice treated with pRNF41-DGNPs. (**H**) High-power image for CD206 and simultaneous detection of EGFP fluorescence in the livers of fibrotic mice treated with pRNF41-DGNPs. (**I**) EGFP fluorescence in the kidneys of fibrotic animals treated with pSCR-DGNPs. (**J**) EGFP fluorescence in the spleens of fibrotic animals treated with pSCR-DGNPs. (**K**) EGFP fluorescence in the lungs of fibrotic mice treated with pSCR-DGNPs. All plasmids constitutively expressed *EGFP* under the control of a CMV promoter. Scale bars, 200 μm (C, E, G, I, J, and K) and 20 μm (D, F, and H). For (B), $^{****}P \leq 0.0001$ versus $CD11b^+$ macrophages using a one-way analysis of variance (ANOVA) with the posthoc Newman-Keuls test. i.p., intraperitoneal; i.v., intravenous.

S11A) and *CD36* (fig. S11B) in fibrotic liver, denoting increased PPAR-γ activation. Last, we validated the therapeutic effects of pRNF41-DGNPs in a second model of liver fibrosis based on intraperitoneal injections of thioacetamide (TAA) (fig. S12A). Livers from fibrotic animals treated with pRNF41-DGNPs displayed a nonfibrotic liver appearance (fig. S12B), a substantial reduction in the fibrosis area (fig. S12C), HSC-related gene expression (fig. S12D), hepatic damage (fig. S12E), macrophage profibrotic genes (fig. S12F), and proinflammatory markers (fig. S12G), along with a substantial increase in anti-inflammatory markers (fig. S12H), liver mass repair (fig. S12I) and *IGF-1* expression (fig. S12J).

Macrophage *RNF41* depletion aggravates inflammation and hepatic damage and reduces survival

Either pshRNF41-DGNPs or pshSCR-DGNPs were intravenously administered to mice with liver fibrosis every 3 days for a total of 10 days (Fig. 5A). *RNF41* expression was considerably reduced in macrophages isolated from fibrotic mice treated with pshRNF41-DGNPs (Fig. 5B). The first observable effect of *RNF41* depletion

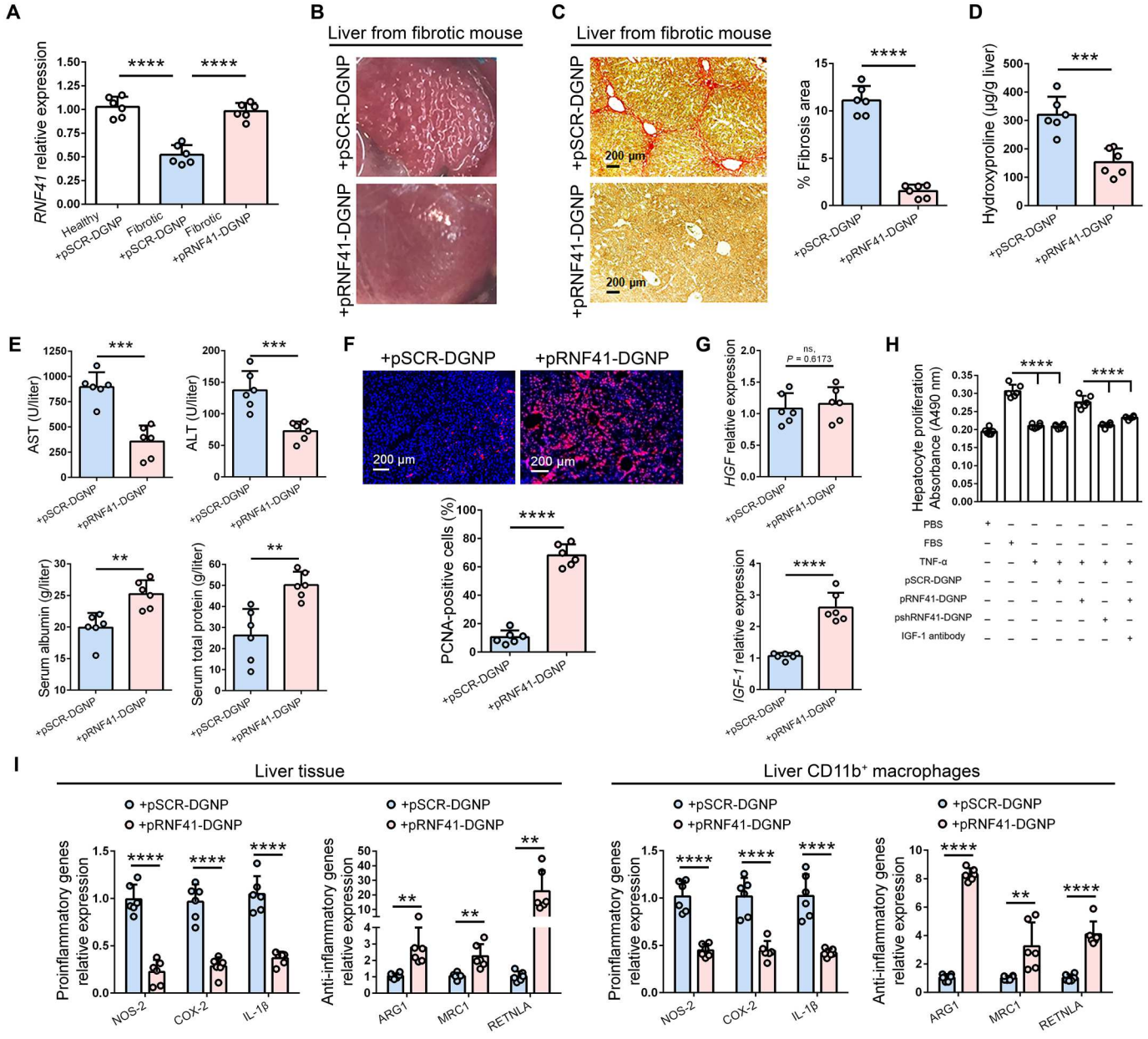

Fig. 4. *RNF41* restoration in macrophages located into the fibrotic liver orchestrates fibrosis and inflammation regression and reduction of hepatic injury in mice. (**A**) *RNF41* abundance in healthy and fibrotic mice treated with dendrimer-graphite nanoparticles linked to plasmid pRNF41 (pRNF41-DGNPs) or scrambled pSCR (pSCR-DGNPs). (**B**) Macroscopic aspect of fibrotic liver after treatment with pRNF41-DGNPs. (**C** to **G**) Sirius Red staining and quantification of liver fibrosis area (C), hydroxyproline measurements (D), serum liver injury parameters [ALT (alanine aminotransferase), AST (aspartate aminotransferase), serum albumin, and serum total protein] (E), hepatic PCNA immunofluorescence staining (F), and hepatic expression of *HGF*and *IGF-1* (G) in fibrotic mice treated with pSCR-DGNPs or pRNF41-DGNPs. (**H**) Cell proliferation in isolated mouse hepatocytes treated for 24 hours with conditioned medium from RAW 264.7 cultures treated with FBS, TNF-α, pSCR-DGNPs, pRNF41-DGNPs, or IGF-1 antibody for 3 days. Experiments were performed in triplicates in two independent experiments. (**I**) Expression of proinflammatory and anti-inflammatory genes in liver tissue and in CD11b$^+$ macrophages isolated from the livers of fibrotic mice treated with pSCR-DGNPs or pRNF41-DGNPs. $n = 6$ animals per group. Student's t test was used for (A), (C) to (G), and (I), and a one-way ANOVA with posthoc Newman-Keuls test was used for (H). Data are shown as means ± SD. $^{**}P \leq 0.01$, $^{***}P \leq 0.001$, and $^{****}P \leq 0.0001$.

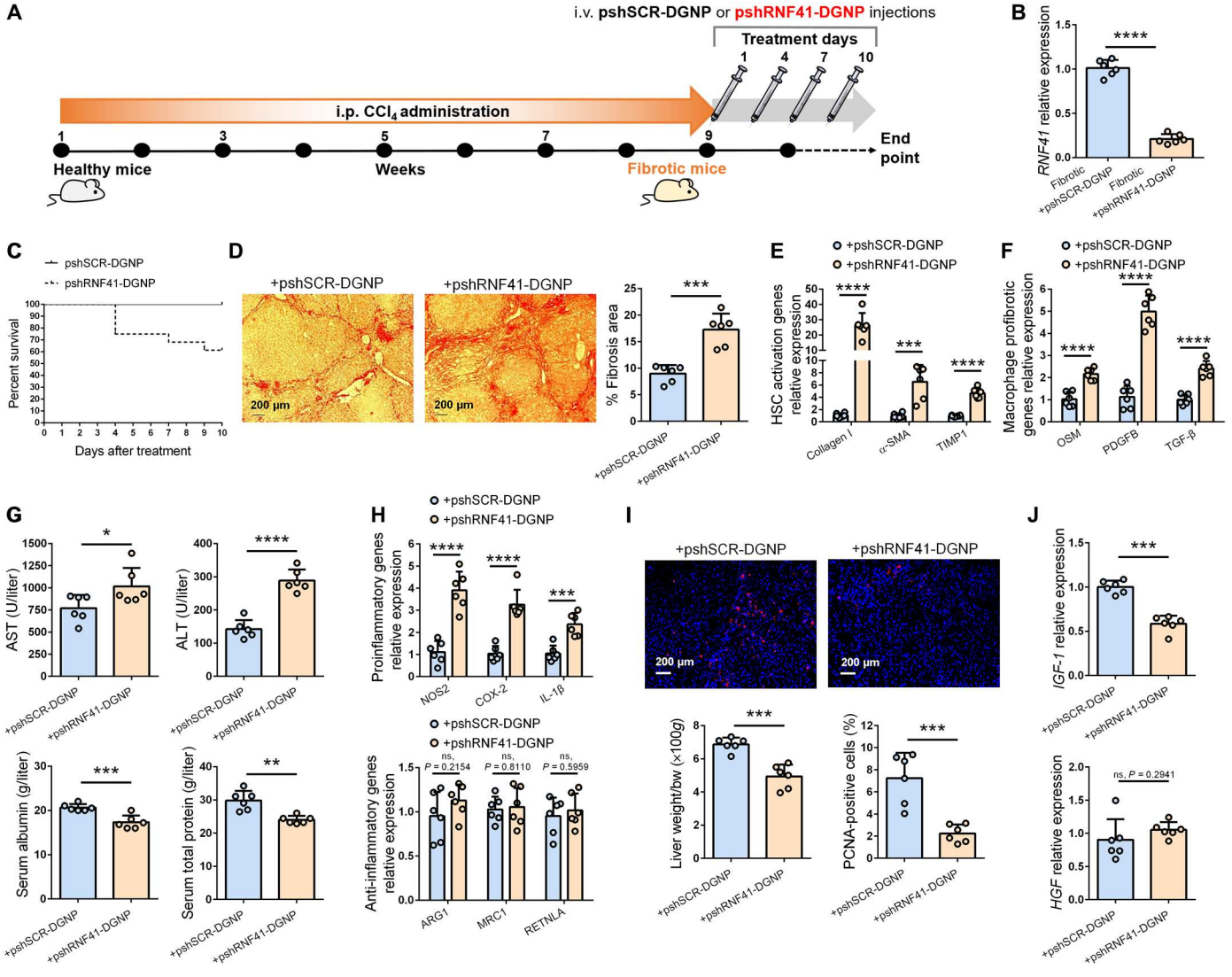

Fig. 5. Depletion of macrophage *RNF41* worsens fibrosis, inflammation, and hepatic damage in mice with liver fibrosis. (**A**) Schematic figure illustrating time points of fibrosis induction with CCl_4 and administration schedule of dendrimer-graphite nanoparticles linked to pshSCR (pshSCR-DGNPs) or pshRNF41 (pshRNF41-DGNPs). (**B** and **C**) Hepatic gene expression of *RNF41* (B) and survival rate (C) of fibrotic mice treated with pshSCR-DGNPs or pshRNF41-DGNPs. (**D** to **J**) Sirius red staining (D), gene expression related to hepatic stellate cell (HSC) activation (E) or profibrogenic agents produced by liver-resident macrophages (F), serum parameters of liver injury (ALT, AST, serum albumin, and serum total protein) (G), expression of inflammatory and anti-inflammatory macrophage genes (H), PCNA immunofluorescence staining (I), and *HGF* and *IGF-1* expression (J) in liver of fibrotic mice treated with pshSCR-DGNPs or pshRNF41-DGNPs. $n = 6$ per group of animals. $^{*}P \leq 0.05$, $^{**}P \leq 0.01$, $^{***}P \leq 0.001$, and $^{****}P \leq 0.0001$ using Student's t test. Data are shown as means ± SD.

was a considerable decrease in survival (Fig. 5C). Collagen fiber staining revealed an increase in fibrosis area in mice receiving pshRNF41-DGNPs (Fig. 5D). This was associated with HSC hyperactivation, as indicated by the increase in *collagen I*, α-*SMA*, and *TIMP-1* (Fig. 5E). Treatment with pshRNF41-DGNPs promoted an increase in hepatic abundance of the macrophage-derived HSC activators *OSM*, *PDGF-BB*, and *TGF*-β (Fig. 5F). Liver injury was also enhanced in fibrotic animals treated with pshRNF41-DGNPs in comparison with fibrotic mice receiving pshSCR-DGNPs (Fig. 5G). These detrimental effects of pshRNF41-DGNP treatment were associated with a further increase in proinflammatory macrophage-derived inflammatory cytokines without affecting anti-inflammatory macrophage genes (Fig. 5H). This exacerbated inflammation resulted in lower hepatocyte proliferation and liver mass repair (Fig. 5I), effects associated with a decrease in *IGF-1* abundance (Fig. 5J). No changes in *HGF* were observed (Fig. 5J).

RNF41 induction promotes hepatic regeneration after hepatectomy

We wondered whether induction of macrophage *RNF41* could also be beneficial in the context of liver resection. Administration of pRNF41-DGNPs to healthy mice undergoing 70% hepatectomy (Fig. 6A) showed greater hepatic restoration than animals receiving pSCR-DGNPs (Fig. 6B). This effect was associated with a higher hepatic proliferative signal, highlighted by the increase in $PCNA^{+}$ cells (Fig. 6C). However, treatment with pRNF41-DGNPs did not

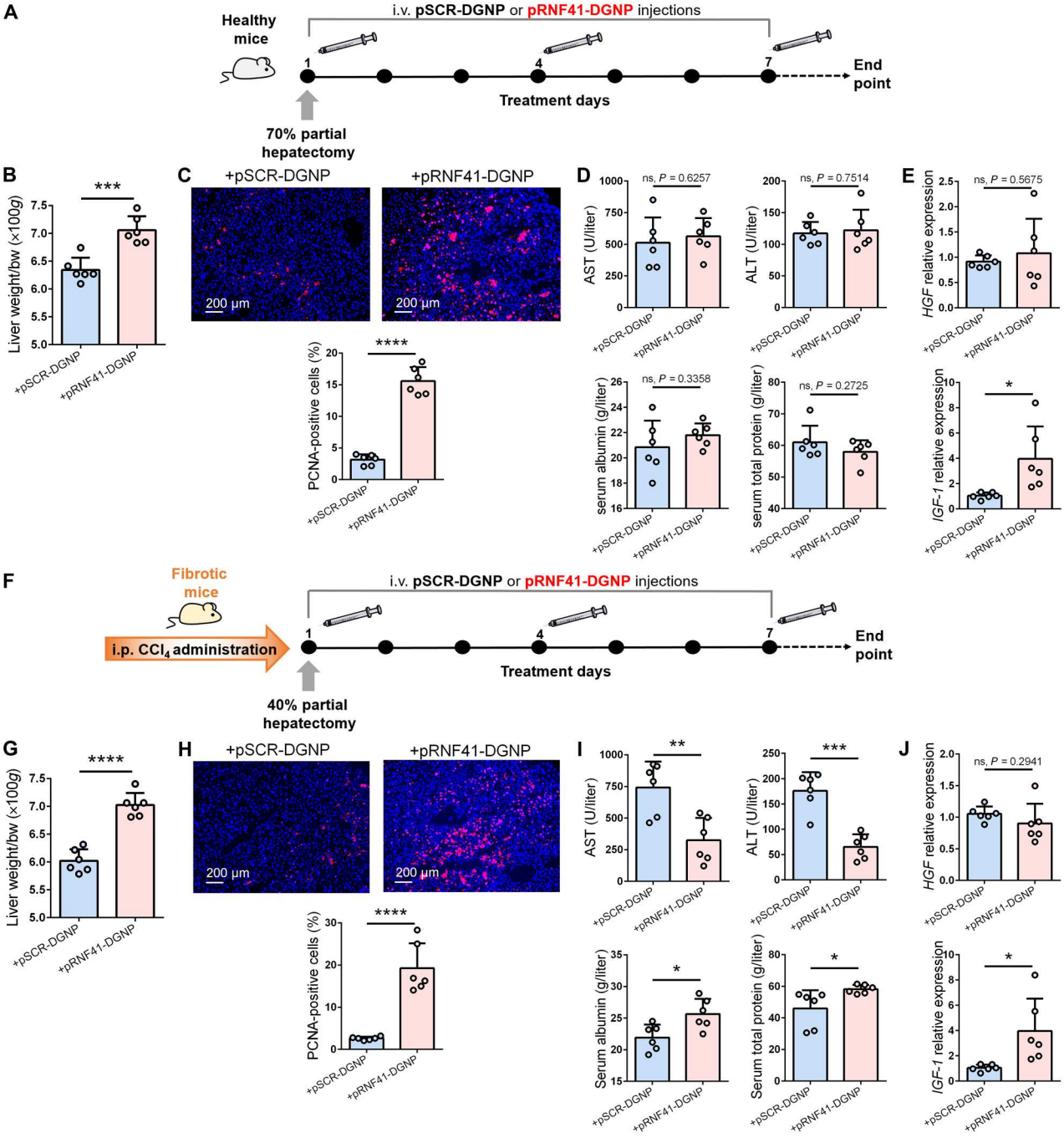

Fig. 6. Macrophage *RNF41* induces liver regeneration after hepatectomy. (**A**) Schematic figure illustrating 70% hepatectomy in healthy mice and administration schedule of dendrimer-graphite nanoparticles linked to pRNF41 (pRNF41-DGNPs) or pSCR (pSCR-DGNPs). (**B** to **E**) Liver restoration rate (B), PCNA immunofluorescence staining (C), serum liver injury parameters [ALT, AST, serum albumin, and serum total protein] (D), and *HGF* and *IGF-1* expression (E) in healthy mice undergoing 70% hepatectomy and treated with pSCR-DGNPs or pRNF41-DGNPs. (**F**) Schematic figure illustrating the time points of fibrosis induction with CCl_4, 40% hepatectomy in fibrotic mice, and the administration schedule of pSCR-DGNPs or pRNF41-DGNPs. (**G** to **J**) Liver restoration rate (G), PCNA immunofluorescence staining (H), serum liver injury parameters (ALT, AST, serum albumin, and serum total protein) (I), and expression of *HGF* and *IGF-1* in the livers of fibrotic mice undergoing 40% hepatectomy and treated with pSCR-DGNPs or pRNF41-DGNPs. $n = 6$ animals per group. *$P \leq 0.05$, **$P \leq 0.01$, ***$P \leq 0.001$, and ****$P \leq 0.0001$ using Student's t test. Data are shown as means ± SD.

reduce hepatocyte damage caused by liver resection, because no changes in serum transaminases, albumin, or proteins were observed compared with animals receiving pSCR-DGNPs (Fig. 6D). In line with the outcomes in fibrotic mice, hepatectomized mice receiving pRNF41-DGNPs did not show up-regulation of *HGF* but did show more abundant *IGF-1* (Fig. 6E) concomitant with increased expression of hepatic PPAR-γ target genes *IL-10* and *CD36* (fig. S11, C and D).

Fibrotic mice operated for 40% hepatectomy and administered pRNF41-DGNPs (Fig. 6F) also displayed a higher liver restoration rate than animals receiving pSCR-DGNPs (Fig. 6G). This effect was proportional with an elevated hepatic proliferative signal demonstrated by the rise in $PCNA^+$ cells (Fig. 6H). In this case, treatment with pRNF41-DGNPs did reduce liver injury (Fig. 6I). In agreement with outcomes in fibrotic mice, hepatectomized mice treated with pRNF41-DGNPs did not display up-regulation of *HGF* but did show higher *IGF-1* (Fig. 6J). Treatment with pRNF41-DGNPs also promoted an increased expression of hepatic PPAR-γ target genes *IL-10* and *CD36* in hepatectomized fibrotic animals (fig. S11, E and F).

DISCUSSION

We sought to determine whether emerging concepts on macrophage RNF41 function are applicable to chronic liver disease and translatable to humans. By examining isolated hepatic macrophages in specimens obtained from cirrhotic patients and mice with liver fibrosis, we tested the hypothesis that macrophage *RNF41* expression is altered in chronic liver disease. We demonstrated that *RNF41* expression is negatively regulated in macrophages isolated from the liver specimens of both states of liver fibrosis: cirrhosis in patients and fibrosis in mice. Our data reveal that sustained inflammatory signals from TNF-α promote down-regulation of macrophage *RNF41* and its stabilizer *USP8*. In contrast, short-term TNF-α exposition induces *RNF41* and *USP8* expression in macrophages, as also described using lipopolysaccharide (*13*). This rapid induction is likely driven by Akt phosphorylation, because TNF-α activates Akt independently of NF-κB (*22*), and Akt regulates the function of RNF41 and its stabilizer USP8 (*21*). Down-regulation of *RNF41* and *USP8* expression under long-term TNF-α stimulation is likely due to the continuous and progressive increase in stress-activated MAPK (*23*), the subsequent Erk-induced Akt down-regulation (*34*), and the reciprocal inhibitory effects between RNF41 and Erk (*35*).

This investigation describes the importance of RNF41 in chronic liver injury. However, it is known that mice deficient for the RNF41-stabilizer USP8 are embryonic lethal, and USP8 inactivation in adulthood causes fatal liver failure (*36*). We speculate that part of the harmful hepatic effects caused by USP8 knockdown could be mediated by RNF41 deficiency in macrophages, but there are no conditional and macrophage-specific knockout mice to study this possibility yet. Here, our investigations substantiate that selective macrophage recovery of *RNF41* in the livers of fibrotic animals using pRNF41-DGNPs promotes the switch of hepatic macrophages from a proinflammatory to anti-inflammatory phenotype. This macrophage switch by induced *RNF41* has also been seen in thioglycollate-elicited peritoneal macrophages (*14*). However, the extraordinary complexity of the hepatic niche defines different macrophage subpopulations from health to disease (*37*). Whereas resident Kupffer cells are the major source in the hepatic macrophage pool in homeostasis, monocyte-derived macrophages predominate in acute and chronic liver injury (*38*). Namely, scar-associated macrophages display a profibrogenic profile and expand similarly in cirrhotic patients and in fibrotic mice (*37*). Notably, pRNF41-DGNPs selectively accumulated into these macrophages within fibrotic septae in mouse fibrotic liver and reduced their synthesis of profibrogenic factors such as OSM, PDGF-BB, or TGF-β1 [the most potent profibrogenic cytokine (*39*)]. In contrast, a further *RNF41* reduction with pshRNF41-DGNPs exerted the opposite effect, an increase in HSC-activating factors. This suggests that RNF41 is a central negative modulator of profibrogenic and proinflammatory signals in scar-associated macrophages during chronic liver disease. RNF41 is behaving as a node connecting the mechanisms driving fibrogenesis with those regulating inflammation (fig. S13). Signals coming from macrophages with low *RNF41* expression seem to perpetuate inflammation and fibrosis that ultimately hampers hepatic function recovery. Hepatocyte damage was diminished by macrophage *RNF41* restoration only in mice with chronic liver injury. This shows that macrophage RNF41 activation is not directly involved in hepatocyte protection. Instead, it leads to inflammation and fibrosis resolution, and these homeostatic effects likely allow for the hepatic function recovery.

A previous study described the predominant effect of macrophage RNF41 on the activation of adenosine 3′,5′-monophosphate response element–binding protein-C/EBP-β cascade (*14*), and because the activation of this cascade has been associated with muscle injury repair (*15*), this prompted us to explore the possible role of RNF41 in hepatic repair after liver resection. In this scenario, we demonstrated that *RNF41* induction in macrophages results in faster hepatic regeneration after liver resection in healthy and fibrotic mice. IGF-1 rather than HGF participates in the proregenerative effects derived from macrophage *RNF41* induction. IGF-1 is not only a trophic factor mainly produced by the liver but also delivered by monocytes/macrophages to stimulate tissue growth (*30*). In chronic liver disease, IGF-1 deficiency is a common condition independent of chronic liver damage etiology (*40*). However, IGF-1 has effects beyond proliferation, including inhibition of HSC activation and activity (*31*). We cannot exclude other participants in the therapeutic effects of macrophage *RNF41* induction in liver injury. The PPAR-γ signaling pathway might, for example, link macrophage biology, inflammation, and insulin-related factor biochemistry. This pathway is involved in the nuclear regulation of inflammation, glucose metabolism, and macrophage phenotype (*33*). Because RNF41 activates C/EBP-β (*14*) and the latter is a PPAR-γ inducer (*41*), this may explain the macrophage phenotype switch observed in fibrotic animals treated with pRNF41-DGNPs. Our findings then combine macrophage RNF41 activation and its downstream phenotypic effects on inflammation, fibrosis, and tissue regeneration, expanding our understanding of the relationship between RNF41, PPAR-γ, and IGF-1 with respect to chronic liver injury and hepatic regeneration. It has long been thought that inflammation is necessary to promote tissue repair and that the mechanisms driving fibrogenesis are distinct from those regulating inflammation; however, we suggest a slightly different paradigm where RNF41 may behave as a central regulator of macrophage behavior, balancing both inflammatory and fibrogenic signals toward tissue repair.

Several limitations and open questions remain. First, human THP-1 cells were used as an alternative to primary human macrophages because of the difficulty of obtaining enough viable primary cells from small control biopsies for experiments involving prolonged incubation with TNF-α. Therefore, other advanced approaches such as precision-cut liver slices or perfusable three-dimensional liver-on-a-chip models are required to better understand the effects of inflammatory factors such as TNF-α on the regulation of RNF41 in human macrophages. Second, the precise role of IGF-1 on the effects driven by macrophage *RNF41* induction needs further investigation to depict the mechanistic link between these two proteins. Third, specific deletion of RNF41 in macrophages would solidify its role in fibrosis resolution and hepatic regeneration. Macrophage-specific conditional gene knockout mice for *RNF41* are still needed to study all the potential downstream effects modulated by macrophage RNF41.

In conclusion, our findings provide evidence that RNF41 may be an immune regulatory node that regulates the response of macrophages to restore homeostasis after tissue injury—down-regulated in chronic liver injury in mice and humans. Therapeutics targeting macrophage RNF41 may represent a therapeutic target for patients with chronic liver disease characterized by inflammation and fibrosis.

MATERIALS AND METHODS

Study design

This study aimed to evaluate *RNF41* expression in macrophages from livers of cirrhotic patients and fibrotic mice and to analyze the influence of macrophage RNF41 modulation in the balance of hepatic fibrosis and repair in response to the inflammatory milieu. To achieve these objectives, we first quantified *RNF41* gene expression in $CD11b^+$ macrophages isolated from the livers of patients with cirrhosis and BALB/c fibrotic mice using a multistep protocol of magnetic-activated cell sorting. We also designed macrophage-selective gene therapy with DGNPs to explore the influence of macrophage RNF41 in liver fibrosis and regeneration. In addition, we designed in vitro studies to explore how macrophage RNF41 influences other hepatic cells to regulate fibrosis and regeneration. Patients (n = 12) with decompensated liver cirrhosis and MELD scores between 13 and 30 from the hospital Clinic of Barcelona were enrolled in this study. Healthy participant samples (n = 8) with normal liver histology were used as controls. For animal studies, we used littermates as much as possible and randomized them in diseased or healthy groups. The study was performed according to the criteria of the Investigation and Ethics Committees of the Hospital Clínic and University of Barcelona and according to Animal Research: Reporting of In Vivo Experiments (ARRIVE) guidelines. Two models of mouse liver fibrosis were performed with intraperitoneal injections of CCl_4 diluted 1:8 (v/v) in corn oil or TAA (200 mg/kg) twice a week for 9 weeks. Mouse models of partial hepatectomy (70% in healthy and 40% in fibrotic mice induced with CCl_4) were also performed. Dispersions of macrophage-selective plasmid-DGNPs were intravenously injected to regulate *RNF41* gene expression. We determined sample size for each experimental group on the basis of our experience with similar studies. The sample size (n) of each experimental group (n = 6) is indicated in the figure legends. For cell culture studies, a minimum of three experimental replicates were performed (exact number of replicates is presented in figure legends).

Human specimens

All protocols conformed to the ethical guidelines of the 1975 Declaration of Helsinki and were approved by the Ethics Committee of the Hospital Clinic of Barcelona. All the patients included in this study provided written and signed informed consent. Human normal liver samples were obtained from small biopsies from donor liver lobules during transplantation (n = 8). All participants had normal hepatic histology and no declared acute or chronic diseases. Human cirrhotic liver samples were obtained from liver explants of patients with end-stage cirrhosis caused by liver disease (n = 12) undergoing liver transplantation.

Animals and in vivo procedures

Male BALB/c mice (7 weeks old) were purchased from Charles River Laboratories (Charles River). All animals were maintained in a temperature-controlled room (22°C) on a 12-hour light-dark cycle. After arrival, mice were continuously fed ad libitum until euthanasia. To induce liver fibrosis, mice were injected intraperitoneally twice a week with CCl_4 diluted 1:8 (v/v) in corn oil for 9 weeks. A second fibrosis mouse model was generated with intraperitoneal injections of TAA (200 mg/kg) twice a week for 9 weeks. Dispersions of plasmid-DGNPs were then intravenously injected (50 μg/kg in a ratio plasmid/DGNP, 1:10) every 3 days for 9 days (four injections in total). Animals were euthanized on day 10 after the start of treatment. Liver samples and serum were collected and frozen for further analysis. Serum parameters were measured using a BS-200E Chemistry Analyzer (Mindray Medical international Ltd.).

Partial hepatectomy (70% in healthy and 40% in fibrotic mice) was performed as previously described (*42*). Hepatectomy was performed at 40% in fibrotic mice to avoid unnecessary animal losses of these already diseased animals according to the criteria of the Investigation and Ethics Committees of the Hospital Clínic and University of Barcelona. Dispersions of plasmid-DGNP were intravenously injected to hepatectomized animals, which were euthanized 7 days after hepatectomy to obtain and analyze tissue and serum samples as described above.

Isolation of hepatic $CD11b^+$-macrophages, stellate cells, and hepatocytes

Freshly isolated primary hepatic $CD11b^+$ macrophages were obtained from the livers of control and cirrhotic patients and from the livers of healthy mice (control) receiving corn oil and fibrotic mouse. Briefly, hepatocytes, macrophages and HSCs were purified after collagenase A (Roche Diagnostics) administration via retrograde perfusion in mice or via an intravenous catheter in human liver samples and subsequent Histodenz gradient (Sigma-Aldrich). Purification was optimized using magnetic beads (magnetic-activated cell sorting system, Miltenyi Biotec) with a modified protocol previously reported (*43*, *44*). First, the gradient fraction corresponding to polymorphonuclear cells was purified using Ly6G (R&D Systems, reference: 25872-1-AP) and PDCA-1 (Invitrogen, reference: PA5-23505) antibodies in mouse and CD15 (R&D Systems, reference: MAB7368) and BDCA-1 (R&D Systems, reference: AF5910) antibodies in human with MACS to remove neutrophils and dendritic cells, respectively. Then, the remaining eluted fraction was incubated with CD11b magnetic beads (Miltenyi

Biotec, reference: 130-049-601), and MACS-purified $CD11b^+$ macrophages were resuspended in TRIzol (Gibco-Invitrogen) for total RNA extraction or in Dulbecco's modified Eagle's medium supplemented with FBS (1%) for prolonged inflammation assays. A 0.5-μg aliquot of total RNA was reverse-transcribed using a complementary DNA synthesis kit (High-Capacity cDNA Reverse Transcription Kit, Applied Biosystems) for further analysis of gene expression using real-time polymerase chain reaction.

Synthesis and functionalization of DGNPs

Carbon GNPs were supplied by Graphene Supermarket. The Generation 5 PAMAM dendrimer was purchased from Dendritech Inc. Scrambled *RNF41* or shRNF41 expression plasmids (fig. S2) were obtained from Cyagen Biosciences. One Shot Top 10 Chemically Competent *Escherichia coli* and the QIAGEN Endofree Plasmid Maxi Kit, used for transformation, amplification, and purification of ultrapure, transfection-grade plasmid DNA, were purchased from Thermo Fisher Scientific Inc. and QIAGEN Inc., respectively. Luria broth (LB broth) and LB agar ampicillin-100 plates for bacterial selection were obtained from Sigma-Aldrich. Deionized water was obtained from a Milli-Q water purification system (Millipore). GNPs were dispersed in deionized water (500 μg/ml) and oxidized using a modified Hofmann method (68% HNO_3/96% H_2SO_4 at a 3:1 ratio in the presence of 70 μM $KClO_3$) in continuous magnetic stirring for 96 hours. Dispersion was then neutralized with NaOH until reaching pH 7 and centrifuged at 21,000*g* for 30 min. Supernatant with small graphene oxide sheets was discarded, and graphite oxide nanoparticles were washed four times with distilled water and centrifuged at 21,000*g* for 30 min. Oxidized GNPs were separated by incubating the dispersion in an ultrasound bath (Selecta) at a frequency of 50 kHz and a potency of 360 W for 15 min. Afterward, 100 μl of GNPs were mixed with 900 μl of EDC/*N*-hydroxysuccinimide (1 mg/ml; 1:1) containing 30 μl of PAMAM dendrimer 25% (v/v) and incubated for 2 hours in the ultrasound bath at a constant temperature (25° ± 2°C). Then, dispersions were centrifuged at 21,000*g* for 10 min and washed three times with PBS for subsequent in vitro and in vivo experiments. Plasmids were incubated with dispersions of DGNP in a ratio of 1:10 for 2 hours in a rotatory shaker, centrifuged, and washed three times with PBS before use for transfection and functional assays. The ratio of plasmid/nanoparticles was established using the variations in zeta potential from positive (DGNP) to negative charge, when coating with plasmid, and evaluated with a Zetasizer Nano ZS (Malvern Instruments Ltd.).

Collagen degradation assay

Gelatin and FITC were obtained from Sigma-Aldrich. The preparation of FITC-conjugated gelatin and the quantitative analysis of collagen degradation assay were performed as previously described (*16*). Briefly, gelatin was dissolved (1 mg/ml) in a buffer containing 61 mM NaCl and 50 mM $Na_2B_4O_7$ (pH 9.3) and then incubated at 37°C for 1 hour. After this incubation period, FITC was added (2 mg/ml) and mixed for 2 hours in complete darkness. This mixture was then dialyzed at room temperature in PBS in complete darkness for 4 days with two or three PBS changes per day. After a quick spin to remove insoluble material, small aliquots were stored in the dark at 4°C. FITC-conjugated gelatin-coated plates were prepared covering the surface of each well with FITC-gelatin and fixed with 1 drop of 0.5% ice-cold formaldehyde in PBS at 4°C for 15 min. Wells were then gently washed three times with PBS and lastly quenched in complete medium for 1 hour at 37°C. Cells were cultured for variable lengths of time up to 7 days, and supernatants were collected. Cells were fixed, washed, and stained with mounting medium containing 4′,6-diamidino-2-phenylindole (DAPI) and visualized with an epifluorescence microscope. Supernatants were centrifuged and fluorescence was quantified with a Hitachi F-2500 Fluorescence Spectrophotometer (Hitachi High Technologies Corp.).

Statistical analysis

All data were expressed as means ± SD. Statistical analysis of the results was performed by one-way analysis of variance (ANOVA) with the post hoc Newman-Keuls test or by Student's *t* tests, where appropriate (GraphPad Prism v6.0a). Data were tested for assumptions before the use of these statistical tests. Differences were considered statistically significant at $P < 0.05$.

Supplementary Materials

This PDF file includes:
Materials and Methods
Figs. S1 to S13
Tables S1 and S2

Other Supplementary Material for this manuscript includes the following:
Data file S1
MDAR Reproducibility Checklist

View/request a protocol for this paper from *Bio-protocol*.

REFERENCES AND NOTES

1. S. K. Asrani, H. Devarbhavi, J. Eaton, P. S. Kamath, Burden of liver diseases in the world. *J. Hepatol.* **70**, 151–171 (2019).
2. P. Melgar-Lesmes, E. R. Edelman, Monocyte-endothelial cell interactions in the regulation of vascular sprouting and liver regeneration in mouse. *J. Hepatol.* **63**, 917–925 (2015).
3. P. Melgar-Lesmes, M. Balcells, E. R. Edelman, Implantation of healthy matrix-embedded endothelial cells rescues dysfunctional endothelium and ischaemic tissue in liver engraftment. *Gut* **66**, 1297–1305 (2017).
4. D. Oro, T. Yudina, G. Fernandez-Varo, E. Casals, V. Reichenbach, G. Casals, B. González de la Presa, S. Sandalinas, S. Carvajal, V. Puntes, W. Jiménez, Cerium oxide nanoparticles reduce steatosis, portal hypertension and display anti-inflammatory properties in rats with liver fibrosis. *J. Hepatol.* **64**, 691–698 (2016).
5. B. Cordoba-Jover, A. Arce-Cerezo, J. Ribera, M. Pauta, D. Oró, G. Casals, G. Fernández-Varo, E. Casals, V. Puntes, W. Jiménez, M. Morales-Ruiz, Cerium oxide nanoparticles improve liver regeneration after acetaminophen-induced liver injury and partial hepatectomy in rats. *J. Nanobiotechnol.* **17**, 112 (2019).
6. S. J. Forbes, N. Rosenthal, Preparing the ground for tissue regeneration: From mechanism to therapy. *Nat. Med.* **20**, 857–869 (2014).
7. T. Tsuchida, S. L. Friedman, Mechanisms of hepatic stellate cell activation. *Nat. Rev. Gastroenterol. Hepatol.* **14**, 397–411 (2017).
8. C. Trautwein, S. L. Friedman, D. Schuppan, M. Pinzani, Hepatic fibrosis: Concept to treatment. *J. Hepatol.* **62**, S15–S24 (2015).
9. C. Sole, E. Sola, M. Morales-Ruiz, G. Fernàndez, P. Huelin, I. Graupera, R. Moreira, G. de Prada, X. Ariza, E. Pose, N. Fabrellas, S. G. Kalko, W. Jiménez, P. Ginès, Characterization of inflammatory response in acute-on-chronic liver failure and relationship with prognosis. *Sci. Rep.* **6**, 32341 (2016).
10. P. Ramachandran, A. Pellicoro, M. A. Vernon, L. Boulter, R. L. Aucott, A. Ali, S. N. Hartland, V. K. Snowdon, A. Cappon, T. T. Gordon-Walker, M. J. Williams, D. R. Dunbar, J. R. Manning, N. van Rooijen, J. A. Fallowfield, S. J. Forbes, J. P. Iredale, Differential Ly-6C expression identifies the recruited macrophage phenotype, which orchestrates the regression of murine liver fibrosis. *Proc. Natl. Acad. Sci. U.S.A.* **109**, E3186–E3195 (2012).

11. F. Moroni, B. J. Dwyer, C. Graham, C. Pass, L. Bailey, L. Ritchie, D. Mitchell, A. Glover, A. Laurie, S. Doig, E. Hargreaves, A. R. Fraser, M. L. Turner, J. D. M. Campbell, N. W. A. McGowan, J. Barry, J. K. Moore, P. C. Hayes, D. J. Leeming, M. J. Nielsen, K. Musa, J. A. Fallowfield, S. J. Forbes, Safety profile of autologous macrophage therapy for liver cirrhosis. *Nat. Med.* **25**, 1560–1565 (2019).
12. J. Wauman, L. De Ceuninck, N. Vanderroost, S. Lievens, J. Tavernier, RNF41 (Nrdp1) controls type 1 cytokine receptor degradation and ectodomain shedding. *J. Cell Sci.* **124**, 921–932 (2011).
13. C. Wang, T. Chen, J. Zhang, M. Yang, N. Li, X. Xu, X. Cao, The E3 ubiquitin ligase Nrdp1 'preferentially' promotes TLR-mediated production of type I interferon. *Nat. Immunol.* **10**, 744–752 (2009).
14. S. Ye, H. Xu, J. Jin, M. Yang, C. Wang, Y. Yu, X. Cao, The E3 ubiquitin ligase neuregulin receptor degradation protein 1 (Nrdp1) promotes M2 macrophage polarization by ubiquitinating and activating transcription factor CCAAT/enhancer-binding protein β (C/EBPβ). *J. Biol. Chem.* **287**, 26740–26748 (2012).
15. D. Ruffell, F. Mourkioti, A. Gambardella, P. Kirstetter, R. G. Lopez, N. Rosenthal, C. Nerlov, A CREB-C/EBPβ cascade induces M2 macrophage-specific gene expression and promotes muscle injury repair. *Proc. Natl. Acad. Sci. U.S.A.* **106**, 17475–17480 (2009).
16. P. Melgar-Lesmes, A. Luquero, M. Parra-Robert, A. Mora, J. Ribera, E. R. Edelman, W. Jiménez, Graphene-dendrimer nanostars for targeted macrophage overexpression of metalloproteinase 9 and hepatic fibrosis precision therapy. *Nano Lett.* **18**, 5839–5845 (2018).
17. X. Wu, L. Yen, L. Irwin, C. Sweeney, K. L. Carraway III, Stabilization of the E3 ubiquitin ligase Nrdp1 by the deubiquitinating enzyme USP8. *Mol. Cell. Biol.* **24**, 7748–7757 (2004).
18. C. Liedtke, T. Luedde, T. Sauerbruch, D. Scholten, K. Streetz, F. Tacke, R. Tolba, C. Trautwein, J. Trebicka, R. Weiskirchen, Experimental liver fibrosis research: Update on animal models, legal issues and translational aspects. *Fibrogenesis Tissue Repair* **6**, 19 (2013).
19. J. Muñoz-Luque, J. Ros, G. Fernandez-Varo, S. Tugues, M. Morales-Ruiz, C. E. Alvarez, S. L. Friedman, V. Arroyo, W. Jiménez, Regression of fibrosis after chronic stimulation of cannabinoid CB2 receptor in cirrhotic rats. *J. Pharmacol. Exp. Ther.* **324**, 475–483 (2008).
20. M. K. Connolly, A. S. Bedrosian, J. Mallen-St Clair, A. P. Mitchell, J. Ibrahim, A. Stroud, H. L. Pachter, D. Bar-Sagi, A. B. Frey, G. Miller, In liver fibrosis, dendritic cells govern hepatic inflammation in mice via TNF-α. *J. Clin. Invest.* **119**, 3213–3225 (2009).
21. Z. Cao, X. Wu, L. Yen, C. Sweeney, K. L. Carraway III, Neuregulin-induced ErbB3 downregulation is mediated by a protein stability cascade involving the E3 ubiquitin ligase Nrdp1. *Mol. Cell. Biol.* **27**, 2180–2188 (2007).
22. L. A. Madge, J. S. Pober, A phosphatidylinositol 3-kinase/Akt pathway, activated by tumor necrosis factor or interleukin-1, inhibits apoptosis but does not activate NFκB in human endothelial cells. *J. Biol. Chem.* **275**, 15458–15465 (2000).
23. G. Sabio, R. J. Davis, TNF and MAP kinase signalling pathways. *Semin. Immunol.* **26**, 237–245 (2014).
24. J. Conde, N. Oliva, M. Atilano, H. S. Song, N. Artzi, Self-assembled RNA-triple-helix hydrogel scaffold for microRNA modulation in the tumour microenvironment. *Nat. Mater.* **15**, 353–363 (2016).
25. H. H. Gustafson, D. Holt-Casper, D. W. Grainger, H. Ghandehari, Nanoparticle uptake: The phagocyte problem. *Nano Today* **10**, 487–510 (2015).
26. J. L. Santos, D. Pandita, J. Rodrigues, A. P. Pêgo, P. L. Granja, G. Balian, H. Tomás, Receptor-mediated gene delivery using PAMAM dendrimers conjugated with peptides recognized by mesenchymal stem cells. *Mol. Pharm.* **7**, 763–774 (2010).
27. M. J. Carroll, A. Kapur, M. Felder, M. S. Patankar, P. K. Kreeger, M2 macrophages induce ovarian cancer cell proliferation via a heparin binding epidermal growth factor/matrix metalloproteinase 9 intercellular feedback loop. *Oncotarget* **7**, 86608–86620 (2016).
28. J. P. Pradere, J. Kluwe, S. De Minicis, J. J. Jiao, G. Y. Gwak, D. H. Dapito, M. K. Jang, N. D. Guenther, I. Mederacke, R. Friedman, A. C. Dragomir, C. Aloman, R. F. Schwabe, Hepatic macrophages but not dendritic cells contribute to liver fibrosis by promoting the survival of activated hepatic stellate cells in mice. *Hepatology* **58**, 1461–1473 (2013).
29. V. Reichenbach, G. Fernandez-Varo, G. Casals, D. Oró, J. Ros, P. Melgar-Lesmes, R. Weiskirchen, M. Morales-Ruiz, W. Jiménez, Adenoviral dominant-negative soluble PDGFRβ improves hepatic collagen, systemic hemodynamics, and portal pressure in fibrotic rats. *J. Hepatol.* **57**, 967–973 (2012).
30. J. Tonkin, L. Temmerman, R. D. Sampson, E. Gallego-Colon, L. Barberi, D. Bilbao, M. D. Schneider, A. Musarò, N. Rosenthal, Monocyte/macrophage-derived IGF-1 orchestrates murine skeletal muscle regeneration and modulates autocrine polarization. *Mol. Ther.* **23**, 1189–1200 (2015).
31. H. Nishizawa, G. Iguchi, H. Fukuoka, M. Takahashi, K. Suda, H. Bando, R. Matsumoto, K. Yoshida, Y. Odake, W. Ogawa, Y. Takahashi, IGF-I induces senescence of hepatic stellate cells and limits fibrosis in a p53-dependent manner. *Sci. Rep.* **6**, 34605 (2016).
32. A. Das, M. Sinha, S. Datta, M. Abas, S. Chaffee, C. K. Sen, S. Roy, Monocyte and macrophage plasticity in tissue repair and regeneration. *Am. J. Pathol.* **185**, 2596–2606 (2015).
33. M. A. Bouhlel, B. Derudas, E. Rigamonti, R. Dièvart, J. Brozek, S. Haulon, C. Zawadzki, B. Jude, G. Torpier, N. Marx, B. Staels, G. Chinetti-Gbaguidi, PPARγ activation primes human monocytes into alternative M2 macrophages with anti-inflammatory properties. *Cell Metab.* **6**, 137–143 (2007).
34. Y. Arkun, Dynamic modeling and analysis of the cross-talk between insulin/AKT and MAPK/ERK signaling pathways. *PLOS ONE* **11**, e0149684 (2016).
35. J. P. Turowec, E. W. T. Lau, X. Wang, K. R. Brown, F. A. Fellouse, K. K. Jawanda, J. Pan, J. Moffat, S. S. Sidhu, Functional genomic characterization of a synthetic anti-HER3 antibody reveals a role for ubiquitination by RNF41 in the anti-proliferative response. *J. Biol. Chem.* **294**, 1396–1409 (2019).
36. L. De Ceuninck, J. Wauman, D. Masschaele, F. Peelman, J. Tavernier, Reciprocal cross-regulation between RNF41 and USP8 controls cytokine receptor sorting and processing. *J. Cell Sci.* **126**, 3770–3781 (2013).
37. P. Ramachandran, R. Dobie, J. R. Wilson-Kanamori, E. F. Dora, B. E. P. Henderson, N. T. Luu, J. R. Portman, K. P. Matchett, M. Brice, J. A. Marwick, R. S. Taylor, M. Efremova, R. Vento-Tormo, N. O. Carragher, T. J. Kendall, J. A. Fallowfield, E. M. Harrison, D. J. Mole, S. J. Wigmore, P. N. Newsome, C. J. Weston, J. P. Iredale, F. Tacke, J. W. Pollard, C. P. Ponting, J. C. Marioni, S. A. Teichmann, N. C. Henderson, Resolving the fibrotic niche of human liver cirrhosis at single-cell level. *Nature* **575**, 512–518 (2019).
38. O. Krenkel, F. Tacke, Liver macrophages in tissue homeostasis and disease. *Nat. Rev. Immunol.* **17**, 306–321 (2017).
39. I. Fabregat, J. Moreno-Caceres, A. Sanchez, S. Dooley, B. Dewidar, G. Giannelli, P. T. Dijke; IT-LIVER Consortium, TGF-β signalling and liver disease. *FEBS J.* **283**, 2219–2232 (2016).
40. K. Bonefeld, S. Moller, Insulin-like growth factor-I and the liver. *Liver Int.* **31**, 911–919 (2011).
41. M. I. Lefterova, Y. Zhang, D. J. Steger, M. Schupp, J. Schug, A. Cristancho, D. Feng, D. Zhuo, C. J. Stoeckert Jr., X. S. Liu, M. A. Lazar, PPARgamma and C/EBP factors orchestrate adipocyte biology via adjacent binding on a genome-wide scale. *Genes Dev.* **22**, 2941–2952 (2008).
42. C. Mitchell, H. Willenbring, A reproducible and well-tolerated method for 2/3 partial hepatectomy in mice. *Nat. Protoc.* **3**, 1167–1170 (2008).
43. I. Mederacke, D. H. Dapito, S. Affo, H. Uchinami, R. F. Schwabe, High-yield and high-purity isolation of hepatic stellate cells from normal and fibrotic mouse livers. *Nat. Protoc.* **10**, 305–315 (2015).
44. J. Ribera, M. Pauta, P. Melgar-Lesmes, B. Córdoba, A. Bosch, M. Calvo, D. Rodrigo-Torres, P. Sancho-Bru, A. Mira, W. Jiménez, M. Morales-Ruiz, A small population of liver endothelial cells undergoes endothelial-to-mesenchymal transition in response to chronic liver injury. *Am. J. Physiol. Gastrointest. Liver Physiol.* **313**, G492–G504 (2017).

Acknowledgments

Funding: This work was supported by grants to P.M-L. and W.J. from Ministerio de Ciencia, Innovación y Universidades (grants RTI2018-094734-B-C21 and PID2021-123426OB-I00/funded by MCIN/AEI/10.13039/501100011033 and by "ERDF A way of making Europe"). P.M-L. was additionally supported by a fellowship from the Ramon y Cajal Program (RYC2018-0Z23971-I) funded by the Spanish Ministerio de Ciencia e Innovación MCIN/AEI/10.13039/501100011033 and FSE invierte en tu futuro. P.M-L. was additionally granted a fellowship from the AGAUR Beatriu de Pinós Program 2016 (BP-00236) of Generalitat de Catalunya and a Research Fellowship Sheila Sherlock from the European Association for the Study of Liver (EASL). A.M.-L. had a Formación de Personal Investigador (FPI) grant from Ministerio de Ciencia, Innovación y Universidades and FSE invierte en tu futuro (reference: PRE2019-088097). M.M-B. had a Formación de Profesorado Universitario (FPU) grant from Ministerio de Ciencia, Innovación y Universidades and FSE invierte en tu futuro (reference: FPU19/03323). E.R.E. was supported by a grant (R01 GM 49039) from the National Institutes of Health. The Centro de Investigación Biomédica en Red de Enfermedades Hepáticas y Digestivas (CIBERehd) is funded by the Instituto de Salud Carlos III. This work was also supported by RedFibro (RED2022-134485-T) of the 2022 call for aid to «RESEARCH NETWORKS», within the framework of the Programa Estatal del Plan Estatal de Investigación Científica, Técnica y de Innovación 2021–2023, and the Consolidated Research Group of the Generalitat de Catalunya AGAUR (2021 SGR 00881).

Author contributions: Conceptualization was carried out by E.R.E., W.J., and P.M.-L. Methodology was performed by A.M.-L., M.M.-B., Y.F., M.P., J.A., M.P.-R., S.B., C.F., and P.M.-L. Investigation was performed by A.M.-L., M.M.-B., and P.M.-L. Project administration was carried out by P.M.-L. Writing—original draft—was carried out by A.M.-L. and P.M.-L. Writing—review and editing—was carried out by A.M.-L., P.M.-L., E.R.E., and W.J. **Competing interests:** The following patent is associated with the study: "Methods and compositions to target and treat macrophages", PCT international application number 18/163.253, by co-inventors P.M.-L. and E.R.E. The other authors declare that they have no competing interests. **Data and materials availability:** All data associated with this study are in the paper or the Supplementary Materials. Raw data from figures are available in data file S1.

Submitted 25 April 2022
Resubmitted 02 March 2023
Accepted 16 June 2023

Published 12 July 2023
10.1126/scitranslmed.abq6225

Science Translational Medicine
AAAS

Supplementary Materials for

RNF41 orchestrates macrophage-driven fibrosis resolution and hepatic regeneration

Alazne Moreno-Lanceta *et al.*

Corresponding author: Pedro Melgar-Lesmes, pmelgar@ub.edu

Sci. Transl. Med. **15**, eabq6225 (2023)
DOI: 10.1126/scitranslmed.abq6225

The PDF file includes:

Materials and Methods
Figs. S1 to S13
Tables S1 and S2
Legend for data file S1

Other Supplementary Material for this manuscript includes the following:

Data file S1
MDAR Reproducibility Checklist

Materials and methods

Physicochemical characterization of nanoparticles

Nanoparticle size was determined by dynamic light scattering (DLS), using a Zetasizer nano ZS (Malvern Instruments Ltd). Measurements were carried out at 25 °C and at fixed angle of 173°, by analyzing the intensity of the scattered light supplied by a helium-neon laser (4 mW, λ = 633 nm). DLS data were calculated from the autocorrelation function of scattered light by means of two mathematical approaches: the cumulants method and Dispersion Technology Software nano v. 5.10 (Malvern Instruments Ltd). Through the cumulants analysis, two important parameters were obtained: the mean hydrodynamic diameter (Z-Average) and the width of the particle size distribution (polydispersity index-PDI). To prepare samples for the measurements, 20 μL of graphite nanoparticle suspension were dispersed in 1480 μL of PBS, in an ordinary cuvette. Reported values of Z-Average and PDI corresponded to the average of approximately 40 measurement runs. The size and morphology of different nanoparticles were characterized by TEM, using a JEOL JEM 1010 microscope (JEOL) equipped with an AMT XR40 digital imaging camera, at a magnification of 75000X and a maximum accelerating voltage of 100 kV. Particle diameter was determined in approximately 300 randomly selected nanoparticles from different TEM images using the morphometry software ImageJ v. 1.44 (U.S. National Institutes of Health). Osmolality was determined from osmometric depression of the freezing point (Advanced Instruments Osmometer 3300).

Cell culture

Primary human umbilical vein endothelial cells (HUVECs), mouse macrophages (RAW 264.7) and human monocytes (THP-1) were supplied by ATCC. Human LX-2 hepatic stellate cells were a generous gift from Dr Scott L Friedman. Human macrophages were obtained from incubation of THP-1 with phorbol myristate acetate (PMA) (100 ng/mL) for 2 days. Freshly isolated primary hepatic $CD11b^{+}$-macrophages were obtained from the livers of healthy mice. Dulbecco's phosphate buffered saline (DPBS), Dulbecco's Modified Eagle Medium (DMEM) and penicillin/streptomycin were purchased from Thermo Fisher Scientific Inc. HUVECs were cultured in pre-gelatinized plates with endothelial growth medium (EGM) supplemented with EGM-2 growth supplements (Lonza), 10% fetal bovine serum (FBS), and 50 U/mL

penicillin/streptomycin. HUVECs were passaged when they reached 80% confluence and passages 2–5 were used for all experiments. RAW 264.7 mouse macrophages, isolated mouse hepatocytes, and hepatic stellate cells were cultured with DMEM supplemented with 10% FBS. Isolated mouse hepatic $CD11b^+$-macrophages were cultured with DMEM supplemented with 1% FBS. Human LX-2 cells were cultured with DMEM supplemented with 2% FBS. All cells were grown at 37 °C and 5% CO_2 in a water jacketed incubator.

Prolonged inflammation assay in macrophages

Mouse RAW 264.7 and human THP-1 macrophages were seeded at 2 x 10^4 cell/cm^2 density with complete DMEM medium supplemented with low FBS (1%) and incubated with TNF-α (5 ng/mL, Life Technologies) for 7 days, with daily renovation of this pro-inflammatory medium. Cells were harvested at different time points; at day 0 (16 hours after seeding with no TNF-α stimulation), and 1, 3, 5 and 7 days after TNF-α stimulation for RNA isolation or protein extraction using the TRIZOL kit (Gibco-Invitrogen) or lysis buffer containing 20 mM Tris-HCl, at pH 7.4, 1% Triton X-100, 0.1% SDS, 50 mM NaCl, 2.5 mM EDTA, 1 mM $Na_4P_2O_7$ $10H_2O$, 20 mM NaF, 1 mM Na_3VO_4, 2 mM Pefabloc and a cocktail of protease inhibitors (Complete Mini, Roche) with protease inhibitors (Thermo Fisher, 87786) and phosphatase inhibitors (Thermo Fisher, 78420), respectively, for Real-time PCR and Western blot experiments. Freshly isolated primary hepatic $CD11b^+$-macrophages from healthy male mice were seeded at 2 x 10^4 cell/cm^2 density with complete DMEM medium supplemented with low FBS (1%) and incubated with TNF-α (5 ng/mL, Life Technologies) for 3 days, with daily renovation of this pro-inflammatory medium. Cells were harvested at different time points; at day 0 (16 hours after seeding with no TNF-α stimulation), and 1, 2 and 3 days after TNF-α stimulation for RNA isolation using TRIZOL kit for Real-time PCR.

Biological characterization of nanoparticles

Plasmid-DGNP cytotoxicity was analyzed on HUVECs using the CellTiter 96 Aqueous One Solution Cell Proliferation Assay (MTS assay, Promega). Briefly, cells were seeded in pre-gelatinized 96-well plates at a cell density of 5×10^3 cells per well, serum starved for 6 h and then incubated with plasmid-DGNP at different concentrations (500, 50 and 5 µg/mL) for 24h. Just before determination of cell viability, cells were washed with PBS and transferred into starvation medium. Cytotoxicity was determined by adding 20 µL of MTS solution to each well. After 2 h,

the absorbance was measured at 490 nm using a microplate spectrophotometer (Varioskan Flash spectrophotometer, Thermofisher Scientific). Cell viability was expressed as the absorbance of cells treated with plasmid-DGNP relative to cells treated with PBS (control). Each condition was performed in quadruplicates and reported as mean ± SD.

Uptake kinetics of plasmid-DGNP

RAW 264.7 mouse macrophages were cultured with DMEM with 10% FBS in 24 wells (10^5 cells/well) for 24 hours and then serum-starved for 6 hours. Afterwards cells were incubated with plasmid-DGNP 100 ng/mL in the presence or absence of TNF-α (5 ng/mL) and images were taken at different time points (30, 60, 120 and 180 minutes) with a light microscope. Black aggregates of plasmid-DGNP were visualized at high magnification to establish the number of cells incorporating plasmid-DGNP. Percentage of cells incorporating plasmid-DGNP is calculated with the formula: number of cells with black aggregates/total number of cells per field x 100. At least 30 different fields were used to calculate the uptake percentage per time point.

Intracellular localization of FITC-DGNP in macrophages

DGNP (10 µg/mL) were incubated with FITC (2 mg/mL, Sigma) for 1 h at room temperature in the dark. Afterwards FITC-DGNP were centrifuged at 21000 Gs for 10 min, washed three times with DMSO, and then three times with PBS for subsequent *in vitro* experiments. FITC-DGNP were incubated with inflamed RAW 264.7 mouse macrophages for 24 h, washed with PBS, and visualized with an epifluorescence microscope (Fluo Zeiss Axio Observer Z1, Zeiss) and a digital imaging system (Ret Exi, Explora Nova). DAPI was used as mounting medium to counterstain cell nuclei.

Functional assay of plasmid transfection efficiency and anti-inflammatory subset switch

The transfection efficiency of plasmid-DGNP complexes was studied in inflamed RAW 264.7 macrophages. Cells were seeded at a concentration of 5×10^4 cells in 2-well Labtek II chamber slides, grown to 80% confluence, and inflamed with TNF-α (5 ng/mL) for 16 h. After that, cells were serum-starved for 6 h and incubated for 3 h with 100 ng/mL plasmid-DGNP containing 10 ng/mL of plasmid DNA expressing RNF41 or EGFP reporter. Cells were then washed and incubated for 3 days. Afterwards, cells were washed with PBS and mounted with a coverslip using a DAPI mounting medium to counterstain cell nuclei. Intracellular presence of

synthesized EGFP was visualized with an epifluorescence microscope. To analyze the possible switch from pro-inflammatory to anti-inflammatory macrophages, cells were stained with rabbit polyclonal anti-mannose receptor (1:100, Abcam, ref: ab64693) and revealed with Cy3-conjugated donkey-anti-rabbit IgG (Jackson ImmunoResearch Laboratories, ref: 711-167-003) incubated for 1h at room temperature. The presence of synthesized mannose receptor was visualized with an epifluorescence microscope.

Detection of EGFP fluorescence in liver isolated cells

Hepatic $CD11b^+$-macrophages, hepatocytes and hepatic stellate cells were isolated from the liver of fibrotic mice 24 hours after treatment with pSCR-DGNP as described in the method section. Liver endothelial cells were obtained after MACS-purification with CD31 specific antibodies (Invitrogen, ref: PA5-14372). Hepatocytes, liver endothelial cells and hepatic stellate cells were MACS-purified using negative selection with Ly6G (RyD Systems, ref: 25872-1-AP) and PDCA-1 (Invitrogen, ref: PA5-23505) antibodies linked to anti-rabbit IgG microbeads (Miltenyi Biotec, ref: 130-048-602) and CD11b magnetic beads (Miltenyi Biotec, 130-049-601) to eliminate any contaminating $CD11b^+$ macrophages. Isolated cells fractions were resuspended in 300 µl of lysis buffer containing 20 mM Tris-HCl, at pH 7.4, 1% Triton X-100, 0.1% SDS, 50 mM NaCl, 2.5 mM EDTA. EGFP cell fluorescence of each fraction was measured using 96-well microplate for fluorescence-based assays (Invitrogen) in a microplate fluorescence reader (Tecan Spark 10M Microplate Reader) with the excitation peak at 488 nm and the emission peak at 510 nm. Liver isolated cells from fibrotic animals without pSCR-DGNP treatment were used as control to normalize relative fluorescence units observed in the cells from pSRC-DGNP treated animals. Fluorescence in isolated cells was expressed as relative fluorescence units (RFU) per miligram of cell fraction. Cell protein content was measured using BCA assay kit (Thermo Fisher Scientific Inc).

Proliferation assay in isolated hepatocytes and pro-fibrogenic activation of LX-2 hepatic stellate cells incubated with macrophage-derived conditioned medium

Effects of macrophage-derived conditioned medium from RAW 264.7 macrophages treated with the different plasmid-DGNP were analyzed in mouse isolated hepatocytes using the CellTiter 96 Aqueous One Solution Cell Proliferation Assay (MTS assay, Promega) and in LX-2 hepatic stellate cells. Isolated mouse hepatocytes and LX-2 were seeded in 96-well plates at a cell

density of 5×10^3 cells per well, serum starved for 6 h, washed with PBS and then incubated with fresh starving medium mixed with conditioned medium 1:1 from RAW 264.7 macrophages treated with PBS, 10% FBS, TNF-α only, TNF-α + pScramble-DGNP, TNF-α + pRNF41-DGNP, TNF-α + pshRNF41-DGNP for 3 days. Conditioned medium was centrifuged, and supernatants stored at -80 ºC for proliferation assays. Conditioned medium from macrophages treated with pRNF41-DGNP was mixed with IGF-1 antibody (ABClonal, ref: A0303) (2 µg/mL) for 2 h before the proliferation assay to evaluate its involvement in the proliferation of hepatocytes. Final conditioned medium mixtures were incubated with hepatocytes for 24 h. Proliferation was determined by adding 20 µL of MTS solution to each well. After 2 h, the absorbance was measured at 490 nm using a microplate spectrophotometer (Varioskan Flash spectrophotometer, Thermofisher Scientific). Cell viability was expressed as absorbance and compared to the absorbance of cells receiving an equal volume of PBS (control). LX-2 hepatic stellate cells were resuspended in TRIZOL to isolate RNA for Real-Time PCR of pro-fibrogenic genes. Each condition was performed in sextuplicate and reported as mean ± SD.

Western Blot

Total protein was extracted from cells with lysis buffer containing 20 mM Tris-HCl, at pH 7.4, 1% Triton X-100, 0.1% SDS, 50 mM NaCl, 2.5 mM EDTA, 1 mM $Na_4P_2O_7$ $10H_2O$, 20 mM NaF, 1 mM Na_3VO_4, 2 mM Pefabloc and a cocktail of protease inhibitors (Complete Mini, Roche) and phosphatase inhibitors (Thermo Fisher, 78420). Proteins were separated on a 10% SDS-polyacrylamide gel (Mini Protean III, BioRad) and transferred for 2 hours at 4°C to nitrocellulose membranes of 0,45 µm (Transblot Transfer Medium, BioRad) that were stained with Ponceau-S red as a primary control for protein loading. The membranes were incubated at 4°C overnight with the following antibodies: rabbit anti-pAkt (Ser127) (1:1000, Cell Signaling, ref: 9271) and anti-Akt (1:1000, Cell Signaling, ref: 9272), rabbit anti-phospho-Erk (1:1000, Cell Signaling, ref: 4370S) and anti-Erk (1:1000, Cell Signaling, ref: 4695) and β-actin (1:2000, Cell Signaling, ref: 4970) as loading control. Next, the membranes were incubated with a donkey ECL-anti-rabbit IgG peroxidase-conjugated secondary antibody at 1:2000 dilution (1:2000, Thermo Fisher, ref: SA1-200) for 1 hour at room temperature. The bands were visualized using Chemidoc Imaging System (Biorad Laboratories, Inc) and quantified by computer-assisted densitometry analysis (ImageJ).

Immunofluorescence and imaging in tissues

Liver was excised and tissue was washed with PBS and fixed with 10% buffered formaldehyde solution for 24h. Afterwards the tissue was cryo-protected with 30% sucrose solution (in PBS) and then embedded using Tissue-Tek OCT compound (Sakura Fineteck) and frozen. Liver sections underwent 1% SDS solution antigen retrieval for 5 minutes at room temperature and then were blocked with 5% normal goat serum. Liver sections were incubated with rabbit polyclonal anti-mannose receptor (1:100, Abcam, ref: ab64693), rabbit polyclonal anti-PCNA antibody (1:50, Abcam, ref: ab152112), rat anti-Ly-6C monoclonal IgG antibody (1:100, Thermofisher Scientific, ref: ER-MP20), rabbit anti-iNOS polyclonal antibody (1:100, Thermofisher Scientific, ref: PA1-036), rabbit anti-COX2 polyclonal antibody (1:100, Proteintech, ref: 12375-1-AP), rabbit anti-Arg1 polyclonal (1:100, Thermofisher Scientific, ref: PA5-85267), rabbit anti-Resistin-like Molecule α polyclonal antibody (1:100, Sigma-Aldrich, ref: AB3365P), rabbit anti-TIMP1 polyclonal antibody (1:100, Bioss, ref: BS-4600R), monoclonal mouse anti-smooth muscle actin (1:100, Dako, ref: M0851), Goat anti- PCNA Polyclonal Antibody (1:50, Invitrogen, ref: PA5-142928), Rabbit anti-ASGR1 Polyclonal Antibody (1:50, Invitrogen, ref: PA5-121041), Monoclonal rat Anti-Endomucin antibody (1:50, Abcam, ref: ab106100), rabbit anti-CD68 Polyclonal Antibody (1:100, Invitrogen, ref: PA5-78996). Primary antibodies were revealed with Cy3-conjugated donkey-anti-rabbit IgG (1:500, Jackson ImmunoResearch Laboratories, ref: 711-167-003), Cy3-conjugated donkey anti-rat IgG (1:500, Jackson ImmunoResearch Laboratories, ref: 712-165-150), donkey-anti-mouse IgG Alexa Fluor 647 (1:500, Thermofisher Scientific, ref: A31571), donkey-anti-rabbit IgG Alexa Fluor 594 (1:500, Jackson ImmunoResearch Laboratories, ref: 711-585-152), Donkey anti-Rabbit IgG Alexa Fluor 488 (1:500, Invitrogen, ref: A-21206), Donkey anti-Rat IgG Alexa Fluor Plus 488 (1:500, Invitrogen, ref: A48269) or Cy3 Donkey Anti-Goat IgG (1:500, Jackson ImmunoResearch Laboratories, ref: 705-165-147) incubated for 1h at room temperature. The presence of mannose receptor, Ly6C, PCNA, COX2, iNOS, Arginase, Resistin-like Molecule α, TIMP1 or anti-smooth muscle actin, ASGPR, endomucin and CD68 was visualized with an epifluorescence microscope. DAPI (Vectashield, Vector laboratories) was used to counterstain cell nuclei. Images were processed by computer-assisted background subtraction (low levels of staining detection, noise and background). Negative controls of immunofluorescence staining were obtained with the

incubation of liver sections with the corresponding Alexa Fluor 594 secondary antibody without the incubation of the primary antibody.

Fibrosis quantification

Liver was excised and tissue was washed with PBS and fixed with 10% buffered formaldehyde solution for 24h. Afterwards, the tissue was embedded using paraffin. Before staining, paraffin was removed using xylene, ethanol, and deionized water. Liver sections (4 µm) were stained in 0.1% Sirius Red F3B (Sigma) with saturated picric acid (Sigma). Relative fibrosis area (expressed as a percentage of total liver area) was analyzed in 20 fields of Sirius red-stained liver sections per animal using the morphometry software ImageJ v 1.44. To evaluate the relative fibrosis area, the measured collagen area was divided by the net field area and then multiplied by 100. From each animal analyzed, the amount of fibrosis as percentage was measured and the average value presented.

Hydroxyproline measurement in liver

Liver hydroxyproline content was measured following the manufacturer's protocol (Hydroxyproline Assay Kit, Sigma-Aldrich). Briefly, 10 mg of liver tissue was homogenized in distilled water, mixed with an equal volume of 10 M concentrated sodium hydroxide, and incubated at 120°C for 1 h. After alkaline hydrolysis, the samples were neutralized, oxidized, and then treated with 4-dimethylaminobenzaldehyde (DMAB) solution. Sample absorbance was measured at 560 nm in duplicate. Hydroxyproline content was expressed at microgram of hydroxyproline per gram liver. Liver protein content was measured using BCA assay kit (Thermo Fisher Scientific Inc).

Gene expression assay with Real-Time PCR

Total RNA from liver was extracted using commercially available kits: RNeasy (Gibco-Invitrogen). A 0.5 µg aliquot of total RNA was reverse transcribed using a complementary DNA synthesis kit (High-Capacity cDNA Reverse Transcription Kit, Applied Biosystems). Primers and probes for gene expression assays (Applied Biosystems) were selected as follows: *RNF41* (Taqman assay reference from Applied Biosystems: Human: Hs01086974_m1; Mouse: Mm01159897_m1), *USP8* (Human: Hs00987105_g1; Mouse: Mm00451077_m1), *IGF-1* (Mm00439560_m1), *HGF* (Mm01135184_m1), *TIMP1* (Human: Hs01092512_g1; Mouse:

Mm01341360_g1), *ACTA2* (*α-SMA*, Human: Hs00426835_g1; Mouse: Mm01204962_gH), *COL1A1* (Human: Hs00164004_m1; Mouse: Mm00801666_g1), *OSM* (Mm01193966_m1), *PDGF-BB* (Mm00440677_m1), *TGF-β* (Mm01178820_m1), *MMP-9* (Mm00442991_m1), *IL-10* (Mm00439614_m1), *CD36* (Mm00432403_m1), *NOS2* (Mm00440502_m1), *COX-2* (Mm00478374_m1), *IL1-β* (Mm00434228_m1), *ARG-1* (Mm00475988_m1), *MRC1* (Mm00485148_m1), *RETNLA* (Mm00445109_m1), *CYP2B9* (Mm00657910_m1) and mouse hypoxanthine phosphoribosyl transferase (*HPRT*, Mm03024075_m1) and human glyceraldehyde-3-phosphate dehydrogenase (*GAPDH*, Hs02786624_g1), used as endogenous standards. Expression assays were designed using the Taqman Gene Expression assay software (Applied Biosystems). Real-time quantitative PCR was analyzed in duplicate and performed with a Lightcycler-480 II (Roche Diagnostics). A 10 µl aliquot of the total volume reaction of diluted 1:8 cDNA, Taqman probe and primers and FastStart TaqMan Master (Applied Biosystems) were used in each PCR. The fluorescence signal was captured during each of the 45 cycles (denaturing 10s at 95 ºC, annealing 15s at 60 ºC and extension 20s at 72 ºC). Water was used as a negative control. Relative quantification was calculated using the comparative threshold cycle (CT), which is inversely related to the abundance of mRNA transcripts in the initial sample. The mean CT of duplicate measurements was used to calculate ΔCT as the difference in CT for target and reference. The relative quantity of the product was expressed as fold induction of the target gene compared with the control primers according to the formula $2^{-\Delta\Delta CT}$, where ΔΔCT represents ΔCT values normalized with the mean ΔCT of control samples.

Supplementary figures

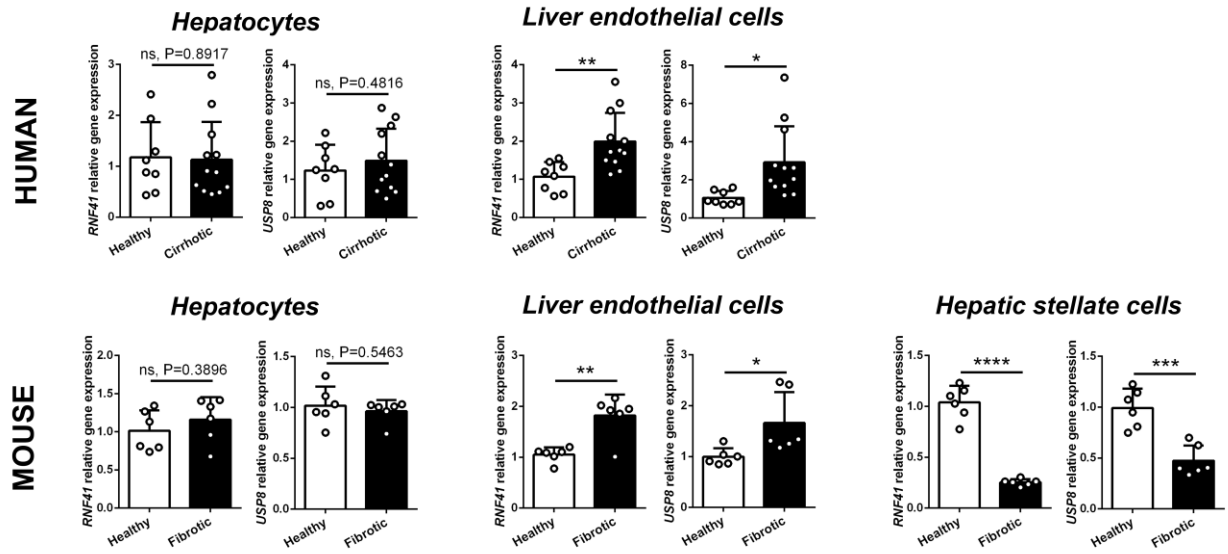

Fig. S1. *RNF41* and its stabilizer *USP8* gene expression in hepatic cells isolated from human and mouse. *RNF41* and *USP8* gene expression in hepatocytes and liver endothelial cells from patients with liver cirrhosis (n=12) and healthy subjects (n=8); and *RNF41* and *USP8* gene expression in hepatocytes, liver endothelial cells and hepatic stellate cells isolated from the liver of healthy and fibrotic mice (n=6 per group). * indicates $P \leq 0.05$, ** indicates $P \leq 0.01$, *** indicates $P \leq 0.001$, **** indicates $P \leq 0.0001$ using a Student's t-test. Data is shown as mean ± S.D.

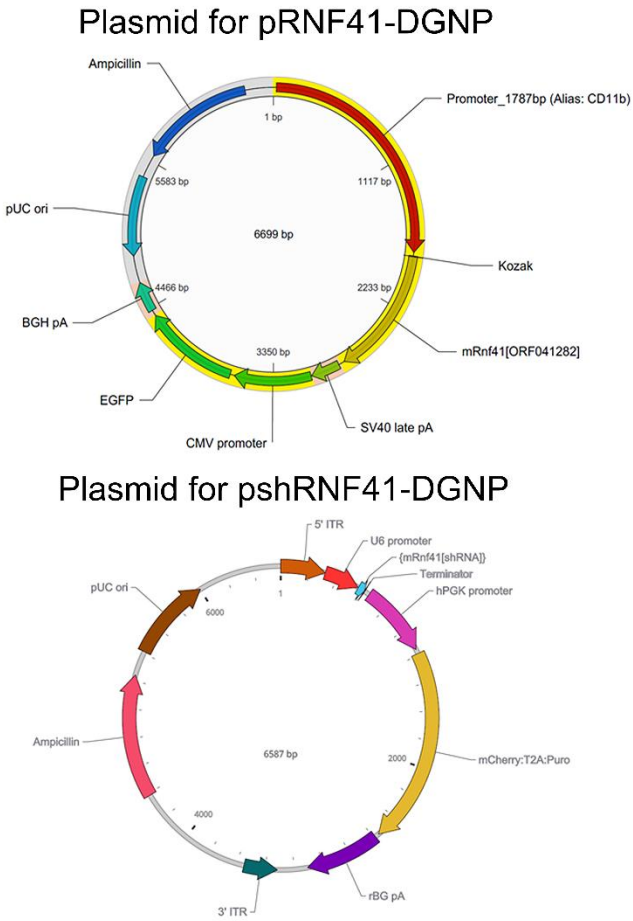

Fig. S2. Structure of pRNF41 and pshRNF41 plasmids.

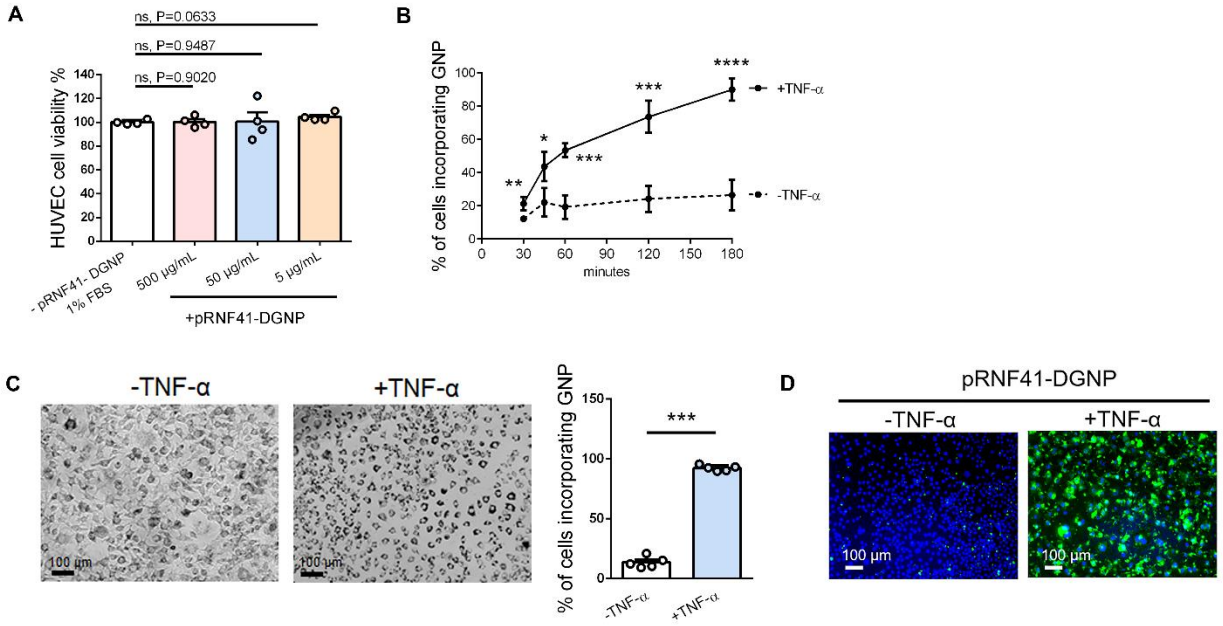

Fig. S3. Toxicity and uptake of plasmid-dendrimer graphite nanoparticles. **(A)** HUVEC viability quantified by MTS in the presence of pRNF41-dendrimer-graphite nanoparticles at concentrations from 5 to 500 µg/mL at 24h (n=4). No significant differences (ns) observed using Student's t-test compared to non-treated control. **(B)** Uptake kinetics in RAW 264.7 macrophages of pRNF41-DGNP in the presence or absence of TNF-α (n=4). * indicates $P \leq 0.05$, ** indicates $P \leq 0.01$, *** indicates $P \leq 0.001$ **** indicates $P \leq 0.0001$ vs. macrophages without TNF-α at the same time point using Student's t-test. **(C)** Uptake percentage in RAW 264.7 macrophages of pRNF41-DGNP at 24h (n=4). *** indicates $P \leq 0.001$ using a Student's t-test. **(D)** Plasmid transfection and expression efficiency highlighted by the presence of high levels of RAW 264.7 macrophage intracellular EGFP in most of cells after 3 days of incubation in TNF-α presence. Data is shown as mean ± S.D.

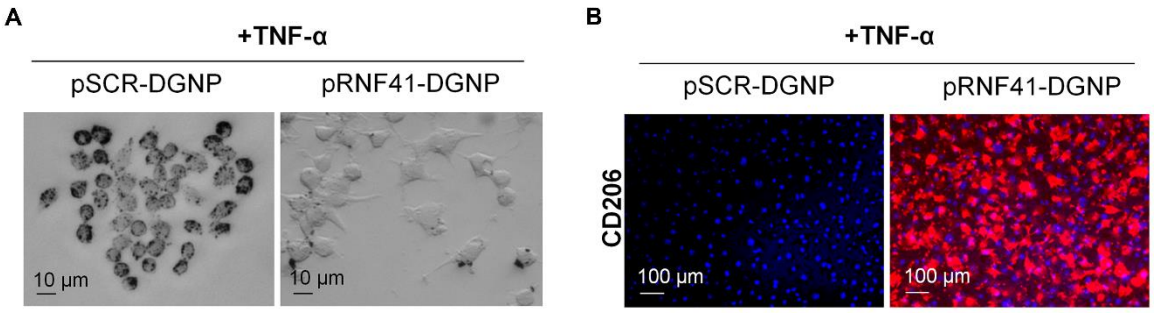

Fig. S4. Macrophage morphology and phenotype switch after pRNF41-DGNP treatment with TNF-α stimulation. (A) Cell morphology of RAW 264.7 macrophage treated with TNF-α and dendrimer-graphite nanoparticles linked to plasmids (pSCR or pRNF41), and observed using light microscopy. **(B)** Immunofluorescence staining for CD206 in RAW 264.7 macrophages treated with TNF-α and dendrimer-graphite nanoparticles linked to plasmids (pSCR or pRNF41).

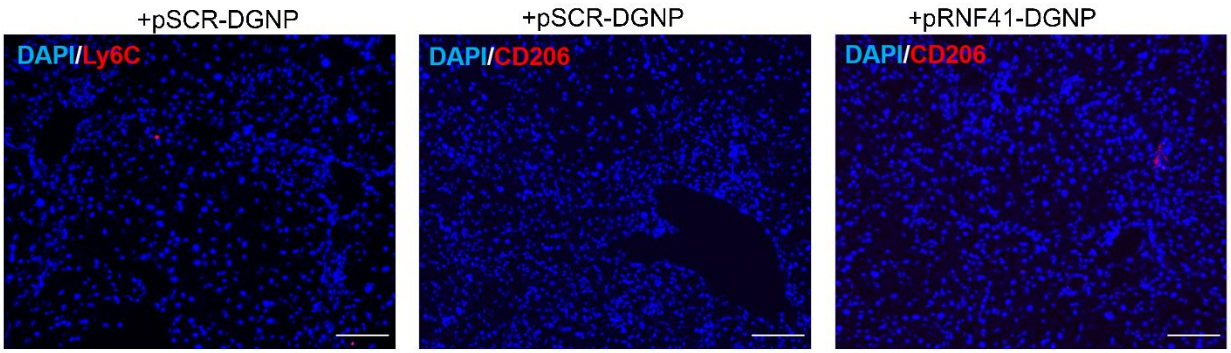

Fig. S5. Negative controls for immunofluorescence stainings. Ly6C and CD206 immunofluorescence staining negative controls in the liver of fibrotic mice treated with dendrimer-graphite nanoparticles linked to pSCR or pRNF41 for images found in Fig. 3. Scale bar: 200 µm.

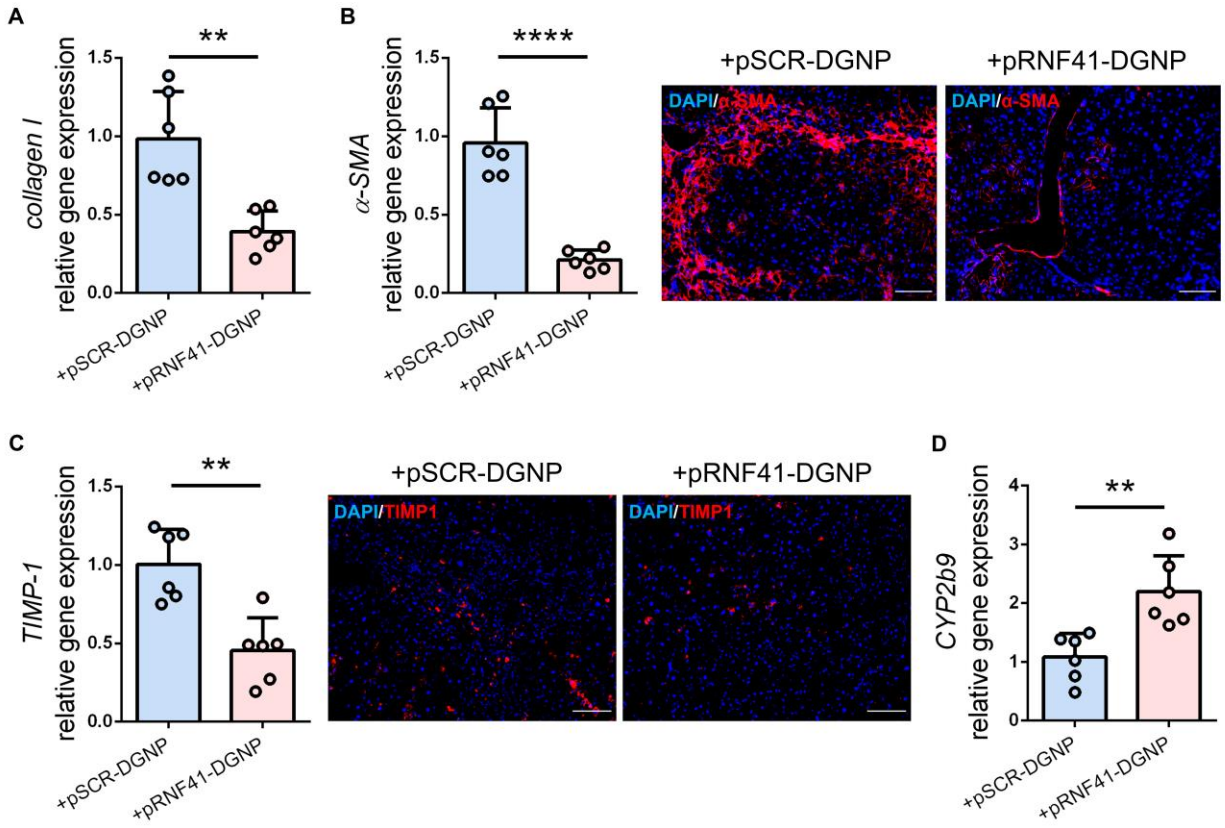

Fig. S6. Hepatic stellate cell inactivation by the treatment with pRNF41-dendrimer-graphite nanoparticles in fibrotic mice. (A) *Collagen I* relative gene expression, **(B)** *α-SMA* relative gene expression and immunofluorescence staining and **(C)** Tissue inhibitor of metalloproteinases-1 ***(****TIMP-1)* relative gene expression and immunofluorescence staining in the liver of fibrotic mice treated with dendrimer-graphite nanoparticles linked to plasmids (pSCR or pRNF41). **(D)** *CYP2B9* relative gene expression in the liver of fibrotic mice treated with dendrimer-graphite nanoparticles linked to plasmids (pSCR or pRNF41). n=6 per group of animals. ** indicates $P \leq 0.01$, **** indicates $P \leq 0.0001$ using a Student's t-test. Data is shown as mean ± S.D. Scale bar: 150 µm.

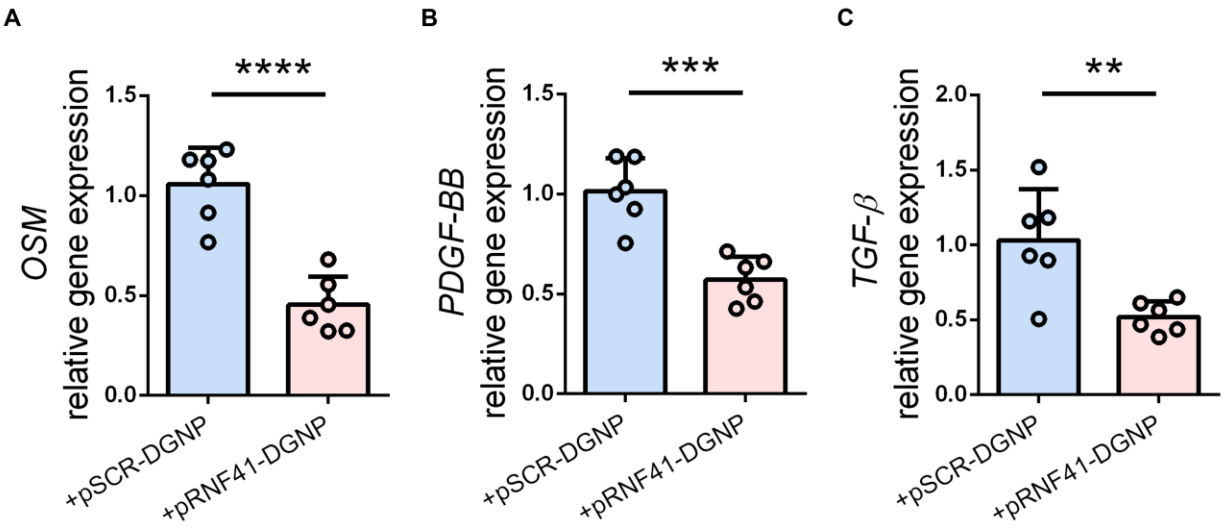

Fig. S7. Therapy with pRNF41-dendrimer-graphite reduces the relative gene expression of macrophage-derived activators of hepatic stellate cells in fibrotic mice. (A) *OSM,* **(B)** *PDGF-BB,* and **(C)** *TGF-* β relative gene expression in the liver of fibrotic mice treated with dendrimer-graphite nanoparticles linked to plasmids (pSCR or pRNF41). n=6 per group of animals. ** indicates $P \leq 0.01$, *** indicates $P \leq 0.001$, **** indicates $P \leq 0.0001$ using a Student's t-test. Data is shown as mean ± S.D.

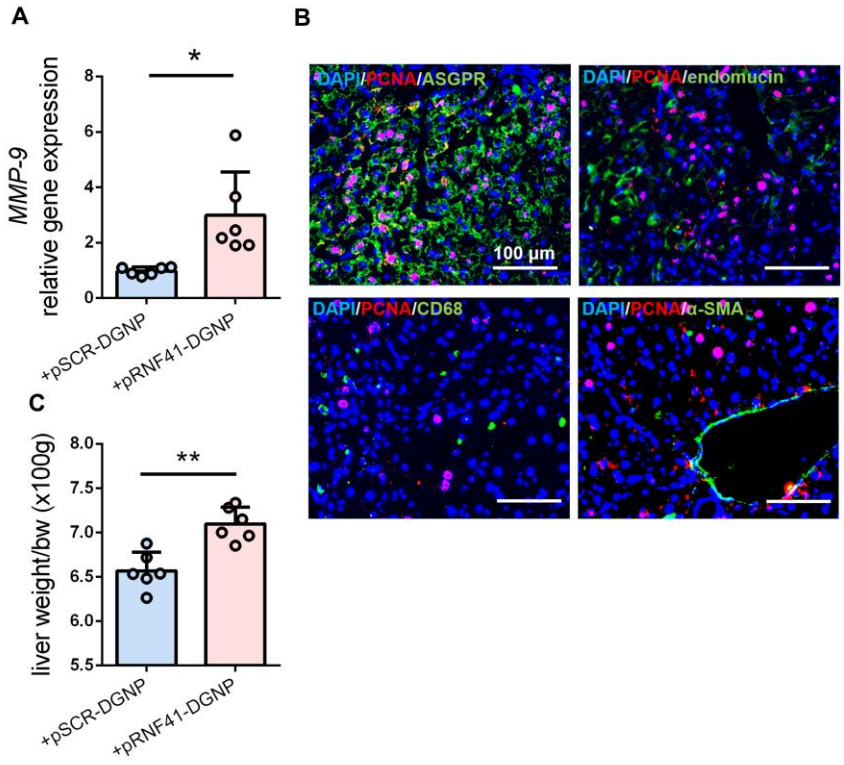

Fig. S8. The treatment with pRNF41-dendrimer-graphite nanoparticles activates the gene expression of MMP-9 and regenerates liver mass in fibrotic mice. (A) Metalloproteinase 9 *(MMP-9)* relative gene expression in the liver of fibrotic mice treated with dendrimer-graphite nanoparticles linked to plasmids (pSCR or pRNF41). **(B)** Immunofluorescence co-staining of PCNA-positive cells and individual hepatic cellular markers (asialoglycoprotein receptor (ASGPR) for hepatocytes, endomucin for liver sinusoidal endothelial cells, CD68 for macrophages and alpha smooth muscle actin (α-SMA) for hepatic stellate cells) in the liver of fibrotic mice treated with dendrimer-graphite nanoparticles linked to pRNF41. **(C)** Liver restoration rate in fibrotic mice treated with dendrimer-graphite nanoparticles linked to plasmids (pSCR or pRNF41). For a and c, n=6 per group of animals. * indicates $P \leq 0.05$, ** indicates $P \leq 0.01$ using a Student's t-test. Data is shown as mean ± S.D.

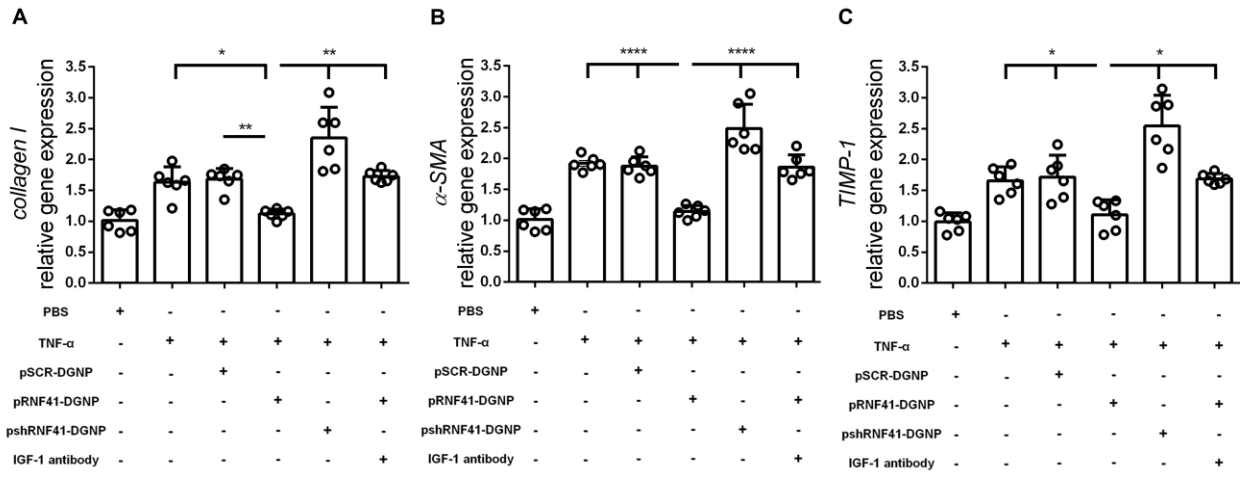

Fig. S9. IGF-1 released by RNF41-activated macrophages reduces pro-fibrogenic activation of LX-2 human hepatic stellate cells. (A) *Collagen I,* **(B)** *α-SMA,* and **(C)** Tissue inhibitor of metalloproteinases-1 *(TIMP-1)* relative gene expression in LX-2 cells treated 24 h with conditioned media from RAW 264.7 cultures treated with FBS, TNF-α, dendrimer-graphite nanoparticles linked to plasmids (pSCR, pRNF41, or pshRNF41) or IGF-1 antibody for 3 days. * indicates $P \leq 0.05$; ** indicates $P \leq 0.01$, **** indicates $P \leq 0.0001$ using a one-way analysis of variance (ANOVA) with the posthoc Newman-Keuls test. Experiments were performed in sextuplicate. Data is shown as mean ± S.D.

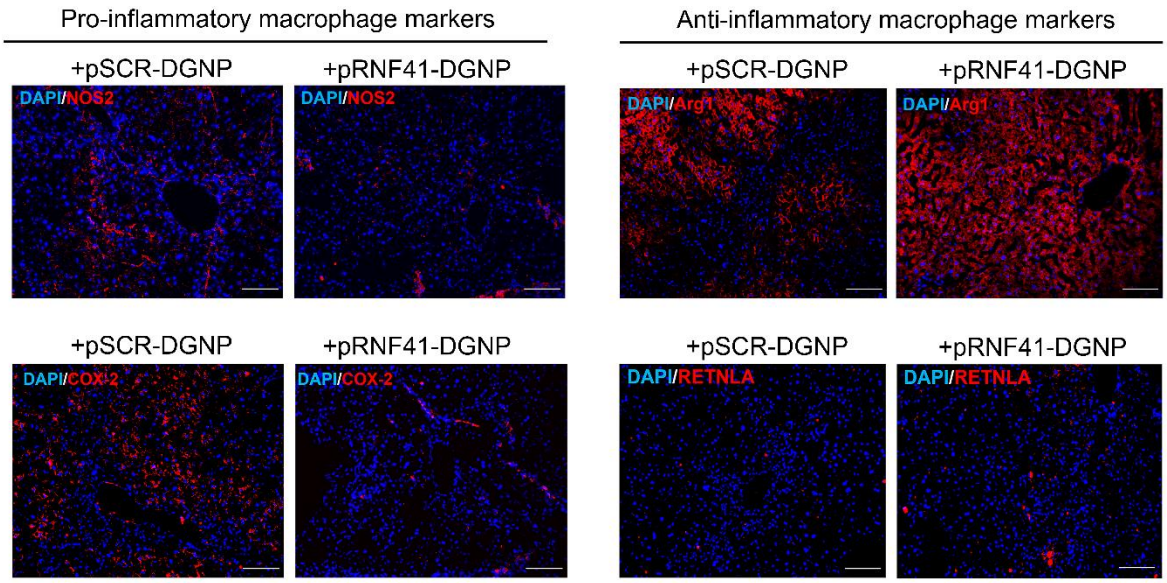

Fig. S10. Immunofluorescent staining of hepatic pro-inflammatory and anti-inflammatory markers. Pro-inflammatory macrophage marker (NOS2 and COX-2) and anti-inflammatory macrophage marker (Arg1 and RETNLA) immunofluorescence staining in the liver of fibrotic mice treated with dendrimer-graphite nanoparticles linked to plasmids (pSCR or pRNF41). Scale bar: 150 μm.

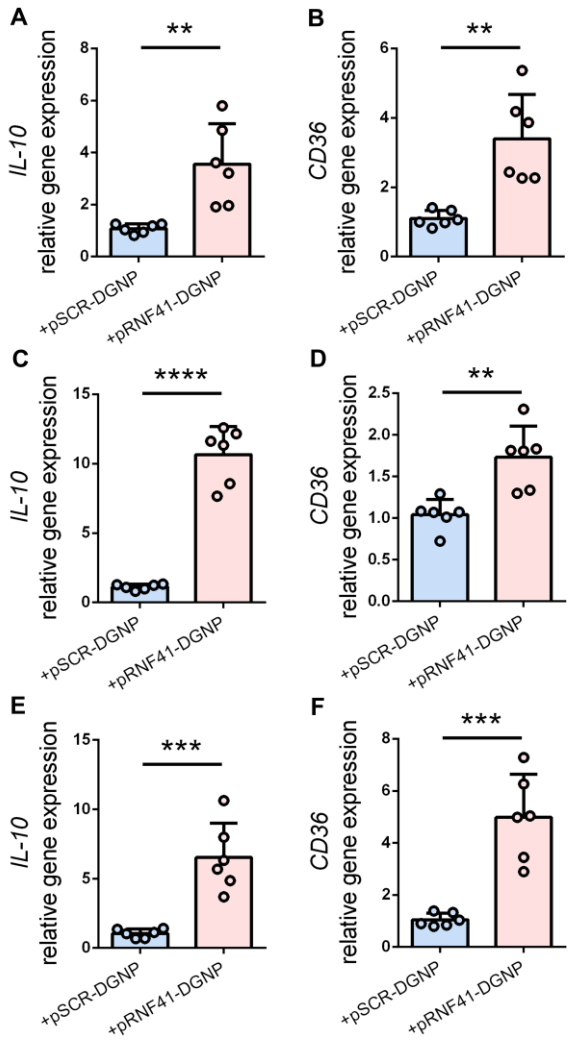

Fig. S11. The treatment with pRNF41-dendrimer-graphite nanoparticles activates the expression of the downstream PPAR-γ genes *IL-10* and *CD36* in the liver. (A) *IL-10* and **(B)** *CD36* relative gene expression in the liver of fibrotic mice treated with dendrimer-graphite nanoparticles linked to plasmids (pSCR or pRNF41). **(C)** *IL-10* and **(D)** *CD36* relative gene expression in the liver of healthy mice undergoing 70% hepatectomy and treated with dendrimer-graphite nanoparticles linked to plasmids (pSCR or pRNF41). **(E)** *IL-10* and **(F)** *CD36* relative gene expression in the liver of fibrotic mice undergoing 40% hepatectomy and treated with dendrimer-graphite nanoparticles linked to plasmids (pSCR or pRNF41). n=6 per group of animals. ** indicates $P \leq 0.01$, *** indicates $P \leq 0.001$, **** indicates $P \leq 0.001$ using a Student's t-test. Data is shown as mean ± S.D.

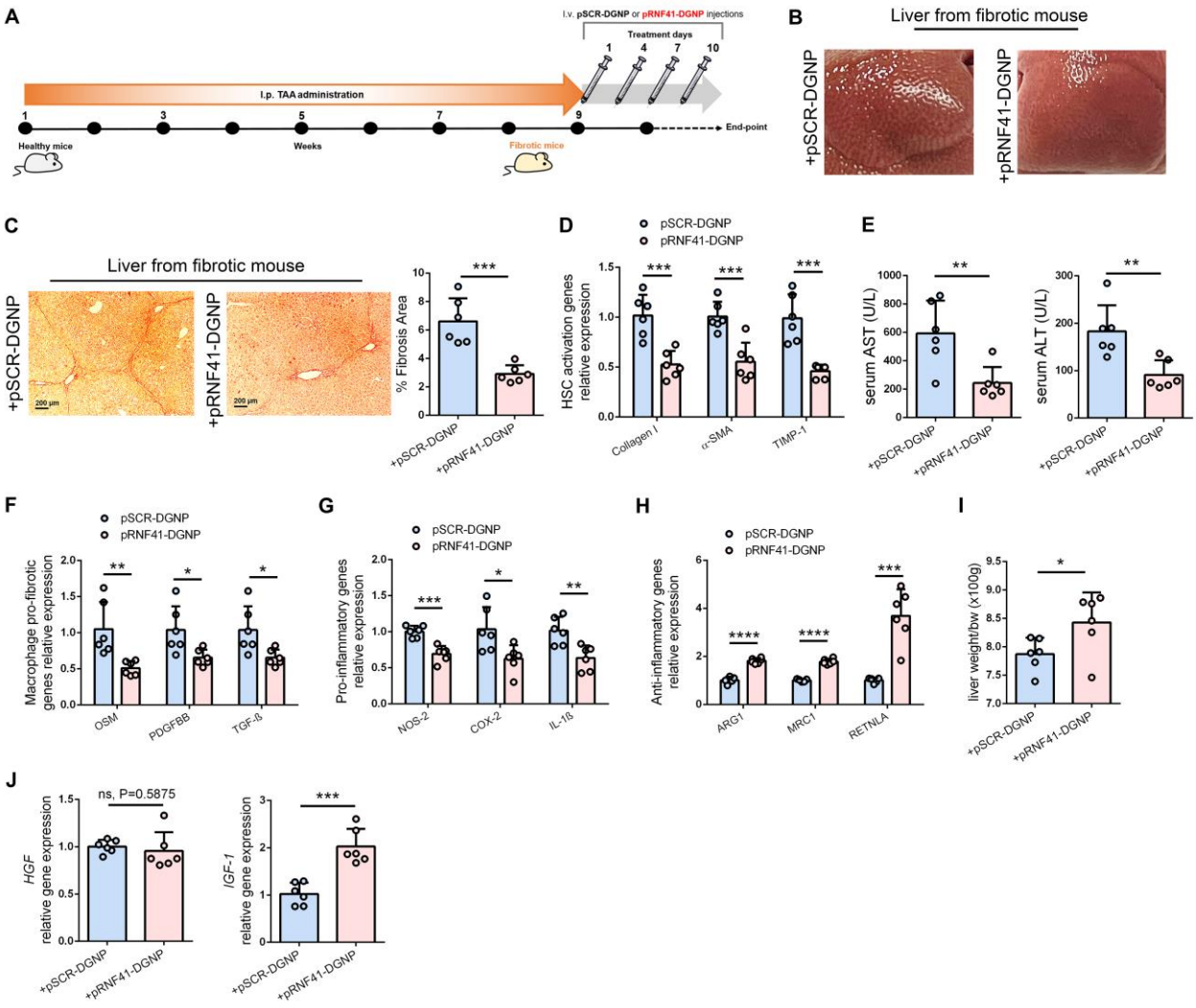

Fig. S12. ***RNF41*** **gene therapy in macrophages located into the fibrotic liver of TAA-induced fibrotic mice orchestrates fibrosis and inflammation regression, and reduction of hepatic injury. (A)** Schematic figure about time points of fibrosis induction with TAA and plasmid-linked (scrambled, pSCR or expressing RNF41, pRNF41) dendrimer-graphite nanoparticle administration. **(B)** Macroscopic aspect of fibrotic liver changing from micronodular fibrotic liver to an apparently low fibrotic liver when treated with pRNF41-DGNP. **(C)** Sirius Red staining and quantification of fibrosis area in the liver of fibrotic mice treated with dendrimer-graphite nanoparticles linked to plasmids (pSCR or pRNF41). **(D)** Expression of genes related to hepatic stellate cell (HSC) activation in the liver of fibrotic mice treated with dendrimer-graphite nanoparticles linked to plasmids (pSCR or pRNF41). **(E)** Serum parameters of liver injury in fibrotic mice treated with dendrimer-graphite nanoparticles linked to plasmids (pSCR or pRNF41). **(F)** Gene expression of pro-fibrogenic agents produced by macrophages in the liver of fibrotic

mice treated with dendrimer-graphite nanoparticles linked to plasmids (pSCR or pRNF41). **(G)** Expression of inflammatory macrophage genes in the liver of fibrotic mice treated with dendrimer-graphite nanoparticles linked to plasmids (pSCR or pRNF41). **(H)** Expression of anti-inflammatory macrophage genes in the liver of fibrotic mice treated with dendrimer-graphite nanoparticles linked to plasmids (pSCR or pRNF41). **(I)** Liver restoration rate in fibrotic mice treated with dendrimer-graphite nanoparticles linked to plasmids (pSCR or pRNF41). **(J)** Hepatic expression of hepatocyte growth factor (*HGF*) and insulin-like growth factor 1 (*IGF-1*) in fibrotic mice treated with dendrimer-graphite nanoparticles linked to plasmids (pSCR or pRNF41). n=6 per group of animals. For c, d, e, f, g, h and I * indicates $P \leq 0.05$, ** indicates $P \leq 0.01$, *** indicates $P \leq 0.001$, **** indicates $P \leq 0.0001$ using a Student's t-test.

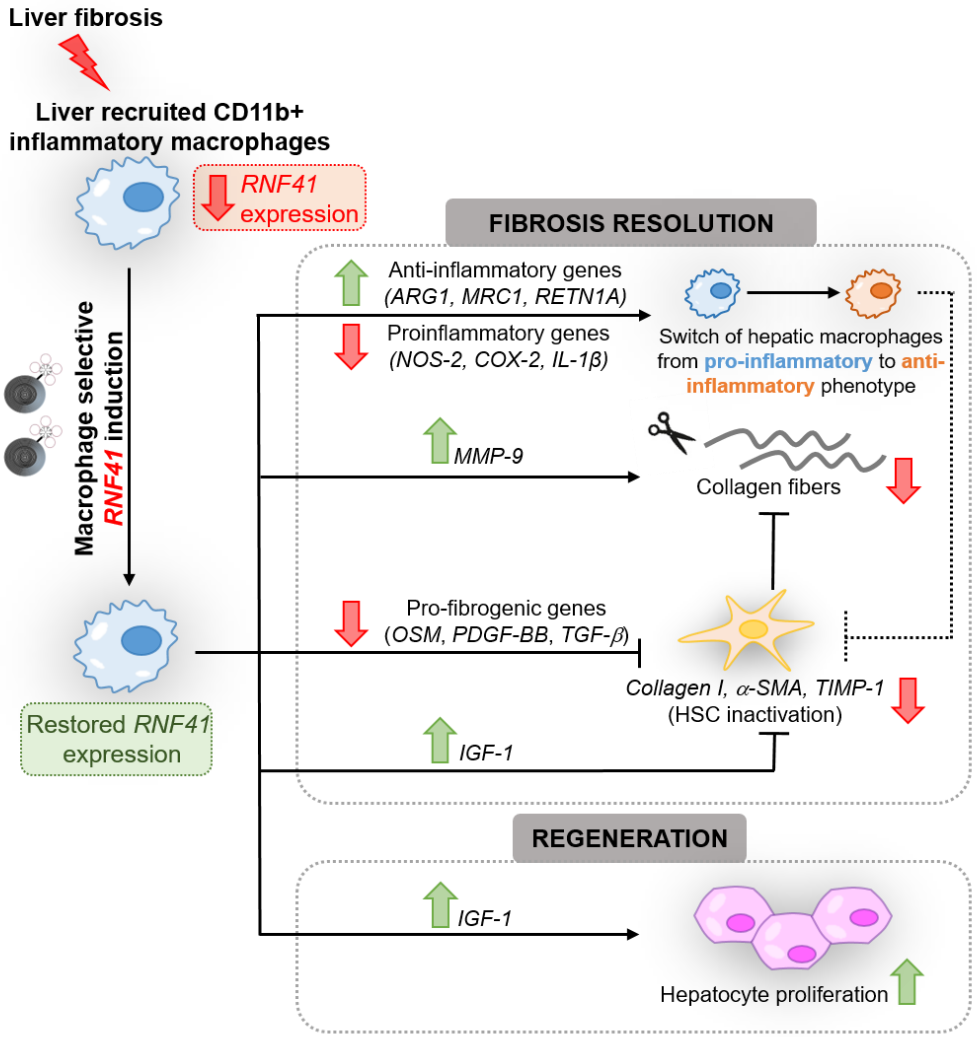

Fig. S13. Summary illustration of the heterogeneous impacts of macrophage *RNF41* restoration on liver fibrosis and regeneration.

Supplementary tables

Table S1: Demographic and baseline characteristics of study participants.

Variables	Cirrhotic n=12	Healthy n=8
Age (years)	58.7 ± 6.1	56.4 ± 19.3
Gender		
Male	9 (75)	3 (37.5)
Female	3 (25)	5 (32.5)
BMI (kg/m^2)	26.9 ± 3	24.5 ± 2.1
Etiology of liver disease		
Alcoholic	7 (58.3)	
Alcoholic + MAFLD	1 (8.3)	
Alcoholic + NASH	2 (16.7)	
PBC	1 (8.3)	
Alcoholic + HCV	1 (8.3)	
Child-Pugh Score		
A	1 (8.3)	
B	3 (25)	
C	8 (66.7)	
MELD score	20.7 ± 5.1	
Cirrhosis duration (years)	4.3 ± 5.8	

Data is shown as Mean ± S.D., or Number of Participants (Percentage, %).

BMI: Body Mass Index; MAFLD: Metabolic associated fatty liver disease; NASH: Non-Alcoholic Steatohepatitis; PBC: Primary Biliary Cirrhosis; HCV: Hepatitis C Virus; MELD: Model for End-Stage Liver Disease

Table S2: Bioinformatic analyses of *RNF41* expression in mouse and human databases.

Bioinformatic source	Species	Tissue or cell type	Disease	*RNF41* Expression levels	Reference/ID
Single-Cell Expression atlas (EBI) Baseline	Human	Liver	Normal	Below cutoff	Kim MS et al. 2014
	Mouse	Kupffer Cell	Normal	12 TPM	Lavin Y et al. 2014
				295 PPB	Azimizar SB et al. 2014
Single-Cell Expression atlas (EBI) Differential	Human	Mononuclear cells	Infected by F. Tularensis	-1.4 Fc	Butchar JP et al. 2008
	Mouse	Liver	Hepatitis (Cnot1 liver-specific KO)	-1.7 Fc	Suzuki T et al. 2020
NCBI Genes	Human	Liver	Hepatitis B virus	Lower levels	Cao K et al. 2016
	Mouse	Isolated Microglia	Inflamed with LPS	Lower levels	Zhu L et al. 2015
GEO profiles	Human	Myelogenous leukemia cell line THP-1	Inflamed with LPS	Value reduction: 95,279	ID: 76881910
	Mouse	Wild type Macrophage	Inflamed with LPS	Value reduction: 58,789	ID: 44617209
Specific Single-cell RNA-seq (Bulk data)	Human	Cycling Scar-associated macrophages	Liver cirrhosis	Reduced expression	Ramachandran P et al. 2019

TPM: transcript per million; PPB: parts per billion; F. Tularensis: Francisella tularensis; Fc: Log2-fold change; Cnot1: CCR4-NOT Transcription Complex Subunit 1; KO: Knock out; NCBI: National Center for Biotechnology Information; LPS: Lipopolysaccharide; GEO: Gene Expression Omnibus.

The online material for this manuscript contains the following Excel file:

Data file S1. Raw data from figures.

DISCUSSION

Liver cirrhosis is an important cause of death worldwide. The presence of a sustained inflammatory milieu and extensive fibrosis are two key pathological features in cirrhotic patients (2,6). Macrophages are key cellular players in both progression and resolution of liver inflammation and fibrosis (42). In recent years, the scientific interest for defining the centrality of macrophages in CLD has increased exponentially. Some elegant new studies using single-cell RNA sequencing technologies have underscored key macrophage subpopulations with pro-fibrogenic roles in human cirrhotic livers (159). Ramachandran et al. performed an exhaustive transcriptomic profile of parenchymal and non-parenchymal cells in human cirrhotic livers and determined that MDMs were one of the most important cell linage contributing to liver fibrosis (160). Indeed, macrophage activation has been associated to medical complications in CLD, such as variceal bleeding and cirrhosis decompensation, and has been proposed as a prognostic parameter for survival in cirrhotic patients (70–72). Thus, the modulation of MDMs has been firmly proposed as a target for the design of novel therapeutic interventions (45). However, macrophages are incredibly plastic cells and key molecular signals governing their polarization are still unknown. In this thesis, we investigated the impacts of a selective macrophage activation of PPARγ signaling pathway (*article 1*) or E3 Ub ligase RNF41 expression (*article 2*) in CLD. Moreover, we explored the therapeutic utility of the modulation of liver MDMs via drug therapy (*article 1*) or gene expression modulation (*article 2*) delivered with selective carbon-based nanotools.

In *article 1*, we sought to evaluate the anti-inflammatory and pro-resolutive potential of macrophage-selective PPARγ activation. PPARγ nuclear receptor activation has been historically associated with anti-inflammatory macrophage polarization (161). PPARγ activation

suppresses the immunoreactive state of macrophages illustrated by the reduction in inflammatory markers such as NOS2, TNF-α, IL-6, and IL-1β (162). On the contrary, PPARγ activation promotes the expression of immunotolerant markers such as CD36, IL-13, Ym1, RETNLA, CD206, IL-4, and IL-10 (163–165). In the absence of PPARγ activation, macrophages display a sustained immune response losing the ability to transdifferentiate into a pro-resolving phenotype (166). These facts prompted us to selectively activate macrophage PPARγ signaling in fibrotic livers, which are characterized by a pro-inflammatory microenvironment. PPARs activation has been previously suggested as a therapeutic strategy for the treatment of CLD and for macrophage anti-inflammatory polarization (99,105,167,168). Boyer-Diaz et al. used a non-selective PPAR agonist to treat cirrhotic rats and hepatic cells isolated from cirrhotic patients (168). The treatment with this agonist ameliorated liver fibrosis and portal hypertension (168). Lefere et al. also used the same non-selective PPAR agonist for the treatment of experimental MASH, reducing inflammation and impairing disease progression (167). However, the use of non-selective agonists is restricted due to severe side effects (111,112). In our study, we used a specific PPARγ agonist, GW1929, with a well-stablished efficacy for macrophage anti-inflammatory polarization (99,107,108). The dose for GW1929 in systemic treatment following intravenous or intraperitoneal administration is usually 10 mg/Kg (109,169,170). We could efficiently design biocompatible NPs with 4-fold less drug dose for mouse intravenous administration. This dose was enough to selectively activate PPARγ signaling in liver macrophages, illustrated by an increase in IL-10 expression. Thus, the selective delivery of the agonist to macrophages using NPs allowed the reduction on the dose, potentially reducing the side effects associated with the use of non-cell-selective agonists administered systemically.

Macrophage PPARγ signaling and its role in macrophage polarization has been well-described in the literature. However, other molecular mechanisms governing macrophage polarization, such as E3 Ub ligases, have been barely studied. RNF41 is an E3 Ub ligase that has been associated to the degradation of pro-inflammatory cytokine receptors, to the inhibition of pro-inflammatory cytokine production and to the induction of macrophage anti-inflammatory polarization (121,124,125). Since RNF41 can activate C/EBPβ (125) and C/EBPβ in turn interacts with PPARγ signaling (171,172), the interaction between RNF41 and PPARγ pathways could be crucial to determine macrophage polarization programs in the liver. Considering all this evidence, we hypothesized that macrophage RNF41 may be altered in CLD. Thus, in *article 2*, we aimed to investigate emerging concepts about the potential immunoregulatory role of macrophage RNF41 in CLD. To our knowledge, this is the first study providing evidence about the role of macrophage RNF41 in CLD.

We first examined RNF41 expression in parenchymal (hepatocytes) and non-parenchymal (CD11b^{high} macrophages, LSECs, and HSC) cells isolated from the liver of cirrhotic patients and mice with liver fibrosis. For macrophage sorting, we used magnetic beads linked to an antibody against CD11b to ensure the isolation of liver CD11b^{high} MDMs. We found that the expression of RNF41 and Ub specific peptidase 8 (USP8), a known stabilizer of RNF41 (173,174), were downregulated in MDMs isolated from the liver of cirrhotic patients and fibrotic mice. The downregulation of macrophage RNF41 was independent of cirrhosis etiology in patients. To confirm our findings about the downregulation of macrophage RNF41 expression in cirrhosis, we analyzed some human and mouse gene expression atlas and bulk data available. Some studies have reported alterations in RNF41 expression in diverse inflammatory settings

(160,175). Importantly, Ramachandran et al. reported a reduced expression of RNF41 in cycling scar-associated macrophages, characterized by triggering receptor expressed on myeloid cells 2 (TREM2) and tetraspanin CD9 surface markers (160). The authors stated that this macrophage subpopulation has a key role in fibrosis progression in human cirrhotic livers (160). We then hypothesized that chronic inflammation could be responsible for the downregulation of macrophage RNF41 expression in CLD. To test this hypothesis, we stimulated human and mouse macrophage cell lines and mouse primary $CD11b^{+}$ liver macrophages with TNF-α for a prolonged period. We used TNF-α because is one of the most prominent cytokines driving inflammation in liver disease (46) and permits a continuous and progressive increase of MAPK and NF-κB pro-inflammatory signaling (176,177), independently of infection or LPS. Although RNF41 and USP8 expression increased during the first 24 hours of TNF-α stimulation, our data revealed that sustained inflammatory signals from TNF-α promotes a downregulation of macrophage RNF41 and USP8 expression in longer periods, mirroring the outcomes that we found in the inflammatory milieu of human and mouse fibrotic livers.

Altogether, our new findings about the role of macrophage RNF41 and previous studies on the function of macrophage PPARγ in chronic inflammation prompted us to investigate the selective modulation of MDMs via gene or drug therapy using novel engineered carbon-based nanotools. We hypothesized that selective MDM polarization towards a pro-resolutive phenotype could exert therapeutic effects on liver inflammation, fibrosis, and regeneration (**Figure 12**).

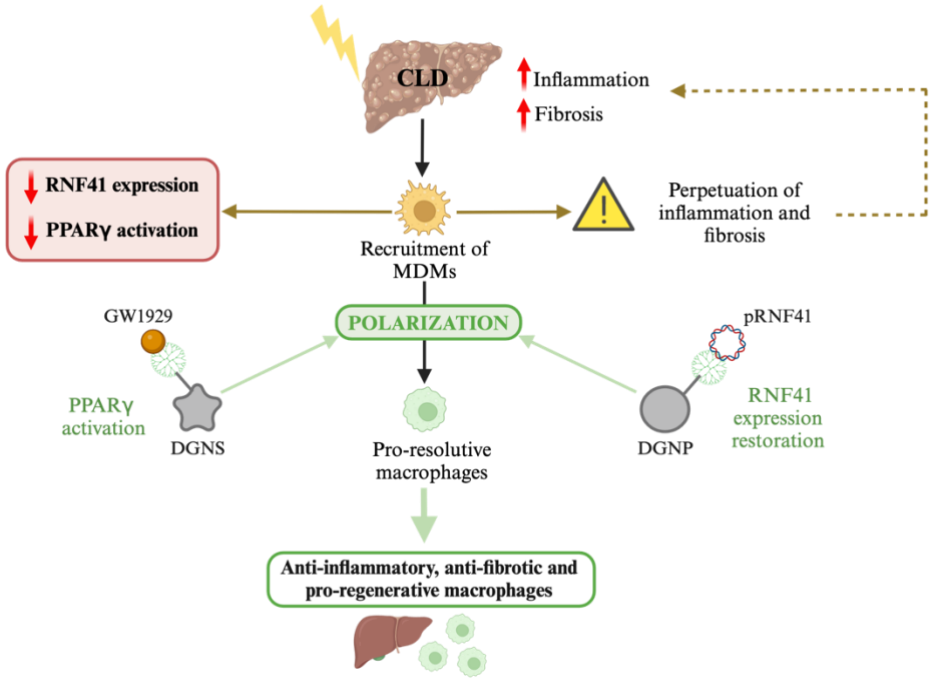

Figure 12: Schematic representation of the state of macrophages in CLD and the therapeutic potential of their polarization. MDMs are key cellular players in inflammation and fibrosis progression, and their polarization towards a pro-resolutive phenotype arises as a promising therapeutic strategy. Abbreviations: CLD, chronic liver disease; MDMs, monocyte-derived macrophages; RNF41, RING finger protein 41; PPARγ, peroxisome proliferator-activated receptor gamma; DGNS, dendrimer-graphene nanostars; DGNP, dendrimer-graphite nanoparticles. *Original image created with Biorender.*

To test this hypothesis, we used carbon-based NPs linked to PAMAM dendrimers as drug or pDNA delivery systems. We used two different carbon-derived nanomaterials as the main core of our engineered NPs, GNSs (*article 1*) and GNPs (*article 2*), which are completely different in structure and chemistry (178). Our results revealed minor differences in size among them, with GNPs being slightly bigger than GNSs. Both GNSs and GNPs were functionalized similarly with dendrimers using the same crosslinking agents to obtain DGNSs and DGNPs respectively. Dendrimers were used to further couple GW1929 PPARγ agonist (DGNS-GW) (*article 1*) or plasmids for RNF41

expression (pRNF41-DGNP) or blockade (pshRNF41-DGNP) (*article 2*). GW1929 agonist was covalently linked to DGNSs, whereas pRNF41 and pshRNF41 were attached to DGNPs through electrostatic interactions. Previous studies have suggested that the electrostatic interaction between pDNA and dendrimers results in a complex that is stable in a wide range of pH and salt conditions (179).

Dendrimers have been previously used as linkers for nucleic acids or small therapeutic molecules in other type of NPs for gene therapy or drug delivery (180). For instance, dendrimers have been used for the functionalization of gold NPs (181–183). However, the use of bare dendrimers for *in vivo* applications may be restricted due to cytotoxic effects. The cytotoxicity of uncoupled dendrimers depends strongly on the nature of functional surface groups. Cationic dendrimers often exhibit high toxicity, whereas anionic dendrimers show slight or no toxic effects (184). Cytotoxicity is primarily due to the interaction between the cationic dendrimer surface and cell membranes, which are negatively charged (185). Thus, dendrimer-coupled NPs should maintain a negative surface charge to be biocompatible (185). In our studies, we obtained isotonic and negatively charged NP dispersions by linking adequate quantities of GW1929 or pDNA to DGNSs or DGNPs, respectively. We tested the biocompatibility of NPs in human endothelial cells, which are the primary cells in blood vessels and the first biological barrier for intravenously administered formulations. Indeed, human endothelial cells have been widely used to assess the biocompatibility of a wide range of NPs (186,187).

We evaluated NP selectivity for targeting pro-inflammatory macrophages, which were the main target cells for our engineered carbon-

based NPs. We observed that TNF-α stimulated murine macrophages were more efficient in capturing and retaining both DGNS-GW (*article 1*) and pRNF41-DGNP (*article 2*), probably due to the carbon core structure and shape. Macrophages may selectively capture carbon NPs by receptor-mediated phagocytosis (188). Moreover, previous reports have indicated that macrophages are more efficient in capturing NPs under pro-inflammatory conditions, such as TNF-α stimulation (26,145). We further verified the selectivity of carbon-based NPs for macrophage targeting *in vivo*. Most NPs administered *in vivo* that are over 200 nm are supposed to be primarily incorporated by macrophages, and in particular by pro-inflammatory macrophages at diseased sites (126,189). Indeed, Melgar-Lesmes et al. demonstrated that functionalized DGNSs were primarily incorporated by liver pro-inflammatory macrophages in fibrotic mice (26). In *article 2*, we also verified that functionalized DGNPs were primarily incorporated by liver pro-inflammatory macrophages in fibrotic mice, indicating that both DGNSs and DGNPs can be similarly captured in macrophages under chronic inflammation. To further ensure the selectivity of pRNF41-DGNP, the expression of RNF41 was controlled under a CD11b promotor, to permit the functional targeting of DGNP to only $CD11b^{high}$ pro-inflammatory MDMs. The selectivity of pRNF41 delivered with DGNPs to liver pro-inflammatory MDMs was confirmed by the observation of its expression only in $CD11b^{high}$ pro-inflammatory macrophages isolated with magnetic cell sorting from the liver of fibrotic mice.

Carbon-based NPs linked to PAMAM dendrimers were therefore safe, efficient, and selective delivery systems to target liver pro-inflammatory MDMs. The next step was to test the therapeutic potential of macrophage-selective PPARγ signaling activation with DGNS-GW

(*article 1*) and RNF41 expression with pRNF41-DGNP (*article 2*) in mouse models of liver inflammation and fibrosis. In both studies, we used BALB/c mouse strain because these mice are more sensitive to liver fibrosis induction (190). We induced toxin-mediated experimental chronic liver injury and fibrosis with CCl_4 intraperitoneal administrations. CCl_4 is a hepatotoxic molecule classically used to promote chronic liver injury, fibrosis, and infiltration of pro-inflammatory macrophages. This toxicity results from the cytochrome P450-dependent reduction of CCl_4 to reactive trichloromethyl radicals (191). CCl_4 periodic administration leads to a robust and highly reproducible model of liver fibrosis (190). Indeed, animal models with CCl_4-induced liver fibrosis have been widely used to perform preclinical research of novel anti-inflammatory and anti-fibrotic drugs for the treatment of CLD (192–194). Thus, we chose this hepatotoxic molecule to stablish liver fibrosis in mice and to test the therapeutic utility of DGNS-GW and pRNF41-DGNP on liver inflammation and fibrosis. To assess the macrophage-selective polarization potential of DGNS-GW and pRNF41-DGNP, we first evaluated the gene and protein expression of inflammation-related genes.

In *article 1*, the livers of fibrotic mice treated with DGNS-GW displayed a reduction in the gene and protein expression of pro-inflammatory factors. PPARγ activation has been linked to the inhibition of the molecular signaling of the nuclear factor NF-κB (195). Activation of PPARγ negatively modulates NF-κB-dependent inflammation by upregulating IκB, a negative regulator of NF-κB, which can ultimately lead to the downregulation of pro-inflammatory genes (195). In *article 2*, selective macrophage induction of RNF41 expression in the livers of fibrotic mice using pRNF41-DGNPs also reduced the gene and protein expression of pro-inflammatory factors. This reduction of pro-

inflammatory gene expression was also observed in liver-isolated $CD11b^+$ macrophages. Interestingly, RNF41 activation has also been linked to NF-κB modulation via the polyubiquitination and degradation of Myd88, which is a TLR adaptor (124,196). Thus, the downregulation of pro-inflammatory genes following DGNS-GW or pRNF41-DGNP treatment is likely mediated by the inactivation of NF-κB signaling pathway in macrophages, but we cannot exclude other molecules or signaling pathways. We also observed an increased gene and protein expression of anti-inflammatory factors in the livers of fibrotic mice treated with DGNS-GW and pRNF41-DGNP. Liver-isolated $CD11b^+$ macrophages also showed an increased anti-inflammatory gene expression following pRNF41-DGNP treatment. These findings evidenced the potential of macrophage-selective PPARγ activation and RNF41 expression restoration to reprogram hepatic macrophages from pro-inflammatory to anti-inflammatory phenotype. It is known that PPARγ activity is essential for the acquisition and long-term maintenance of macrophage anti-inflammatory phenotype (197). Since RNF41 activates C/EBP-β (125), and C/EBP-β is a PPARγ inducer (198), we further hypothesized that macrophage RNF41 restoration could be inducing macrophage anti-inflammatory signaling through PPARγ activation. To assess this hypothesis, we evaluated the expression of some PPARγ downstream genes in the livers of fibrotic mice treated with pRNF41-DGNP (*article 2*). We found an increased expression on the PPARγ downstream genes IL-10 and CD36 in the livers of fibrotic mice treated with pRNF41-DGNP, suggesting an interplay between RNF41 and PPARγ. However, the precise molecular mechanisms that link RNF41 and PPARγ remain unclear and need further investigation. Altogether, our results reinforce the fact that PPARγ acts as an essential nuclear regulator of inflammation

in macrophages and RNF41 may be modulating macrophage anti-inflammatory phenotype partially through PPARγ activation.

Since chronic liver inflammation and fibrosis are two phenomena that are tightly associated (6), we wondered whether the polarization of macrophages towards an anti-inflammatory phenotype was also influencing liver fibrosis. Our results in *article 1* and *article 2* indicated a reduction in liver fibrosis following DGNS-GW and pRNF41-DGNP administration to fibrotic mice. In *article 1*, the reduction of liver fibrosis area following DGNS-GW administration was accompanied with a decreased expression of liver α-SMA. The modulation of PPARγ has been previously described to attenuate HSC activation and to reduce liver fibrosis (105), in part because the expression of IL-10 has been directly correlated to α-SMA reduction (199–201). However, we did not observe a significant reduction in collagen I and TIMPs gene expression following selective macrophage PPARγ activation, which indicated that the treatment with DGNS-GW may not directly modulate HSC activity. Interestingly, we found proliferative cells along fibrotic tracts in the liver of fibrotic mice treated with DGNS-GW, together with an increased expression of VEGF. Since PPARγ activation has been associated with VEGF production in macrophage cell lines (65,202) and VEGF has been linked to fibrosis resolution through the stimulation of pro-resolutive scar-associated macrophages (64), we think that macrophage-selective PPARγ activation may also favor the proliferation of pro-resolutive macrophage lineages located in fibrotic tracts. The antifibrotic effects of DGNS-GW were attributed to an increase in the liver expression of gelatinase MMP-2 and MMP-9, indicating that PPARγ activation directly influences the collagenolytic enzymatic secretome of macrophages to boost ECM remodeling.

In *article 2*, we also observed an increase in liver MMP-9 expression due to RNF41 induction in macrophages, which was accompanied with a reduction in the liver expression of macrophage-derived pro-fibrogenic factors and genes related to HSC activity. These outcomes indicated that macrophage polarization following induction of RNF41 expression influences ECM remodeling by both increasing collagenolytic enzymes and impairing HSC activity. These results were corroborated in a second independent cohort of mice treated with pRNF41-DGNP and thioacetamide (TAA), which is a hepatotoxic molecule that causes oxidative stress and centrilobular necrosis (203). These results were consistent with those observed in fibrotic mice treated with pRNF41-DGNP after fibrosis induction with CCl_4. Thus, our study reinforced the fact that macrophages polarized to an anti-inflammatory state are key cells contributing to HSC inactivation in fibrotic livers (204–206). Interestingly, HSCs were not the only cells influenced by macrophage RNF41 recovered expression. Our results indicated that hepatocyte proliferation was also favored by macrophage RNF41 restoration in mice with chronic liver injury. This hepatocyte proliferation correlated with augmented liver expression of IGF-1, and not by HGF, which is probably the most potent growth factor driving hepatocyte proliferation (207). IGF-1 deficiency is a common condition in chronic liver disease independently of the etiology of chronic liver damage (208–210). IGF-1 is not only a trophic factor produced by the liver but is also secreted by monocytes and macrophages to stimulate tissue growth (63). Previous studies have suggested that IGF-1 secreted from macrophages not only affects hepatocyte proliferation but also promotes HSC inactivation (62,63), influencing both fibrosis resolution and liver regeneration. In our study, we speculated that the increase of liver IGF-1 following macrophage RNF41 restoration has a dual influence on both fibrosis resolution and hepatocyte regeneration. Macrophage-selective blockade of RNF41

expression with pshRNF41-DGNP exerted the opposite effects, thereby reducing IGF-1 liver expression and hepatocyte proliferation, and increasing the expression of macrophage pro-fibrogenic factors and genes related to HSC activity. The detrimental effects of macrophage RNF41 blockade resulted in a substantial increase on liver fibrosis and an impairment of liver function, which was accompanied by a pro-inflammatory cytokine storm, and ultimately reduced survival in fibrotic mice. Thus, macrophage RNF41 orchestrates fibrosis regression by modulating the inflammatory phenotype of macrophages but also promoting the inactivation of HSC and influencing the recovery of hepatocyte proliferation.

Since macrophage RNF41 restoration influenced hepatocyte proliferation, we finally wondered whether induction of macrophage RNF41 could also be beneficial in the context of liver resection. A previous study described the predominant effect of macrophage RNF41 on the activation of CREB-C/EBP-β cascade (211), and the activation of this cascade has been associated with muscle injury repair (86). Moreover, the activity of anti-inflammatory macrophages has also been associated to tissue repair (59). Since pRNF41-DGNP treatment switched macrophage phenotype towards an anti-inflammatory state, we tested macrophage RNF41 function in healthy and fibrotic mice undergoing partial hepatectomy. Partial hepatectomy (70% or 2/3) represents the most commonly used model for the study of liver regeneration (212,213). We performed 70% partial hepatectomy in healthy mice and 40% partial hepatectomy in fibrotic mice, to reduce possible unnecessary animal loss, and evaluated the regeneration rate following pRNF41-DGNP administration. Macrophage RNF41 induction in either healthy or fibrotic mice resulted in a faster hepatic regeneration after liver resection, and in a reduction of liver injury in fibrotic mice. The regenerative process was

accompanied by an increase in the expression of hepatic IGF-1 and also PPARγ downstream genes illustrated by an increased liver expression of CD36 and IL-10. PPARγ signaling has been previously described as an essential pathway for the correct regeneration in the liver (214). Thus, we think that macrophage RNF41 may coordinate a well-orchestrated regeneration process by inducing macrophage anti-inflammatory phenotype and also influencing signaling cascades related to regeneration such as IGF-1 and the PPARγ signaling pathway.

In conclusion, the results of this thesis expand our understanding on macrophage biology in the context of CLD, reporting insights into the relationship between RNF41 and PPARγ in chronic liver injury and hepatic regeneration. The heterogeneous cellular impacts of macrophage-selective PPARγ activation with DGNS-GW (*article 1*) and RNF41 restoration with pRNF41-DGNP (*article 2*) on liver inflammation, fibrosis, and regeneration are illustrated in **Figure 13**.

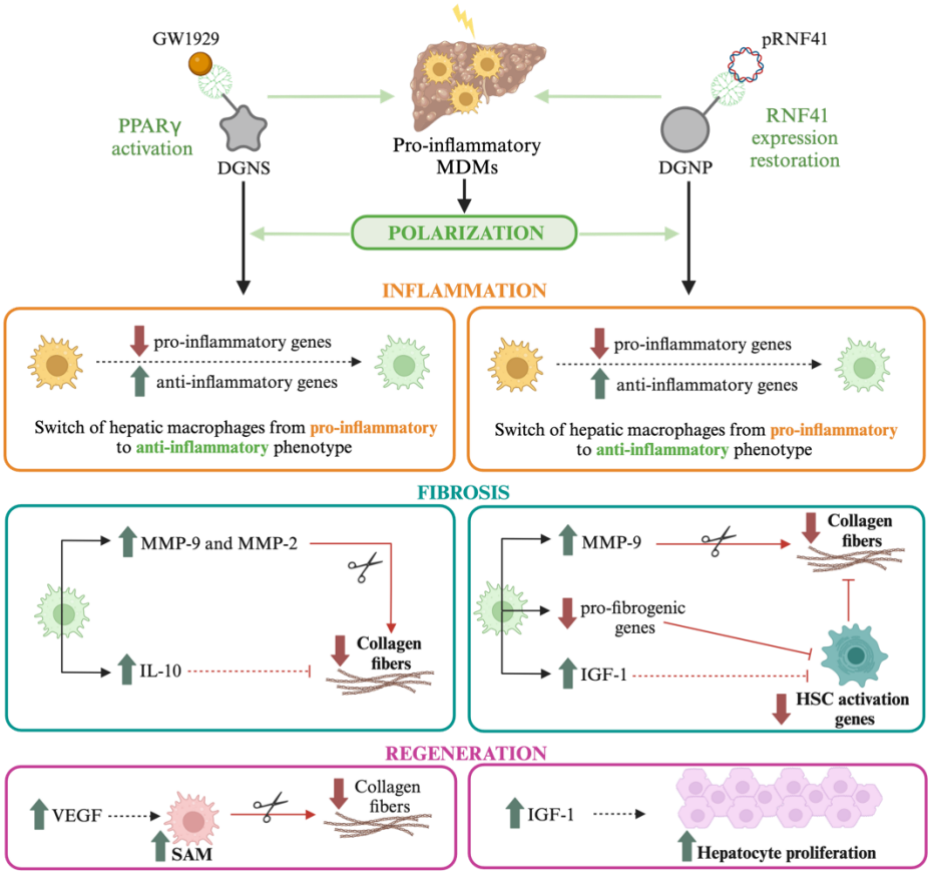

Figure 13: Schematic illustration of the effects of macrophage-selective PPARγ activation and RNF41 restoration in liver inflammation, fibrosis, and regeneration. Abbreviations: PPARγ, peroxisome proliferator-activated receptor gamma; DGNS, dendrimer-graphene nanostars; MDMs, monocyte-derived macrophages; DGNP, dendrimer-graphite nanoparticles; pRNF41, plasmid expressing RNF41; MMP-2, metalloproteinase 2; MMP-9, metalloproteinase 9; IL-10, interleukin 10; IGF-1, insulin-like growth factor 1; HSC, hepatic stellate cells; VEGF, vascular endothelial growth factor; SAM, scar-associated macrophages. *Original image created with Biorender.*

This thesis defines macrophages as central cellular regulators in liver inflammation, fibrosis, and regeneration, and highlights the potential of novel carbon-based nanoscale therapies for macrophage targeting and modulation. However, these studies present some limitations and there are still open questions that need to be further investigated. First, although the importance of macrophage RNF41 was elucidated in macrophages isolated from human cirrhotic livers, all experiments related to the uptake

and selective drug or plasmid delivery of DGNS and DGNP were investigated in murine macrophage cell lines and in animal models. NP uptake and delivery of GW1929 or pDNA should be also investigated in human macrophages, such as in $CD11b^{high}$ macrophages isolated from human cirrhotic livers. However, the enormous difficulties to obtain enough sample from human origin for efficient macrophage isolation limits the performance of these experiments. Second, more mechanistic studies are needed to fully understand the molecular connection between RNF41 activity and PPARγ activation in macrophage anti-inflammatory and pro-resolutive polarization. We think that both RNF41 and PPARγ are key molecular players governing macrophage polarization programs in chronic liver inflammation, but we cannot exclude other molecular mechanisms. Third, the therapeutic utility of carbon-based NPs was elucidated in mice with toxin-induced liver fibrosis. The results obtained in this thesis regarding the therapeutic utility of these NPs should be corroborated in other models, such as fibrotic animals with steatosis, human precision-cut liver slices, or *ex vivo* liver perfusion systems.

CONCLUSIONS

The conclusions obtained in this doctoral thesis can be summarized as follows:

1) Dendrimer-graphene nanostars linked to a low dose of GW1929 peroxisome proliferator-activated receptor gamma (PPARγ) agonist (DGNS-GW) preferentially accumulate in tumor necrosis factor alpha (TNF-α)-stimulated murine macrophages.
2) GW1929 delivered with dendrimer-graphene nanostars efficiently activates macrophage PPARγ signaling, illustrated by an increase in interleukine-10 expression, both in TNF-α-stimulated murine macrophages and in the liver of fibrotic mice.
3) Treatment with DGNS-GW reduces the expression of pro-inflammatory genes in TNF-α-stimulated murine macrophages without altering the expression of anti-inflammatory genes.
4) Selective macrophage PPARγ activation by DGNS-GW switches macrophages from pro-inflammatory to anti-inflammatory phenotype in the liver of fibrotic mice.
5) Treatment with DGNS-GW significantly reduces fibrosis in the liver of fibrotic mice likely due to an increase in the expression of collagenolytic enzymes.
6) Treatment with DGNS-GW promotes liver regeneration in fibrotic mice, which is associated with an augmented liver expression of vascular endothelial growth factor.
7) Macrophage E3 ubiquitin ligase RING finger 41 (RNF41) expression is downregulated in $CD11b^{high}$ macrophages isolated from the liver of fibrotic mice and cirrhotic patients regardless of cirrhosis etiology.
8) Macrophage RNF41 downregulation is in part mediated by prolonged inflammatory stimuli.

9) Dendrimer-graphite nanoparticles selectively and efficiently transfect a RNF41-encoding plasmid into macrophages infiltrated in mouse fibrotic livers.
10) Selective restoration of RNF41 in macrophages using dendrimer-graphite nanoparticles linked to a RNF41-encoding plasmid (pRNF41-DGNP) promotes an anti-inflammatory phenotype in hepatic macrophages, induces fibrosis regression, and reduces liver injury in fibrotic mice, in part, mediated by insulin-like growth factor 1 upregulation.
11) Selective blockade of macrophage RNF41 expression with pshRNF41-DGNP increases fibrosis and liver damage in the liver of fibrotic mice, induces a pro-inflammatory phenotype in macrophages, and reduces mouse survival.
12) Selective induction of RNF41 expression in macrophages using pRNF41-DGNP promotes hepatic regeneration after liver resection.

According to the results obtained in this doctoral thesis, it may be concluded that the selective activation of the anti-inflammatory pathways PPARγ or RNF41 in liver monocyte-derived macrophages can stimulate a pro-resolutive phenotype in macrophages resulting in a decrease of liver inflammation and fibrosis and an increase of hepatic regeneration. The use of carbon-based nanotools linked to dendrimers are promising nanoscale therapeutic approaches to target and treat liver pro-inflammatory macrophages through the delivery of drug or gene therapies. The findings of this thesis provide a rationale for personalized therapeutic strategies in chronic liver disease and potentially for other diseases characterized by inflammation and fibrosis.

REFERENCES

1. Parola M, Pinzani M. Liver fibrosis: Pathophysiology, pathogenetic targets and clinical issues. Mol Aspects Med. 2019; 65:37–55.
2. Devarbhavi H, Asrani SK, Arab JP, Nartey YA, Pose E, Kamath PS, et al. Global burden of liver disease: 2023 update. J Hepatol. 2023; 79(2):516–37.
3. Bataller R, Brenner D. Liver fibrosis. J Clin Invest. 2005; 115(2):209–18.
4. Pellicoro A, Ramachandran P, Iredale JP, Fallowfield JA. Liver fibrosis and repair: Immune regulation of wound healing in a solid organ. Nat Rev Immunol. 2014; 14(3):181–94.
5. Fattovich G, Stroffolini T, Zagni I, Donato F. Hepatocellular carcinoma in cirrhosis: Incidence and risk factors. Gastroenterology. 2004; 127(5):35–50.
6. Hammerich L, Tacke F. Hepatic inflammatory responses in liver fibrosis. Nat Rev Gastroenterol Hepatol. 2023; 20(10):633–46.
7. Costa D, Simbrunner B, Jachs M, Hartl L, Bauer D, Paternostro R, et al. Systemic inflammation increases across distinct stages of advanced chronic liver disease and correlates with decompensation and mortality. J Hepatol. 2021; 74(4):819–28.
8. Simbrunner B, Villesen IF, Königshofer P, Scheiner B, Bauer D, Paternostro R, et al. Systemic inflammation is linked to liver fibrogenesis in patients with advanced chronic liver disease. Liver Int. 2022; 42(11):2501–12.
9. Burra P, Burroughs A, Graziadei I, Pirenne J, Valdecasas JC, Muiesan P, et al. EASL Clinical Practice Guidelines: Liver transplantation. J Hepatol. 2016; 64(2):433–85.
10. Mathur AK, Ashby VB, Fuller DS, Zhang M, Merion RM, Leichtman A, et al. Variation in access to the liver transplant waiting list in the United States. Transplantation. 2014; 98(1):94–9.
11. Wynn TA, Ramalingam TR. Mechanisms of fibrosis: Therapeutic translation for fibrotic disease. Nat Med. 2012; 18(7):1028–40.
12. Pinzani M. Liver fibrosis. Springer Semin Immunopathol. 2000; 21:475–90.
13. Wang J, Qin T, Sun J, Li S, Cao L, Lu X. Non-invasive methods to evaluate liver fibrosis in patients with non-alcoholic fatty liver disease. Front Physiol. 2022; 13:1–11.
14. de Lédinghen V, Vergniol J. Transient elastography (FibroScan). Gastroenterol Clin Biol. 2008; 32(6):58–67.

15. Roehlen N, Crouchet E, Baumen TE. Liver Fibrosis: Mechanistic Concepts and. Cells. 2020. 1–43 p.
16. Kruepunga N, Hakvoort TBM, Hikspoors JPJM, Köhler SE, Lamers WH. Anatomy of rodent and human livers: What are the differences? Biochim Biophys Acta - Mol Basis Dis. 2019; 1865(5):869–78.
17. Ben-Moshe S, Itzkovitz S. Spatial heterogeneity in the mammalian liver. Nat Rev Gastroenterol Hepatol. 2019; 16(7):395–410.
18. Kisseleva T, Brenner D. Molecular and cellular mechanisms of liver fibrosis and its regression. Nat Rev Gastroenterol Hepatol. 2021; 18(3):151–66.
19. Tsuchida T, Friedman SL. Mechanisms of hepatic stellate cell activation. Nat Rev Gastroenterol Hepatol. 2017; 14(7):397–411.
20. Ying HZ, Chen Q, Zhang WY, Zhang HH, Ma Y, Zhang SZ, et al. PDGF signaling pathway in hepatic fibrosis pathogenesis and therapeutics (Review). Mol Med Rep. 2017; 16(6):7879–89.
21. Elpek GÖ. Cellular and molecular mechanisms in the pathogenesis of liver fibrosis: An update. World J Gastroenterol. 2014; 20(23):7260–76.
22. Pradere JP, Kluwe J, De Minicis S, Jiao JJ, Gwak GY, Dapito DH, et al. Hepatic macrophages but not dendritic cells contribute to liver fibrosis by promoting the survival of activated hepatic stellate cells in mice. Hepatology. 2013; 58(4).
23. Iwaisako K, Jiang C, Zhang M, Cong M, Moore-Morris TJ, Park TJ, et al. Origin of myofibroblasts in the fibrotic liver in mice. Proc Natl Acad Sci U S A. 2014; 111(32).
24. Arthur MJP. Reversibility of liver fibrosis and cirrhosis following treatment for hepatitis C. Gastroenterology. 2002; 122(5):1525–8.
25. Rockey DC, Friedman SL. Fibrosis Regression After Eradication of Hepatitis C Virus: From Bench to Bedside. Gastroenterology. 2021; 160(5):1502-1520.e1.
26. Melgar-lesmes P, Luquero A, Parra-robert M, Mora A, Ribera J, Edelman ER, et al. Graphene-dendrimer nanostars for targeted macrophage overexpression of metalloproteinase 9 and hepatic fibrosis precision therapy. Nano Lett. 2019; 18(9):5839–45.
27. Perramón M, Navalón-López M, Fernández-Varo G, Moreno-Lanceta A, García-Pérez R, Faneca J, et al. Liver-targeted nanoparticles delivering nitric oxide reduce portal hypertension in

cirrhotic rats. Biomed Pharmacother. 2024; 171: 116143.
28. Perramón M, Carvajal S, Reichenbach V, Fernández-Varo G, Boix L, Macias-Muñoz L, et al. The pituitary tumour-transforming gene 1/delta-like homologue 1 pathway plays a key role in liver fibrogenesis. Liver Int. 2022; 42(3):651–62.
29. Koda Y, Teratani T, Chu PS, Hagihara Y, Mikami Y, Harada Y, et al. CD8+ tissue-resident memory T cells promote liver fibrosis resolution by inducing apoptosis of hepatic stellate cells. Nat Commun. 2021; 12(1):1–15.
30. DeFrances GKM and MC. Liver Regeneration. Science. 1997; 276:60–6.
31. Mehendale HM. Tissue Repair: An Important Determinant of Final Outcome of Toxicant-Induced Injury. Toxicol Pathol. 2005; 33(1):41–51.
32. Nagasue N, Yukaya H, Ogawa Y, Kohno H, Nakamura T. Human liver regeneration after major hepatic resection. A study of normal liver and livers with chronic hepatitis and cirrhosis. Ann Surg. 1987; 206(1):30–9.
33. Michalopoulos GK, Bhushan B. Liver regeneration: biological and pathological mechanisms and implications. Nat Rev Gastroenterol Hepatol. 2021; 18(1):40–55.
34. Michalopoulos GK. Liver Regeneration. J Cell Physiol. 2007; 213(2):286–300.
35. Zhang C, Sun C, Zhao Y, Ye B, Yu GY. Signaling pathways of liver regeneration: Biological mechanisms and implications. iScience. 2024; 27(1):108683.
36. Melgar-Lesmes P, Edelman ER. Monocyte-endothelial cell interactions in the regulation of vascular sprouting and liver regeneration in mouse. J Hepatol. 2015; 63(4):917–25.
37. Medrano-Bosch M, Simón-Codina B, Jiménez W, Edelman ER, Melgar-Lesmes P. Monocyte-endothelial cell interactions in vascular and tissue remodeling. Front Immunol. 2023; 14:1–21.
38. Hirayama D, Iida T, Nakase H. The phagocytic function of macrophage-enforcing innate immunity and tissue homeostasis. Int J Mol Sci. 2018; 19(1): 92.
39. Germic N, Frangez Z, Yousefi S, Simon HU. Regulation of the innate immune system by autophagy: monocytes, macrophages, dendritic cells and antigen presentation. Cell Death Differ. 2019;

26(4):715–27.
40. Martín-Orozco N, Isibasi A, Ortiz-Navarrete V. Macrophages present exogenous antigens by class I major histocompatibility complex molecules via a secretory pathway as a consequence of interferon-γ activation. Immunology. 2001; 103(1):41–8.
41. Sreejit G, Fleetwood AJ, Murphy AJ, Nagareddy PR. Origins and diversity of macrophages in health and disease. Clin Transl Immunol. 2020; 9(12):1–19.
42. Krenkel O, Tacke F. Liver macrophages in tissue homeostasis and disease. Nat Rev Immunol. 2017; 17(5):306–21.
43. Freitas-Lopes MA, Mafra K, David BA, Carvalho-Gontijo R, Menezes GB. Differential location and distribution of hepatic immune cells. Cells. 2017; 6(4):1–22.
44. Ehling J, Bartneck M, Wei X, Gremse F, Fech V, Möckel D, et al. CCL2-dependent infiltrating macrophages promote angiogenesis in progressive liver fibrosis. Gut. 2014; 63(12):1960–71.
45. Ju C, Tacke F. Hepatic macrophages in homeostasis and liver diseases: From pathogenesis to novel therapeutic strategies. Cell Mol Immunol. 2016; 13(3):316–27.
46. Connolly MK, Bedrosian AS, Mallen-St. Clair J, Mitchell AP, Ibrahim J, Stroud A, et al. In liver fibrosis, dendritic cells govern hepatic inflammation in mice via TNF-α. J Clin Invest. 2009; 119(11):3213–25.
47. Auguet T, Vidal F, López-Dupla M, Broch M, Gutiérrez C, Olona M, et al. A study on the TNF-α system in Caucasian Spanish patients with alcoholic liver disease. Drug Alcohol Depend. 2008; 92(1–3):91–9.
48. Kadomoto S, Izumi K, Mizokami A. Macrophage Polarity and Disease Control. Int J Mol Sci. 2022; 23(1): 144.
49. Yang H, Xuefeng Y, Shandong W, Jianhua X. COX-2 in liver fibrosis. Clin Chim Acta. 2020; 506:196–203.
50. Li YH, Zhang Y, Pan G, Xiang LX, Luo DC, Shao JZ. Occurrences and Functions of Ly6Chi and Ly6Clo Macrophages in Health and Disease. Front Immunol. 2022; 13:1–9.
51. Mills CD, Kincaid K, Alt JM, Heilman MJ, Hill AM. M-1/M-2 Macrophages and the Th1/Th2 Paradigm. J Immunol. 2000; 164(12):6166–6173.
52. Medzhitov R. Origin and physiological roles of inflammation.

Nature. 2008; 454(7203):428–35.
53. Das A, Sinha M, Datta S, Abas M, Chaffee S, Sen CK, et al. Monocyte and Macrophage Plasticity in Tissue Repair and Regeneration. Am J Pathol. 2015; 185(10):2596–606.
54. Wynn TA, Vannella KM. Macrophages in Tissue Repair, Regeneration, and Fibrosis. Immunity. 2016; 44(3):450–62.
55. Jablonski KA, Amici SA, Webb LM, Ruiz-Rosado JDD, Popovich PG, Partida-Sanchez S, et al. Novel markers to delineate murine M1 and M2 macrophages. PLoS One. 2015; 10(12):5–11.
56. Orecchioni M, Ghosheh Y, Pramod AB, Ley K. Macrophage polarization: Different gene signatures in M1(Lps+) vs. Classically and M2(LPS-) vs. Alternatively activated macrophages. Front Immunol. 2019; 10:1–14.
57. Geervliet E, Bansal R. Matrix Metalloproteinases as Potential Biomarkers. J Cells. 2020; 9(1212):2–20.
58. Naim A, Pan Q, Baig MS. Matrix Metalloproteinases (MMPs) in Liver Diseases. J Clin Exp Hepatol. 2017; 7(4):367–72.
59. Wen Y. The Role of Immune Cells in Liver Regeneration. Livers. 2023; 3(3):383–96.
60. Li N, Hua J. Immune cells in liver regeneration Review. Oncotarget. 2017; 8(2):3628–39.
61. Zhao Y, Ye W, Wang YD, Chen WD. HGF/c-Met: A Key Promoter in Liver Regeneration. Front Pharmacol. 2022; 13:1–10.
62. Nishizawa H, Iguchi G, Fukuoka H, Takahashi M, Suda K, Bando H, et al. IGF-I induces senescence of hepatic stellate cells and limits fibrosis in a p53-dependent manner. Sci Rep. 2016; 6:1–11.
63. Tonkin J, Temmerman L, Sampson RD, Gallego-Colon E, Barberi L, Bilbao D, et al. Monocyte/macrophage-derived IGF-1 orchestrates murine skeletal muscle regeneration and modulates autocrine polarization. Mol Ther. 2015; 23(7):1189–200.
64. Yang L, Kwon J, Popov Y, Gajdos GB, Ordog T, Brekken RA, et al. Vascular Endothelial Growth Factor Promotes Fibrosis Resolution and Repair in Mice. Gastroenterology. 2014; 146(5):1339–50.
65. Jozkowicz A, Dulak J, Piatkowska E, Placha W, Dembinska-Kiec A. Ligands of peroxisome proliferator-activated receptor-gamma increase the generation of vascular endothelial growth factor in vascular smooth muscle cells and in macrophages. Acta Biochim Pol. 2000; 47(4):1147–57.

66. Shi C, Pamer EG. Monocyte recruitment during infection and inflammation. Nat Rev Immunol. 2011; 11(11):762–74.
67. Pahl HL, Rosmarin AG, Tenen DG. Characterization of the myeloid-speciflc CD11b promoter. Blood. 1992; 79(4):865–70.
68. Diamond MS, Staunton DE, De Fougerolles AR, Stacker SA, Garcia-Aguilar J, Hibbs ML, et al. ICAM-1 (CD54): A counter-receptor for Mac-1 (CD11b/CD18). J Cell Biol. 1990; 111(6):3129–39.
69. Möst J, Schwaeble W, Drach J, Sommerauer A, Dierich MP. Regulation of the expression of ICAM-1 on human monocytes and monocytic tumor cell lines. J Immunol. 1992; 148(6):1635–42.
70. Rode A, Nicoll A, Møller HJ, Lim L, Angus PW, Kronborg I, et al. Hepatic macrophage activation predicts clinical decompensation in chronic liver disease. Gut. 2013; 62(8):1231–2.
71. Nielsen MC, Gantzel RH, Cl J, Trebicka J, Møller HJ, Grønbæk H. Macrophage Activation Markers, CD163 and CD206, in Acute-on-Chronic Liver Failure. Cells. 2020; 9:1175.
72. Waidmann O, Brunner F, Herrmann E, Zeuzem S, Piiper A, Kronenberger B. Macrophage activation is a prognostic parameter for variceal bleeding and overall survival in patients with liver cirrhosis. J Hepatol. 2013; 58(5):956–61.
73. Yao Y, Xu XH, Jin L. Macrophage polarization in physiological and pathological pregnancy. Front Immunol. 2019; 10:1–13.
74. Liu YC. Ubiquitin ligases and the immune response. Annu Rev Immunol. 2004; 22:81–127.
75. Wang X, Lupardus P, LaPorte SL, Garcia KC. Structural Biology of Shared Cytokine Receptors. Annu Rev Immunol 2009; 27:29–60.
76. Shi JH, Sun SC. Tumor necrosis factor receptor-associated factor regulation of nuclear factor κB and mitogen-activated protein kinase pathways. Front Immunol. 2018; 9:1–13.
77. Hu X, Li J, Fu M, Zhao X, Wang W. The JAK/STAT signaling pathway: from bench to clinic. Signal Transduct Target Ther. 2021; 6(1):402.
78. Gadina M, Gazaniga N, Vian L, Furumoto Y. Small molecules to the rescue: Inhibition of cytokine signaling in immune-mediated diseases. J Autoimmun. 2017; 85(301):20–31.
79. Mitchell S, Vargas J, Hoffmann A. Signaling via the NFκB system. Wiley Interdiscip Rev Syst Biol Med. 2016; 8(3):227–41.

80. Moens U, Kostenko S, Sveinbjørnsson B. The role of mitogen-activated protein kinase-activated protein kinases (MAPKAPKs) in inflammation. Genes (Basel). 2013; 4(2):101–33.
81. Darling NJ, Cook SJ. The role of MAPK signalling pathways in the response to endoplasmic reticulum stress. Biochim Biophys Acta - Mol Cell Res. 2014; 1843(10):2150–63.
82. Hu Q, Bian Q, Rong D, Wang L, Song J, Huang HS, et al. JAK/STAT pathway: Extracellular signals, diseases, immunity, and therapeutic regimens. Front Bioeng Biotechnol. 2023; 11:1–24.
83. Mueller TD, Zhang JL, Sebald W, Duschl A. Structure, binding, and antagonists in the IL-4/IL-13 receptor system. Biochim Biophys Acta - Mol Cell Res. 2002; 1592(3):237–50.
84. Shea JJO, Paul WE, Cells CDT. Mechanisms Underlying Lineage Commitment and Plasticity of Helper CD4+ T Cells. Science. 2010; 327:1098–103.
85. Gordon S, Martinez FO. Alternative activation of macrophages: Mechanism and functions. Immunity. 2010; 32(5):593–604.
86. Ruffell D, Mourkioti F, Gambardella A, Kirstetter P, Lopez RG, Rosenthal N, et al. A CREB-C/EBPβ cascade induces M2 macrophage-specific gene expression and promotes muscle injury repair. Proc Natl Acad Sci U S A. 2009; 106(41):17475–80.
87. Moore KJ, Rosen ED, Fitzgerald ML, Randow F, Andersson LP, Altshuler D, et al. The role of PPAR-γ in macrophage differentiation and cholesterol uptake. Nat Med. 2001; 7:41–7.
88. Guo L, Li X, Tang QQ. Transcriptional regulation of adipocyte differentiation: A central role for CCAAT/ enhancer-binding protein (C/EBP) β. J Biol Chem. 2015; 290(2):755–61.
89. Bradley MN, Zhou L, Smale ST. C/EBP beta Regulation in Lipopolysaccharide-Stimulated Macrophages. 2003; 23(14):4841–58.
90. Zhou J, Li H, Xia X, Herrera A, Pollock N, Reebye V, et al. Anti-inflammatory Activity of MTL-CEBPA, a Small Activating RNA Drug, in LPS-Stimulated Monocytes and Humanized Mice. Mol Ther. 2019; 27(5):999–1016.
91. Greene ME, Blumberg B, McBride OW, Yi HF, Kronquist K, Kwan K, et al. isolation of the human peroxisome proliferator activated receptor gamma cDNA: Expression in hematopoietic cells and chromosomal mapping. Gene Expr. 1995; 4(4–5):281–99.

92. Chandra V, Huang P, Hamuro Y, Raghuram S, Wang Y, Burris TP, et al. Structure of the intact PPAR-γ–RXR-α nuclear receptor complex on DNA. Nature. 2008; 456(7220):350–6.
93. Greenberg ME, Sun M, Zhang R, Febbraio M, Silverstein R, Hazen SL. Oxidized phosphatidylserine-CD36 interactions play an essential role in macrophage-dependent phagocytosis of apoptotic cells. J Exp Med. 2006; 203(12):2613–25.
94. Pennathur S, Pasichnyk K, Bahrami NM, Zeng L, Febbraio M, Yamaguchi I, et al. The Macrophage Phagocytic Receptor CD36 Promotes Fibrogenic Pathways on Removal of Apoptotic Cells during Chronic Kidney Injury. Am J Pathol. 2015; 185(8):2232–45.
95. Garg M, Johri S, Sagar S, Mundhada A, Agrawal A, Ray P, et al. Cardiolipin-mediated PPARγ S112 phosphorylation impairs IL-10 production and inflammation resolution during bacterial pneumonia. Cell Rep. 2021; 34(6):108736.
96. Yu L, Gao Y, Aaron N, Qiang L. A glimpse of the connection between PPARγ and macrophage. Front Pharmacol. 2023; 14:1–9.
97. de Carvalho M V., Gonçalves-De-albuquerque CF, Silva AR. PPAR gamma: From definition to molecular targets and therapy of lung diseases. Int J Mol Sci. 2021; 22(2):1–20.
98. Wang C, Ma C, Gong L, Guo Y, Fu K, Zhang Y, et al. Macrophage Polarization and Its Role in Liver Disease. Front Immunol. 2021; 12:1–25.
99. Bouhlel MA, Derudas B, Rigamonti E, Dièvart R, Brozek J, Haulon S, et al. PPARγ Activation Primes Human Monocytes into Alternative M2 Macrophages with Anti-inflammatory Properties. Cell Metab. 2007; 6(2):137–43.
100. Tan CK, Zhuang Y, Wahli W. Synthetic and natural Peroxisome Proliferator-Activated Receptor (PPAR) agonists as candidates for the therapy of the metabolic syndrome. Expert Opin Ther Targets. 2017; 21(3):333–48.
101. Yi W, Shi J, Zhao G, Zhou XE, Suino-Powell K, Melcher K, et al. Identification of a novel selective PPARλ 3 ligand with a unique binding mode and improved therapeutic profile in vitro. Sci Rep. 2017; 7:1–11.
102. Zhao D, Zhu Z, Li D, Xu R, Wang T, Liu K. Pioglitazone Suppresses CXCR7 Expression to Inhibit Human Macrophage Chemotaxis through Peroxisome Proliferator-Activated Receptor γ.

Biochemistry. 2015; 54(45):6806–14.
103. Wu D, Eeda V, Undi RB, Mann S, Stout M, Lim HY, et al. A novel peroxisome proliferator-activated receptor gamma ligand improves insulin sensitivity and promotes browning of white adipose tissue in obese mice. Mol Metab. 2021; 54:101363.
104. Rizos CV, Elisaf MS, Mikhailidis DP, Liberopoulos EN. How safe is the use of thiazolidinediones in clinical practice? Expert Opin Drug Saf. 2009; 8(1):15–32.
105. Li J, Guo C, Wu J. The agonists of peroxisome proliferator-activated receptor-γ for liver fibrosis. Drug Des Devel Ther. 2021; 15:2619–28.
106. Willson TM, Brown PJ, Sternbach DD, Henke BR. The PPARs: From orphan receptors to drug discovery. J Med Chem. 2000; 43(4):527–50.
107. Tsoyi K, Ha YM, Kim YM, Lee YS, Kim HJ, Kim HJ, et al. Activation of PPAR-γ by carbon monoxide from CORM-2 leads to the inhibition of iNOS but not COX-2 expression in LPS-stimulated macrophages. Inflammation. 2009; 32(6):364–71.
108. Paukkeri EL, Leppänen T, Lindholm M, Yam MF, Asmawi MZ, Kolmonen A, et al. Anti-inflammatory properties of a dual PPARgamma/alpha agonist muraglitazar in in vitro and in vivo models. Arthritis Res Ther. 2013; 15(2):R51.
109. Kaundal RK, Sharma SS. GW1929: A nonthiazolidinedione PPARγ agonist, ameliorates neurological damage in global cerebral ischemic-reperfusion injury through reduction in inflammation and DNA fragmentation. Behav Brain Res. 2011; 216(2):606–12.
110. Xi Y, Zhang Y, Zhu S, Luo Y, Xu P, Huang Z. PPAR-Mediated Toxicology and Applied Pharmacology. Cells. 2020; 9(2):352.
111. Wright MB, Bortolini M, Tadayyon M, Bopst M. Minireview: Challenges and opportunities in development of ppar agonists. Mol Endocrinol. 2014; 28(11):1756–68.
112. Bortolini M, Wright MB, Bopst M, Balas B. Examining the safety of PPAR agonists - Current trends and future prospects. Expert Opin Drug Saf. 2013; 12(1):65–79.
113. Lin X, Zhang H, Boyce BF, Xing L. Ubiquitination of interleukin-1α is associated with increased pro-inflammatory polarization of murine macrophages deficient in the E3 ligase ITCH. J Biol Chem. 2020; 295(33):11764–75.

114. Zhong J, Wang H, Chen W, Sun Z, Chen J, Xu Y, et al. Ubiquitylation of MFHAS1 by the ubiquitin ligase praja2 promotes M1 macrophage polarization by activating JNK and p38 pathways. Cell Death Dis. 2017; 8(5):1–10.
115. Cao W, Chen J, Zhang E, Cai Z. E3 Ubiquitin Ligase TRIM21 Enhances Macrophage-Mediated Bortezomib Resistance By Inducing M2 Polarization in Multiple Myeloma. Blood. 2023; 142:5730–5730.
116. Zheng N, Shabek N. Ubiquitin ligases: Structure, function, and regulation. Annu Rev Biochem. 2017; 86:129–57.
117. Deshaies RJ, Joazeiro CAP. RING domain E3 ubiquitin ligases. Annu Rev Biochem. 2009; 78:399–434.
118. Rotin D, Kumar S. Physiological functions of the HECT family of ubiquitin ligases. Nat Rev Mol Cell Biol. 2009; 10(6):398–409.
119. Cai C, Tang YD, Zhai J, Zheng C. The RING finger protein family in health and disease. Signal Transduct Target Ther. 2022; 7(1):300.
120. Chen H, Chew G, Devapragash N, Loh JZ, Huang KY, Guo J, et al. The E3 ubiquitin ligase WWP2 regulates pro-fibrogenic monocyte infiltration and activity in heart fibrosis. Nat Commun. 2022; 13(1):1–21.
121. Wauman J, De Ceuninck L, Vanderroost N, Lievens S, Tavernier J. RNF41 (Nrdp1) controls type 1 cytokine receptor degradation and ectodomain shedding. J Cell Sci. 2011; 124(6):921–32.
122. Vainchenker W, Leroy E, Gilles L, Marty C, Plo I, Constantinescu SN. JAK inhibitors for the treatment of myeloproliferative neoplasms and other disorders. F1000Research. 2018; 7(0):1–19.
123. Desai HR, Sivasubramaniyam T, Revelo XS, Schroer SA, Luk CT, Rikkala PR, et al. Macrophage JAK2 deficiency protects against high-fat diet-induced inflammation. Sci Rep. 2017; 7(1):1–15.
124. Wang C, Chen T, Zhang J, Yang M, Li N, Xu X, et al. The E3 ubiquitin ligase Nrdp1 “preferentially” promotes TLR-mediated production of type I interferon. Nat Immunol. 2009; 10(7):744–52.
125. Wu X, Chen Z, Chen Q, Lin C, Zheng X, Yuan B. Nrdp1-mediated Macrophage Phenotypic Regulation Promotes Functional Recovery in Mice with Mild Neurological Impairment after Intracerebral Hemorrhage. Neuroscience. 2024; 545:16–30.
126. Medrano-Bosch M, Moreno-Lanceta A, Melgar-Lesmes P. Nanoparticles to target and treat macrophages: The ockham’s

concept? Pharmaceutics. 2021; 13(9):1–27.
127. Soares S, Sousa J, Pais A, Vitorino C. Nanomedicine: Principles, properties, and regulatory issues. Front Chem. 2018; 6:1–15.
128. Anselmo AC, Mitragotri S. Nanoparticles in the clinic: An update post COVID-19 vaccines. Bioeng Transl Med. 2021; 6(3):1–20.
129. Joudeh N, Linke D. Nanoparticle classification, physicochemical properties, characterization, and applications: a comprehensive review for biologists. J Nanobiotechnology. 2022; 20(1):1–29.
130. Asad S, Jacobsen AC, Teleki A. Inorganic nanoparticles for oral drug delivery: opportunities, barriers, and future perspectives. Curr Opin Chem Eng. 2022; 38:100869.
131. Mendes BB, Conniot J, Avital A, Yao D, Jiang X, Zhou X, et al. Nanodelivery of nucleic acids. Nat Rev Methods Prim. 2022; 2(1).
132. Tiwari G, Tiwari R, Bannerjee S, Bhati L, Pandey S, Pandey P, et al. Drug delivery systems: An updated review. Int J Pharm Investig. 2012; 2(1):2.
133. Hu G, Guo M, Xu J, Wu F, Fan J, Huang Q, et al. Nanoparticles targeting macrophages as potential clinical therapeutic agents against cancer and inflammation. Front Immunol. 2019; 10:1–14.
134. Nakkala JR, Li Z, Ahmad W, Wang K, Gao C. Immunomodulatory biomaterials and their application in therapies for chronic inflammation-related diseases. Acta Biomater. 2021; 123:1–30.
135. Warner JB, Guenthner SC, Hardesty JE, McClain CJ, Warner DR, Kirpich IA. Liver-specific drug delivery platforms: Applications for the treatment of alcohol-associated liver disease. World J Gastroenterol. 2022; 28(36):5280–99.
136. Zhang YN, Poon W, Tavares AJ, McGilvray ID, Chan WCW. Nanoparticle–liver interactions: Cellular uptake and hepatobiliary elimination. J Control Release. 2016; 240:332–48.
137. Tsoi KM, Macparland SA, Ma XZ, Spetzler VN, Echeverri J, Ouyang B, et al. Mechanism of hard-nanomaterial clearance by the liver. Nat Mater. 2016; 15(11):1212–21.
138. Carvajal S, Perramón M, Casals G, Oró D, Ribera J, Morales-Ruiz M, et al. Cerium oxide nanoparticles protect against oxidant injury and interfere with oxidative mediated kinase signaling in human-derived hepatocytes. Int J Mol Sci. 2019; 20(23):1–22.
139. Xiong Y, Wu B, Guo X, Shi D, Xia H, Xu H, et al. Galangin delivered by retinoic acid-modified nanoparticles targeted hepatic

stellate cells for the treatment of hepatic fibrosis. RSC Adv. 2023; 13(16):10987–1001.
140. Younis MA, Sato Y, Elewa YHA, Harashima H. Reprogramming activated hepatic stellate cells by siRNA-loaded nanocarriers reverses liver fibrosis in mice. J Control Release. 2023; 361:592–603.
141. Xia S, Liu Z, Cai J, Ren H, Li Q, Zhang H, et al. Liver fibrosis therapy based on biomimetic nanoparticles which deplete activated hepatic stellate cells. J Control Release. 2023; 355:54–67.
142. Carambia A, Gottwick C, Schwinge D, Stein S, Digigow R, Şeleci M, et al. Nanoparticle-mediated targeting of autoantigen peptide to cross-presenting liver sinusoidal endothelial cells protects from CD8 T-cell-driven autoimmune cholangitis. Immunology. 2021; 162(4):452–63.
143. Hashem MA, Alotaibi BS, Elsayed MMA, Alosaimi ME, Hussein AK, Abduljabbar MH, et al. Characterization and Bio-Evaluation of the Synergistic Effect of Simvastatin and Folic Acid as Wound Dressings on the Healing Process. Pharmaceutics. 2023; 15(10):2463.
144. Zhou JE, Sun L, Liu L, Jia Y, Han Y, Shao J, et al. Hepatic macrophage targeted siRNA lipid nanoparticles treat non-alcoholic steatohepatitis. J Control Release. 2022; 343:175–86.
145. Martinez-Campanario MC, Cortés M, Moreno-Lanceta A, Han L, Ninfali C, Domínguez V, et al. Atherosclerotic plaque development in mice is enhanced by myeloid ZEB1 downregulation. Nat Commun. 2023; 14(1).
146. Duan BW, Liu YJ, Li XN, Han MM, Yu HY, Hong HY, et al. An Autologous Macrophage-Based Phenotypic Transformation-Collagen Degradation System Treating Advanced Liver Fibrosis. Adv Sci. 2024; 11(7):1–15.
147. Han S, Bao X, Zou Y, Wang L, Li Y, Yang L, et al. D-lactate modulates M2 tumor-associated macrophages and remodels immunosuppressive tumor microenvironment for hepatocellular carcinoma. Sci Adv. 2023; 9(29):1–17.
148. Zheng J, Yang N, Wan Y, Cheng W, Zhang G, Yu S, et al. Celastrol-loaded biomimetic nanodrug ameliorates APAP-induced liver injury through modulating macrophage polarization. J Mol Med. 2023; 101(6):699–716.

149. Shin M, Lim J, Park Y, Lee JY, Yoon J, Choi JW. Carbon-based nanocomposites for biomedical applications. RSC Adv. 2024; 14(10):7142–56.
150. Fahmy HM, Abu Serea ES, Salah-Eldin RE, Al-Hafiry SA, Ali MK, Shalan AE, et al. Recent Progress in Graphene- and Related Carbon-Nanomaterial-based Electrochemical Biosensors for Early Disease Detection. ACS Biomater Sci Eng. 2022; 8(3):964–1000.
151. Ehrenfreund P, Irvine W, Becker L, Blank J, Brucato JR, Colangeli L, et al. Astrophysical and astrochemical insights into the origin of life. Reports Prog Phys. 2002; 65(10):1427–87.
152. Witmer-Pack MD, Crowley MT, Inaba K, Steinman RM. Macrophages, but not dendritic cells, accumulate colloidal carbon following administration in situ. J Cell Sci. 1993; 105(4):965–73.
153. Yuan X, Zhang X, Sun L, Wei Y, Wei X. Cellular Toxicity and Immunological Effects of Carbon-based Nanomaterials. Part Fibre Toxicol. 2019; 16(1):18.
154. Geim AK, Novoselov KS. The rise of graphene. Nat Mater. 2007; 6(3):183–91.
155. Moreno-Lanceta A, Medrano-Bosch M, Melgar-Lesmes P. Single-walled carbon nanohorns as promising nanotube-derived delivery systems to treat cancer. Pharmaceutics. 2020; 12(9):850.
156. Khatik N, Sachdeva H. Graphite-based nanomaterials for drug delivery. Mater Today Proc. 2022; 69:30–5.
157. Sinclair R, Li H, Madsen S, Dai H. HREM analysis of graphite-encapsulated metallic nanoparticles for possible medical applications. Ultramicroscopy. 2013; 134:167–74.
158. Abedi-gaballu F, Dehghan G, Ghaffari M, Yekta R, Abbaspour-ravasjani S, Baradaran B, et al. PAMAM dendrimers as efficient drug and gene delivery nanosystems for cancer therapy. Appl Mater Today. 2018; 12:177–90.
159. Ramachandran P, Matchett KP, Dobie R, Wilson-Kanamori JR, Henderson NC. Single-cell technologies in hepatology: new insights into liver biology and disease pathogenesis. Nat Rev Gastroenterol Hepatol. 2020; 17(8):457–72.
160. Ramachandran P, Dobie R, Wilson-Kanamori JR, Dora EF, Henderson BEP, Luu NT, et al. Resolving the fibrotic niche of human liver cirrhosis at single-cell level. Nature. 2019; 575(7783):512-518

161. Toobian D, Ghosh P, Katkar GD. Parsing the Role of PPARs in Macrophage Processes. Front Immunol. 2021; 12:1–17.
162. Su M, Cao J, Huang J, Liu S, Im DS, Yoo JW, et al. The in vitro and in vivo anti-inflammatory effects of a phthalimide PPAR-γ agonist. Mar Drugs. 2017; 15(1):7.
163. Tian Y, Yang C, Yao Q, Qian L, Liu J, Xie X, et al. Procyanidin B2 activates PPARγ to induce M2 polarization in mouse macrophages. Front Immunol. 2019; 10:1–12.
164. Nelson VL, Nguyen HCB, Garcìa-Cañaveras JC, Briggs ER, Ho WY, Dispirito JR, et al. PPARγ is a nexus controlling alternative activation of macrophages via glutamine metabolism. Genes Dev. 2018; 32(15–16):1035–44.
165. Coste A, Dubourdeau M, Linas MD, Cassaing S, Lepert JC, Balard P, et al. PPARγ promotes mannose receptor gene expression in murine macrophages and contributes to the induction of this receptor by IL-13. Immunity. 2003; 19(3):329–39.
166. Heming M, Gran S, Jauch SL, Fischer-Riepe L, Russo A, Klotz L, et al. Peroxisome proliferator-activated receptor-γ modulates the response of macrophages to lipopolysaccharide and glucocorticoids. Front Immunol. 2018; 9:893.
167. Lefere S, Puengel T, Hundertmark J, Penners C, Frank AK, Guillot A, et al. Differential effects of selective- and pan-PPAR agonists on experimental steatohepatitis and hepatic macrophages. J Hepatol. 2020; 73(4):757–70.
168. Boyer-Diaz Z, Aristu-Zabalza P, Andrés-Rozas M, Robert C, Ortega-Ribera M, Fernández-Iglesias A, et al. Pan-PPAR agonist lanifibranor improves portal hypertension and hepatic fibrosis in experimental advanced chronic liver disease. J Hepatol. 2021; 74(5):1188–99.
169. Yan S, Ding J, Wang Z, Zhang F, Li J, Zhang Y, et al. CTRP6 regulates M1 macrophage polarization via the PPAR-γ/NF-κB pathway and reprogramming glycolysis in recurrent spontaneous abortion. Int Immunopharmacol. 2023; 124(PA):110840.
170. Moore-Carrasco R, Figueras M, Ametller E, López-Soriano FJ, Argilés JM, Busquets S. Effects of the PPARγ agonist GW1929 on muscle wasting in tumour-bearing mice. Oncol Rep. 2008; 19(1):253–6.
171. Nanbu-Wakao R, Fujitani Y, Masuho Y, Muramatu MA, Wakao H.

Prolactin enhances CCAAT enhancer-binding protein-β (C/EBPβ) and peroxisome proliferator-activated receptor γ (PPARγ) messenger RNA expression and stimulates adipogenic conversion of NIH-3T3 cells. Mol Endocrinol. 2000; 14(2):307–16.
172. Lefterova MI, Zhang Y, Steger DJ, Schupp M, Schug J, Cristancho A, et al. PPARγ and C/EBP factors orchestrate adipocyte biology via adjacent binding on a genome-wide scale. Genes Dev. 2008; 22(21):2941–52.
173. Wu X, Yen L, Irwin L, Sweeney C, Carraway KL. Stabilization of the E3 Ubiquitin Ligase Nrdp1 by the Deubiquitinating Enzyme USP8. Mol Cell Biol. 2004; 24(17):7748–57.
174. Islam MT, Chen F, Chen H. The oncogenic role of ubiquitin specific peptidase (USP8) and its signaling pathways targeting for cancer therapeutics. Arch Biochem Biophys. 2021; 701:108811.
175. Butchar JP, Cremer TJ, Clay CD, Gavrilin MA, Wewers MD, Marsh CB, et al. Microarray analysis of human monocytes infected with Francisella tularensis identifies new targets of host response subversion. PLoS One. 2008; 3(8):1–8.
176. Hayden MS, Ghosh S. Regulation of NF-κB by TNF Family Cytokines. Semin Immunol. 2014; 26(3):253–66.
177. Sabio G, Davis RJ. TNF and MAP kinase signaling pathways. Semin Immunol. 2014; 26(3):237–45.
178. Low I, Albetran HM, Degiorgio M. Structural Characterization of Commercial Graphite and Graphene Materials. J Nanotechnol Nanomater. 2020; 1(1):23–30.
179. Bielinska AU, Kukowska-Latallo JF, Baker JR. The interaction of plasmid DNA with polyamidoamine dendrimers: Mechanism of complex formation and analysis of alterations induced in nuclease sensitivity and transcriptional activity of the complexed DNA. Biochim Biophys Acta - Gene Struct Expr. 1997; 1353(2):180–90.
180. Chis AA, Dobrea CM, Rus LL, Frum A, Morgovan C, Butuca A, et al. Dendrimers as non-viral vectors in gene-directed enzyme prodrug therapy. Molecules. 2021; 26(19):5976.
181. Li J, Shen M, Shi X. Poly(amidoamine) Dendrimer-Gold Nanohybrids in Cancer Gene Therapy: A Concise Overview. ACS Appl Bio Mater. 2020; 3(9):5590–605.
182. A-Kadhim MM-H, Kelkawi AHA. The Role of Gold Nanoparticles/Au-PEG-PAMAM as Drug Delivery System for

Treatment of Breast Cancer. Biomed Chem Sci. 2023; 2(2):76–82.
183. Lin L, Fan Y, Gao F, Jin L, Li D, Sun W, et al. UTMD-promoted co-delivery of gemcitabine and miR-21 inhibitor by dendrimer-entrapped gold nanoparticles for pancreatic cancer therapy. Theranostics. 2018; 8(7):1923–39.
184. Janaszewska A, Lazniewska J, Trzepiński P, Marcinkowska M, Klajnert-Maculewicz B. Cytotoxicity of dendrimers. Biomolecules. 2019; 9(8):1–23.
185. Zenze M, Daniels A, Singh M. Dendrimers as Modifiers of Inorganic Nanoparticles for Therapeutic Delivery in Cancer. Pharmaceutics. 2023; 15(2):398.
186. Wigner P, Zielinski K, Michlewska S, Danielska P, Marczak A, Ricci EJ, et al. Disturbance of cellular homeostasis as a molecular risk evaluation of human endothelial cells exposed to nanoparticles. Sci Rep. 2021; 11(1):1–16.
187. Bauer AT, Strozyk EA, Gorzelanny C, Westerhausen C, Desch A, Schneider MF, et al. Cytotoxicity of silica nanoparticles through exocytosis of von Willebrand factor and necrotic cell death in primary human endothelial cells. Biomaterials. 2011; 32(33):8385–93.
188. Dunphy A, Patel K, Belperain S, Pennington A, Chiu NHL, Yin Z, et al. Modulation of macrophage polarization by carbon nanodots and elucidation of carbon nanodot uptake routes in macrophages. Nanomaterials. 2021; 11(5):1–16.
189. Gustafson HH, Holt-Casper D, Grainger DW, Ghandehari H. Nanoparticle uptake: The phagocyte problem. Nano Today. 2015; 10(4):487–510.
190. Liedtke C, Luedde T, Sauerbruch T, Scholten D, Streetz K, Tacke F, et al. Experimental liver fibrosis research: Update on animal models, legal issues and translational aspects. Fibrogenes Tissue Repair. 2013; 6(1):19.
191. Zangar RC, Benson JM, Burnett VL, Springer DL. Cytochrome P450 2E1 is the primary enzyme responsible for low-dose carbon tetrachloride metabolism in human liver microsomes. Chem Biol Interact. 2000; 125(3):233–43.
192. Bangen JM, Hammerich L, Sonntag R, Baues M, Haas U, Lambertz D, et al. Targeting CCl4-induced liver fibrosis by RNA interference–mediated inhibition of cyclin E1 in mice. Hepatology. 2017;

66(4):1242–57.
193. Scholten D, Trebicka J, Liedtke C, Weiskirchen R. The carbon tetrachloride model in mice. Lab Anim. 2015; 49:4–11.
194. Kolaric TO, Kuna L, Covic M, Roguljic H, Matic A, Sikora R, et al. Preclinical Models and Promising Pharmacotherapeutic Strategies in Liver Fibrosis: An Update. Curr Issues Mol Biol. 2023; 45(5):4246–60.
195. Scirpo R, Fiorotto R, Villani A, Amenduni M, Spirili C, Strazzabosco M. Stimulation of nuclear receptor PPAR-γ limits NF-kB-dependent inflammation in mouse cystic fibrosis biliary epithelium. Hepatology. 2016; 62(5):1551–62.
196. Meng Z, Xu R, Xie L, Wu Y, He Q, Gao P, et al. A20/Nrdp1 interaction alters the inflammatory signaling profile by mediating K48- And K63-linked polyubiquitination of effectors MyD88 and TBK1. J Biol Chem. 2021; 297(1):100811.
197. Chawla A. Control of macrophage activation and function by PPARs. Circ Res. 2010; 106(10):1559–69.
198. Wu Z, Xie Y, Bucher NLR, Farmer SR. Conditional ectopic expression of C/EBPβ in NIH-3T3 cells induces PPARγ and stimulates adipogenesis. Genes Dev. 1995; 9(19):2350–63.
199. Shi J, Li J, Guan H, Cai W, Bai X, Fang X, et al. Anti-fibrotic actions of interleukin-10 against hypertrophic scarring by activation of PI3K/AKT and STAT3 signaling pathways in scar-forming fibroblasts. PLoS One. 2014; 9(5):1–10.
200. Huang YH, Chen MH, Guo QL, Chen ZX, Chen QD, Wang XZ. Interleukin-10 induces senescence of activated hepatic stellate cells via STAT3-p53 pathway to attenuate liver fibrosis. Cell Signal. 2020; 66:109445.
201. Zhang LJ, Zheng WD, Shi MN, XZ Li-Wang. Effects of interleukin-10 on activation and apoptosis of hepatic stellate cells in fibrotic rat liver. World J Gastroenterol. 2006; 12(12):1918–23.
202. Wagner N, Wagner KD. Ppars and angiogenesis—implications in pathology. Int J Mol Sci. 2020; 21(16):1–23.
203. Ezhilarasan D. Molecular mechanisms in thioacetamide-induced acute and chronic liver injury models. Environ Toxicol Pharmacol. 2023; 99(162):104093.
204. Matsuda M, Tsurusaki S, Miyata N, Saijou E, Okochi H, Miyajima A, et al. Oncostatin M causes liver fibrosis by regulating

cooperation between hepatic stellate cells and macrophages in mice. Hepatology. 2018; 67(1):296–312.
205. Chu PS, Nakamoto N, Ebinuma H, Usui S, Saeki K, Matsumoto A, et al. C-C motif chemokine receptor 9 positive macrophages activate hepatic stellate cells and promote liver fibrosis in mice. Hepatology. 2013; 58(1):337–50.
206. Imamura M, Ogawa T, Sasaguri Y, Chayama K, Ueno H. Suppression of macrophage infiltration inhibits activation of hepatic stellate cells and liver fibrogenesis in rats. Gastroenterology. 2005; 128(1):138–46.
207. Szücs A, Paku S, Sebestyén E, Nagy P, Dezso K. Postnatal, ontogenic liver growth accomplished by biliary/oval cell proliferation and differentiation. PLoS One. 2020; 15(5):1–13.
208. Bonefeld K, Møller S. Insulin-like growth factor-I and the liver. Liver Int. 2011; 31(7):911–9.
209. de la Garza RG, Morales-Garza LA, Martin-Estal I, Castilla-Cortazar I. Insulin-Like Growth Factor-1 Deficiency and Cirrhosis Establishment. J Clin Med Res. 2017; 9(4):233–47.
210. Miyauchi S, Miyake T, Miyazaki M, Eguchi T, Niiya T, Yamamoto S, et al. Insulin-like growth factor-1 is inversely associated with liver fibrotic markers in patients with type 2 diabetes mellitus. J Diabetes Investig. 2019; 10(4):1083–91.
211. Ye S, Xu H, Jin J, Yang M, Wang C, Yu Y, et al. The E3 ubiquitin ligase neuregulin receptor degradation protein 1 (Nrdp1) promotes M2 macrophage polarization by ubiquitinating and activating transcription factor CCAAT/enhancer-binding protein β (C/EBPβ). J Biol Chem. 2012; 287(32):26740–8.
212. Boyce S, Harrison D. A detailed methodology of partial hepatectomy in the mouse. Lab Anim (NY). 2008; 37(11):529–32.
213. Mitchell C, Willenbring H. A reproducible and well-tolerated method for 2/3 partial hepatectomy in mice. Nat Protoc. 2008; 3(7):1167–70.
214. Gazit V, Huang J, Weymann A, Rudnick DA. Analysis of the role of hepatic PPARγ expression during mouse liver regeneration. Hepatology. 2012; 56(4):1489–98.